



Université Catholique de Louvain

Faculté des Sciences
Institut de Recherche en Mathématique et Physique
Center for Cosmology, Particle Physics and Phenomenology

*Effective field theories in the
Standard Model and beyond*

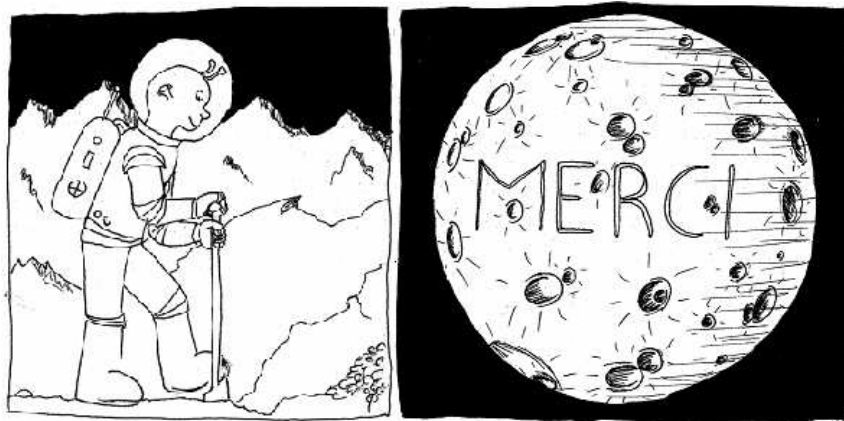
Céline Degrande

Jury de thèse:

Y. Félix (UCL) *Président*
J. M. Gérard (UCL-CP3) *Promoteur*
G. Bruno (UCL-CP3)
C. Grojean (CERN)
F. Maltoni (UCL-CP3)
S. Willenbrock (UIUC)

September 2011

Remerciements



*A mon promoteur, mes collaborateurs et mes collègues,
aux membres du jury,
à mon mari, mes parents, ma soeur, ma famille et ma belle-famille,
à mes amis.*

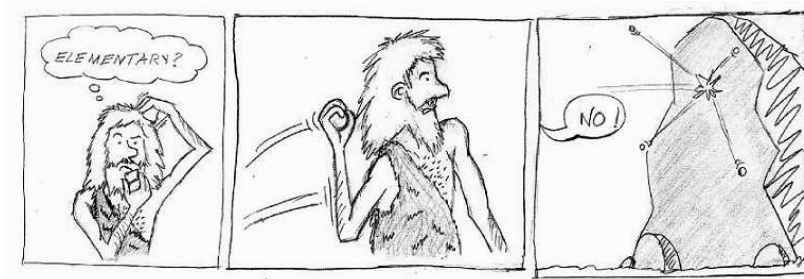
Contents

Introduction	9
1 An introduction to elementary particle physics	13
1.1 Standard Model	14
1.1.1 The gauge Lagrangian	14
1.1.2 The Higgs mechanism	15
1.1.3 The Yukawa Lagrangian	17
1.1.4 Custodial symmetry	18
1.1.5 The strong interaction	18
1.2 Effective field theories	20
1.2.1 Fermi theory	20
1.2.2 The expansion	21
1.2.3 Integrating out heavy degrees of freedom	23
1.2.4 Scale hierarchy from spontaneously broken symmetries	24
1.2.5 Loops in effective field theories	25
1.3 Top scenery	27
1.3.1 $t\bar{t}$ total cross-section and invariant mass distribution	28
1.3.2 Forward-backward Asymmetry	29
1.3.3 Spin correlations	31
1.3.4 Beyond $t\bar{t}$	32

2	A Theoretical determination of the $\eta - \eta'$ mixing	35
2.1	An effective theory at leading order in p^2 and $\frac{1}{N_c}$	36
2.2	One-loop corrections to the $\eta - \eta'$ inverse propagator matrix	41
2.3	One-loop corrections to the $\eta' \rightarrow \eta\pi\pi$ decay amplitude	44
2.3.1	Tree-level amplitude	45
2.3.2	One-loop amplitude	45
2.4	Concluding remarks	46
3	Effective theory for the top pair productions	49
3.1	Effective Lagrangians	50
3.1.1	Dimension-six operators for opposite sign top pair production	51
3.1.2	Dimension-six operators for same sign top pair production . .	56
3.2	Connection with composite top and heavy boson exchange models . .	57
3.2.1	Composite models	57
3.2.2	s - and t -channel exchanges	60
3.3	Corrections to the Higgs production	64
3.3.1	The chromomagnetic operator	64
3.3.2	Composite Higgs	65
3.4	Z decay constraints	66
4	Phenomenology of top pair productions	71
4.1	Opposite sign top pair production	72
4.1.1	Partonic differential cross-sections	72
4.1.2	Total cross-section	74
4.1.3	$t\bar{t}$ invariant-mass, p_T and η distributions	80
4.1.4	Forward-backward asymmetry	82
4.1.5	Spin correlations	85
4.1.6	Bosons exchanges	87

4.2	Same Sign top pair production	91
4.3	Associated top pair productions	94
4.3.1	$t\bar{t}b\bar{b}$ and $t\bar{t}t\bar{t}$ productions at the LHC	94
4.3.2	$t\bar{t}$ production in association with a Higgs	97
4.4	Summary	99
	Conclusion	103
	A Appendix for top pair productions	107
A.1	Fierz transformations	107
A.2	Feynman diagrams for $t\bar{t}$ production at order $\mathcal{O}(\Lambda^{-2})$	108
A.3	Helicity amplitude for $t\bar{t}$	108

Introduction



Particle physics aims at identifying the elementary constituents of our Universe and understanding their interactions. Four elementary building blocks of ordinary matter have been discovered so far : the electron, the neutrino and the two constituents of the proton and the neutron, the up and down quarks. Moreover, two heavier replicas were found for each matter particle. The observed picture is completed by the four forces that carry the information between the twelve elementary fermions. In the 20th century, the weak and the strong nuclear interactions were added to the well-known gravitational and electromagnetic ones. However, the gravitational interaction does not fit in the same theoretical framework as the three others. Since its effects are tiny in (4-dimensional) particle physics, gravitation will be discarded in the following.

In this theoretical picture of elementary particle physics, the Standard Model (SM), local symmetries are the keys of our understanding of the fundamental interactions. They ensure predictivity at the quantum level, *i.e.* only a finite number of free parameters are needed to absorb all the divergences of the model. However, they also imply that the mediators are massless. Consequently, particles should interact at large

distance. While this property is confirmed for the electromagnetic interaction, it disagrees with the observed behavior of the weak and strong interactions. We can actually see, for example, the attraction or the repulsion between magnets due to the electromagnetic force. On the contrary, nuclear forces did never show up in any every day experiments.

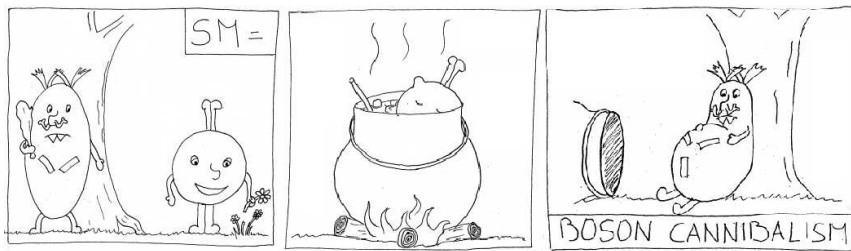
The issue was solved differently for the two interactions in the SM. On the one hand, the strong interaction is hidden at large distances through confinement. Similarly as neutral atoms and molecules mask the electromagnetic interaction, only quark bound states, neutral for the strong interaction, are allowed. The drawback is that only those composite hadrons can be directly seen in any detector. Moreover, accurate relations with the fundamental parameters are hard to obtain due to the large value of the strong coupling. Consequently, many questions about the strong dynamics are still unanswered. On the other hand, the weak interaction can only act at short distances due to the masses of its mediators. The price to avoid an explicit breaking of the local symmetry by the masses is the introduction of a new scalar, the Higgs boson. Despite its very good agreement with the experimental data, this minimal solution brings its own issues. First of all, the elementary scalar predicted by the model has not been discovered so far and requires further experimental investigation. Additionally, scalar masses are very sensitive to the ultraviolet content of the model. If there are some new particles at higher energy, it is hard to stabilize the electroweak scale at its measured value. There are several reasons to expect those new states. In particular, the known matter is only 5% of the Universe content. There are basically two ways out : either the new physics scale is close to the electroweak one or the electroweak symmetry breaking (EWSB) is not due to an elementary scalar. Even in the second case, new phenomenons should happen around the TeV. As a matter of fact, sizeable deviations from the SM in the weak bosons scattering are expected at this scale if there is no Higgs particle.

While our knowledge of the strong interaction is mainly theoretically limited, the questions about the EWSB mechanism can only be answered by experiments. The Tevatron and the Large Hadron Collider (LHC) were precisely built for that reason. Little hope remains for a discovery at the Tevatron before its closure in September. However, LHC has just started last year to collect data and is performing extremely well. Both at the Tevatron and at the LHC, the strong processes dominate since they are hadron machines. Weak bosons are thus harder to produce than the colored particles. Fortunately, the fermion mass generation is also related to the symmetry breaking of the weak sector in the SM. The heavier a particle is, the stronger it couples to the EWSB sector. Being the heaviest matter particle, the top quark is thus a natural probe of the EWSB mechanism.

In this thesis, we use the same tool, effective field theories, to further explore confinement and electroweak spontaneous symmetry breaking. Effective field theories are introduced in the first chapter as well as the Standard Model and the relevant measurements in top physics. The second chapter focuses on the lightest strong bound states. Their low masses compared to the confinement scale of the strong interaction make the light mesons suitable for an effective treatment. The associated effective theory allows us to understand their interactions from the various symmetries of the fundamental Lagrangian. In particular, we focus on the $\eta - \eta'$ mixing which is sensitive to the dynamical breaking of the global axial symmetry by the strong interaction [1]. After this first contact with the well-known effective theory for the light mesons, we further use this tool for the search of new physics in top pair productions [2, 3]. The effective theory, described in the third chapter, provides a model independent way to parametrize the new physics effects. Our analysis is thus not restricted to new physics related to EWSB, but also includes many other types of new physics coupled to the top quark. The constraints on the parameter space from the Tevatron and LHC measurements are derived in the last chapter. The new physics effects for the LHC are then computed in the allowed region.

Chapter 1

An introduction to elementary particle physics



This chapter does not attempt to provide a complete introduction to elementary particle physics. Its aim is to give the necessary ingredients for the following chapters in a pedagogical way. First, the current theoretical picture of the fundamental interactions, *i.e.* the Standard Model (SM), is briefly introduced. Even if there are several reasons to go beyond the SM, its successes in explaining the experimental data prove that the SM is at least a good approximation in the energy range probed so far. The second part is dedicated to the effective field theories. They will be used to explore the SM in Chap. 2 but mainly to go beyond in Chap. 3. Finally, the more relevant experimental measurements in the top quark sector will be summarized. In Chap. 4, our extension of the SM will be confronted to those data.

1.1 Standard Model

1.1.1 The gauge Lagrangian

The Standard Model is a gauge theory based on the groups $SU(3)_c \otimes SU(2)_L \otimes U(1)_Y$. The fermion fields transformations under the local symmetry are given by

$$\Psi \rightarrow e^{ig_s \alpha(x) T^A + ig \beta^I(x) \frac{\sigma^I}{2} + ig' \gamma(x) Y} \Psi \quad (1.1)$$

where Y is the hypercharge, σ^I are the $SU(2)_L$ generators¹ normalized as $\text{tr}(\sigma^I \sigma^J) = 2\delta^{IJ}$ and T^A are the $SU(3)_c$ generators normalized as $\text{tr}(T^A T^B) = \frac{1}{2}\delta^{AB}$. The matter content of the SM as well as their quantum numbers are displayed in Table 1.1.

	L_L	l_R	q_L	u_R	d_R
$SU(3)_c$	1	1	3	3	3
$SU(2)_L$	2	1	2	1	1
Y	$-\frac{1}{2}$	-1	$\frac{1}{6}$	$\frac{2}{3}$	$-\frac{1}{3}$

Table 1.1: Quantum numbers of the SM fermions where $L_L = (\nu_L, l_L)^T$ and $q_L = (u_L, d_L)^T$.

The remaining particles of the SM are the mediators of the interactions between the matter fields. The gluons G^A and the electroweak bosons W^I and B are the gauge bosons of $SU(3)_c$, $SU(2)_L$ and $U(1)_Y$ respectively and transform as

$$F_\mu^A \rightarrow F_\mu^A + \partial_\mu \phi(x)^A + g_i f^{ABC} F_\mu^B \phi^C \quad (1.2)$$

where $\phi(x)$ is a generic label for $\alpha(x)$, $\beta(x)$ and $\gamma(x)$, g_i for g_s , g and g' and f^{ABC} are the structure constants of the associated group. With this particle content, the most generic renormalizable Lagrangian is

$$\mathcal{L}^{gauge} = \sum i \bar{\Psi} \not{D} \Psi - \frac{1}{4} G_{\mu\nu}^A G^{\mu\nu A} - \frac{\alpha_s}{8\pi} \theta \tilde{G}_{\mu\nu}^A G^{\mu\nu A} - \frac{1}{4} W_{\mu\nu}^I W^{\mu\nu I} - \frac{1}{4} B_{\mu\nu} B^{\mu\nu} \quad (1.3)$$

where

$$D_\mu \equiv \partial_\mu - ig_s G_\mu^A T^A - i \frac{1}{2} g W_\mu^I \sigma^I - ig' B_\mu Y \quad (1.4)$$

¹Since the SM only contains $SU(2)_L$ doublets or singlets, σ^I will be also used to denote the Pauli matrices.

is the covariant derivative, the $G_{\mu\nu}^A$, $W_{\mu\nu}^I$ and $B_{\mu\nu}$ are the strength field tensors defined by

$$F_{\mu\nu}^A \equiv \partial_\mu F_\nu^A - \partial_\nu F_\mu^A + g_i f^{ABC} F_\mu^B F_\nu^C, \quad (1.5)$$

$\alpha_s \equiv \frac{g_s^2}{4\pi}$ and $\tilde{G}_{\mu\nu} = \epsilon_{\mu\nu\rho\sigma} G^{\rho\sigma}$. The parameter θ is constrained to be very small by the measurement of the neutron electric dipole moment² so we will assume that $\theta = 0$ in the following. There is no such term for $SU(2)_W$ since the Lagrangian for the weak interaction is equivalent to a chiral QCD-like theory.

It should be noted that \mathcal{L}^{gauge} only contains gauge interactions and kinetic terms. Consequently, all the fields are massless so far. On the one hand, gauge symmetry guarantees that the mediators are massless. On the other hand, no Dirac mass term can be formed for the fermions since their right- and left-handed components belong to different representations of the electroweak symmetry group.

1.1.2 The Higgs mechanism

However, almost all the observed elementary particles are massive. In the SM, this problem is solved by breaking spontaneously the gauge group of the electroweak interactions $SU(2)_L \otimes U(1)_Y$ to $U(1)_{EM}$. In practice, this mechanism is implemented by a scalar field denoted H and transforming as $(1, 2, 1/2)$ under the SM gauge groups. We can now write down the full SM Lagrangian,

$$\mathcal{L}^{SM} = \mathcal{L}^{gauge} + |D_\mu H|^2 - V(H) + \mathcal{L}_{Yukawa}. \quad (1.6)$$

where

$$V(H) = -\mu^2 H^\dagger H + \lambda (H^\dagger H)^2 \quad (1.7)$$

is the scalar potential and \mathcal{L}_{Yukawa} contains the interactions between the new scalar doublet and the matter fields (see Sect. 1.1.3).

The scalar potential is bounded from below if λ is positive. If $\mu^2 > 0$, the scalar field has a non vanishing value at the minimum

$$\langle |H|^2 \rangle = \frac{\mu^2}{2\lambda} \equiv \frac{v^2}{2}, \quad (1.8)$$

²If the determinant of the mass matrix for the light quarks is real.

where v is the vacuum expectation value (vev). Using gauge invariance, H can be written as

$$H = \begin{pmatrix} 0 \\ \frac{v+h(x)}{\sqrt{2}} \end{pmatrix} \quad (1.9)$$

where $h(x)$ is the surviving physical Higgs boson. The upper component can actually be gauged away by a $SU(2)_L$ transformation. The phase of the lower component can be then removed thanks to the generator $\frac{1}{2}\sigma_3 - Y$. Consequently, the orthogonal combination, corresponding to the unbroken $U(1)_{EM}$, is still not fixed by our choice of gauge. A massless vector boson has two degrees of freedom, its two transverse polarizations. However, a massive vector boson has also a longitudinal polarization and has thus three degrees of freedom. The three missing real scalar fields of the doublet provide the additional degrees of freedom required by the three massive vector bosons, *i.e.* they are eaten by the gauge bosons. In practice, the mass terms of the weak gauge bosons are obtained by replacing H accordingly to Eq. (1.9),

$$|DH|^2 \ni \frac{v^2}{8} (g'B - gW_3)^2 + \frac{g^2}{4} v^2 W^+ W^- \quad (1.10)$$

where we have omitted the Lorentz indices and $W^\pm \equiv (W_1 \mp iW_2)/\sqrt{2}$. The masses of the bosons are

$$M_W = \frac{v}{2}g, \quad M_Z = \frac{v}{2}\sqrt{g^2 + g'^2} \quad \text{et} \quad M_A = 0. \quad (1.11)$$

The neutral mass eigenstates are

$$\begin{pmatrix} Z \\ A \end{pmatrix} = \begin{pmatrix} \cos \theta_W & -\sin \theta_W \\ \sin \theta_W & \cos \theta_W \end{pmatrix} \begin{pmatrix} W_3 \\ B \end{pmatrix} \quad (1.12)$$

with $\cos \theta_W \equiv M_W/M_Z$.

In term of the physical field, the covariant derivative reads

$$\begin{aligned} D &= \partial - ig_s G_A T^A - ig' \cos \theta_W \left(\frac{1}{2}\sigma_3 + Y \right) A - i\frac{g}{\sqrt{2}} (W^+ \sigma^+ + W^- \sigma^-) \\ &\quad - i \left(g\frac{1}{2}\sigma_3 \cos \theta_W - g' \sin \theta_W Y \right) Z. \end{aligned} \quad (1.13)$$

where $\sigma^\pm \equiv \frac{\sigma_1 \pm i\sigma_2}{2}$. The massless boson A is identified as the photon. Consequently,

$$e = g' \cos \theta_W \quad \text{and} \quad Q = \frac{1}{2}\sigma_3 + Y. \quad (1.14)$$

The fourth and fifth terms in Eq. (1.13) give rise to the weak charged and neutral currents respectively.

1.1.3 The Yukawa Lagrangian

In the SM, the scalar doublet does not only give their masses to the weak gauge bosons, but also to the fermions. The last piece of the Lagrangian is

$$\mathcal{L}_{Yukawa} = -\bar{L}_L H y^l l_R - \bar{Q}_L \tilde{H} y^u u_R - \bar{Q}_L H y^d d_R + h.c. \quad (1.15)$$

where $\tilde{H} = i\sigma_2 H^*$ and L_L, Q_L, l_R, u_R and d_R are vectors in the three dimensional flavor space. Consequently, y^F are 3×3 arbitrary complex matrices. The fermion mass matrices,

$$M^F = \frac{y^F v}{\sqrt{2}}, \quad F = l, u, d, \quad (1.16)$$

are thus free parameters. They are, in principle, not diagonal, but can be diagonalized by unitary transformations :

$$M_{diag}^F = U_L^F M^F U_R^{F\dagger}. \quad (1.17)$$

The mass eigenstates are linear combinations of the interaction eigenstates, the latter being now denoted by $'$,

$$u_R = U_R^u u'_R, \quad d_R = U_R^d d'_R \quad (1.18)$$

$$u_L = U_L^u u'_L, \quad d_L = U_L^d d'_L. \quad (1.19)$$

The full SM Lagrangian can be rewritten in term of the mass eigenstates. Nothing changes for the neutral currents since the associated generators are diagonal. On the contrary, the charged currents mix up and down quarks and are at the origin of flavor violation at the tree-level, *i.e.*

$$\begin{aligned} \frac{g}{2\sqrt{2}} \bar{Q}' (W_\mu^+ \sigma^- \gamma^\mu) Q' + h.c. &= \frac{g}{\sqrt{2}} \bar{u}'_L (W_\mu^+ \gamma^\mu) d'_L + h.c. \\ &= \frac{g}{\sqrt{2}} \bar{u}_L (W_\mu^+ \gamma^\mu) V_{CKM} d_L + h.c. \end{aligned} \quad (1.20)$$

where $V_{CKM} = U_L^u U_L^{d\dagger}$ is the unitary Cabibbo, Kobayashi, Maskawa mixing matrix. This matrix can be described by three mixing angles and one physical phase. This phase is the only source of CP violation in the SM.

The Yukawa Lagrangian is responsible for most of the free parameters of the SM. In fact, it contains 13 physical parameters (3×3 masses, 3 angles and 1 phase) while the gauge and the Higgs Lagrangian only depend respectively on 3 and 2 parameters. While most of those 13 parameters are small, the top yukawa coupling turns out to be large ($y_t = \frac{\sqrt{2}m_t}{v} \sim 1$).

Neutrinos are massless since we have not introduced their right-handed components. There are many other ways to provide the neutrinos with a mass [4]. However, we are not concerned here about neutrino masses and mixing.

1.1.4 Custodial symmetry

The scalar potential of the SM has an accidental $SU(2)_L \otimes SU(2)_R$ symmetry. Defining

$$M \equiv \begin{pmatrix} \tilde{H} & H \end{pmatrix}, \quad (1.21)$$

the scalar potential is only a function of $\text{tr}(M^\dagger M) = 2H^\dagger H$ and is invariant under the transformation

$$M \rightarrow U_L^\dagger M U_R. \quad (1.22)$$

After spontaneous symmetry breaking, $SU(2)_L \otimes SU(2)_R$ is broken to the custodial $SU(2)_V$ symmetry. The three eaten scalar bosons transform as a triplet under the custodial symmetry. Their mass degeneracy is transferred to the triplet of gauge bosons (W^\pm, W_3). As a consequence, this symmetry implies the tree-level relation

$$\rho \equiv \frac{M_W^2}{M_Z^2 \cos^2 \theta_W} = \frac{M_W^2}{M_{W_3}^2} = 1 \quad (1.23)$$

and protects it from quantum corrections quadratic in the Higgs mass. However, the custodial symmetry is broken both by the gauge and the yukawa interactions. The largest one-loop correction to the ρ parameter is due to the top mass,

$$\delta\rho = \frac{3G}{8\sqrt{2}\pi^2} m_t^2. \quad (1.24)$$

Its precise measurement at LEP [5],

$$\rho = 1.00412 \pm 0.00124, \quad (1.25)$$

was used to estimate the top mass [6] before its discovery at the Tevatron [7, 8].

1.1.5 The strong interaction

The strong interaction is mediated by the gluons. The associated quantum field theory is called quantum chromodynamics (QCD) since its charges are the colors. At low energy, those interactions are much stronger than the electromagnetic and weak

interactions. As a consequence, the same computation technique, perturbative expansion, cannot be applied. However, the coupling constant of the strong interaction at the energy μ is given by

$$\alpha_s(\mu^2) = \frac{4\pi}{b_0 \log\left(\frac{\mu^2}{\Lambda_{QCD}^2}\right)} \quad (1.26)$$

where Λ_{QCD} is a reference scale. At one-loop,

$$b_0 = 11 - \frac{2}{3}n_F \quad (1.27)$$

where n_F is the number of fermions in the fundamental representation of $SU(3)_c$. The contribution of the gluons, given by the first term, is positive. On the contrary, b_0 decreases due to the fermions loops. b_0 is positive if $n_F < \frac{33}{2}$, i.e. if there are at most 16 colored fermions. Consequently, the strong coupling constant decreases with the energy in the SM as illustrated on Fig. 1.1. At high energy, the quarks behave like free particles, they are asymptotically free. It also insures that perturbative computation is valid in QCD at high energy, but breaks down at low energy.

The non abelian structure of the group is necessary to have gauge bosons self-interactions as shown in Eq. (1.5). Consequently, abelian gauge theories like QED are not asymptotically free.

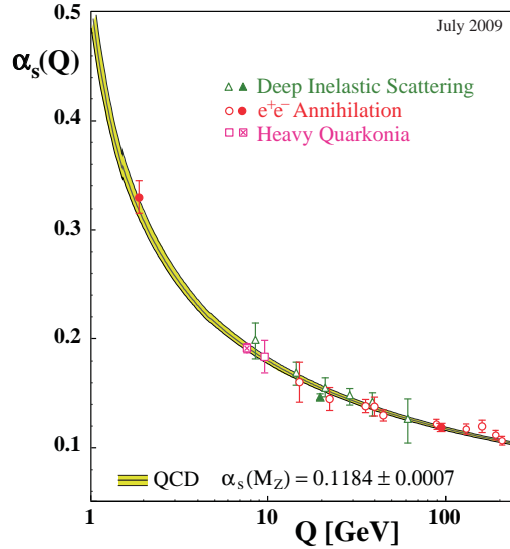


Figure 1.1: Running of the strong coupling constant [9].

1.2 Effective field theories

Many problems can be simplified by only using the relevant scale(s) of the studied process. The chemical properties of the hydrogen atom can be well described without knowing the details on how the quarks interact inside the proton. The proton can be considered as an elementary object because the binding energy of its constituents is much bigger than the energy of the orbiting electron. The separation of the different scales of the system is the key ingredient for effective theories.

Effective field theories are very useful in different areas. Predictive effective theories can be constructed for strongly coupled theories where perturbative expansion cannot be trusted anymore. The typical example is QCD at low energy which will be studied in Chap. 2. Heavy quark effective theory (HQET) has been also used for the strong interaction if the mesons contain one heavy quark. In addition, effective theories also provide a model independent approach to look for new physics in a bottom up way. The same effective theory can correspond to several high energy fundamental theories since it does not depend on all the details of the full theory. This is the cornerstone of Chap. 3.

In this section, the main ideas of effective field theories are introduced with the help of one of the most famous examples. The main properties relevant for the following chapters are then discussed. This introduction is based on Refs. [10–13] and more information can be found therein.

1.2.1 Fermi theory

In the early days of particle physics, Fermi proposed explaining the charged currents leading to β -decay by contact interactions, *i.e.* products of currents [14]. The Fermi effective Lagrangian is now written as

$$\mathcal{L}^{Fermi} = -\frac{G_F}{\sqrt{2}} J^\mu J_\mu^\dagger \quad (1.28)$$

where G_F is the Fermi constant. Since the Fermi constant has the dimension of the inverse of an energy squared, let us define the energy Λ_F such that

$$\frac{G_F}{\sqrt{2}} \equiv \frac{1}{\Lambda_F^2}. \quad (1.29)$$

The current in the Fermi Lagrangian can be split into the hadronic, J_μ^h , and the leptonic, J_μ^l , currents

$$J_\mu = J_\mu^h + J_\mu^l. \quad (1.30)$$

For simplicity, let us focus on lepton interactions where the current is defined by

$$J_\mu^l = \sum_l \bar{\nu}_l \gamma_\mu (1 - \gamma_5) l. \quad (1.31)$$

This effective Lagrangian could have been built from the symmetries of the SM only. Assuming that only the left-handed leptons are doublets under $SU(2)_L$ and that the interactions are flavor universal, one easily proves that Eq. (1.28) contains the only dimension-six operator with charged currents. However, the opposite way was followed historically. Charged currents were measured to be flavor universal. Parity violation of the weak interaction was discovered later and led to the V-A structure. The $SU(2)$ symmetry was then postulated and the existence of neutral currents predicted. Their discovery was one of the great success of what became later the SM.

From the effective Fermi Lagrangian, the decay width of the muon into an electron and two neutrinos is given by

$$\Gamma(\mu \rightarrow e \bar{\nu}_e \nu_\mu) \cong \frac{1}{96\pi^3} \frac{m_\mu^5}{\Lambda_F^4}. \quad (1.32)$$

The scale Λ_F , or equivalently G_F , can be extracted from the measured value of this decay

$$\Lambda_F \cong 348 \text{ GeV}. \quad (1.33)$$

The same result holds for the tau decay such that the Λ_F -independent ratio

$$\frac{\Gamma(\mu \rightarrow e \bar{\nu}_e \nu_\mu)}{\Gamma(\tau \rightarrow e \bar{\nu}_e \nu_\tau)} \cong \frac{m_\mu^5}{m_\tau^5} \approx 7.4 \cdot 10^{-7} \quad (1.34)$$

agrees with the experimental value. Similarly, several other processes like electron-neutrino diffusion can be now computed as well.

1.2.2 The expansion

The muon decay can also be computed starting from the SM Lagrangian. Since the momenta involved in this process are small compared to the mass of the W boson, the denominator of its propagator can be expanded as

$$\frac{1}{p^2 - M_W^2} = -\frac{1}{M_W^2} - \frac{p^2}{M_W^4} + \dots \quad (1.35)$$

Keeping only the first term, we obtain the same result as in Eq. (1.32) with the identification

$$\frac{g^2}{8} \frac{1}{M_W^2} = \frac{1}{\Lambda_F^2} = \frac{G_F}{\sqrt{2}}, \quad (1.36)$$

from which we extract the value of the Higgs vev as,

$$v = \left(\sqrt{2} G_F \right)^{-\frac{1}{2}} = 246 \text{ GeV}. \quad (1.37)$$

The effective Fermi theory is thus equivalent to the SM up to corrections of the order of $\frac{p^2}{M_W^2}$. The scale Λ_F is of the order of the mass of the heavy states in the fundamental theory.

The effective Lagrangian of Eq. (1.28) is in fact the first term of the same expansion in $\frac{1}{M_W^2}$ as in Eq. (1.35) applied to the full Lagrangian. The advantage is that the expansion on Lagrangian is done once for all in opposition to the expansion of the propagator which should be done for each amplitude. Momenta in an amplitude are equivalent to derivatives in the Lagrangian. Since each derivative increases the dimension of the operator by one unit, this operator should be suppressed by one extra power of the new physics scale Λ compared to the other operators. However, an effective Lagrangian is more than just an expansion in the number of derivatives. In general, each operator will be suppressed by Λ^{4-d} with d being the dimension of the operator. The suppression of an operator does not only increase with its number of derivatives but also with its fields content. This generalization to the fields is necessary if we want to keep gauge invariance because covariant derivatives and strength field tensors are sum of derivatives and vector fields. Moreover, this extension is necessary for the Fermi theory. Despite the lack of derivatives, Fermi Lagrangian is still suppressed by the square of the mass of the heavy particles, the W boson, because the operator is of dimension six.

An effective theory is thus nothing more than a Taylor expansion in the ratio of two scales. The convergence is warranted by the gap between the scales. As we saw in the previous example, the only remnants of the full theory at low energies are the symmetries and the values of the coupling constants. However, effective theories are still predictive even if we do not know the values of those coupling constants. In fact, the series can be truncated if the expansion parameter is small. Consequently, the Lagrangian only contains a finite number of free coefficients. The drawback of the truncation is that the predictions have errors. However, the errors are of the same order as the truncated piece of the Lagrangian.

The general rules for effective field theories can be stated as follows :

1. The dynamics at low energies does not depend on details of the dynamics at high energies.
2. Determine the relevant degrees of freedom at the scale of your process.
3. Build all the operators allowed by the symmetries of the theory up to the required precision knowing that each operator is suppressed by Λ^{4-d} with d being the dimension of the operator and Λ being the scale associated with the heavy particles of the fundamental theory.

1.2.3 Integrating out heavy degrees of freedom

It is not always possible to go (easily) from the fundamental to the effective theory. However, if the theory is perturbative, we can integrate out the heavy particles. The tree-level relations between the fundamental parameters and the effective couplings are then directly obtained without passing through amplitudes computation. This procedure is illustrated in the following for heavy bosons (spin 0 or 1). This choice of particles is motivated by their use in Chap 3. However, it can also be applied for fermions or tensors.

The generic renormalizable Lagrangian for a vector field is given by

$$\mathcal{L}^V = \text{kin. term} + M^2 V_\mu^\dagger V^\mu + \sum_i g_i V_\mu J_i^\mu + h.c. \quad (1.38)$$

where M^2 should be replaced by $\frac{M^2}{2}$ if the vector field is self-conjugate. The kinetic term can be neglected for a heavy vector. The Lagrange equation for V_μ^\dagger then implies

$$V^\mu = -\frac{1}{M^2} \sum_i g_i J_i^\mu. \quad (1.39)$$

After replacing V^μ according to Eq. (1.39), *i.e.* integrating out the heavy vector, the Lagrangian of Eq. (1.38) becomes

$$\mathcal{L}_{eff}^V = -\frac{(\sum_i g_i J_i^\mu)(\sum_i g_i J_i^\mu)^\dagger}{M^2}. \quad (1.40)$$

Using the definition of the leptonic current of Eq. (1.31), the Lagrangian in Eq. (1.3) implies $g_l = \frac{g}{2\sqrt{2}}$. Fermi's Lagrangian follows with the identification of Eq. (1.36).

Similarly, if the vector field is self-conjugate, we obtain

$$\mathcal{L}_{eff}^V = -\frac{(\sum_i g_i J_i^\mu + h.c.)^2}{2M^2}. \quad (1.41)$$

Finally, if the heavy degree of freedom is a scalar, the full Lagrangian is

$$\mathcal{L}^S = \text{kin. term} - M^2 \phi \phi^\dagger + \sum_i g_i \phi d_i + h.c.. \quad (1.42)$$

After integrating out this heavy scalar field, the Lagrangian becomes

$$\mathcal{L}_{eff}^S = \frac{(\sum_i g_i d_i) (\sum_i g_i d_i)^\dagger}{M^2}. \quad (1.43)$$

1.2.4 Scale hierarchy from spontaneously broken symmetries

Symmetries of the fundamental theory are often unbroken in the effective theory. However, broken global symmetry can also be helpful for effective field theories. If a global continuous symmetry is spontaneously broken, Goldstone theorem implies the existence of a massless particle, a Goldstone boson, for each broken generator. If the symmetry is only approximate, the particles are not massless but remain lighter than the fields associated with the unbroken generators. Consequently, their interactions can be well described by an effective Lagrangian. As we will see in Chap. 2, the light pseudoscalar mesons are an example of pseudo-Goldstone bosons. Their masses are truly below those of the scalar mesons, *i.e.* $\Lambda = 1 \text{ GeV}$.

Proof of the Goldstone theorem : We assume that the Lagrangian depends on several scalar fields ϕ^a and is invariant under a continuous global symmetry

$$\phi^a \rightarrow \phi^a + i \alpha G_{ab}^k \phi^b \quad (1.44)$$

where α is the expansion parameter and G^k are the generators of the group. Since the kinetic term is left unchanged by the symmetry, the potential should also be invariant,

$$V(\phi^a) = V(\phi^a + i \alpha G_{ab}^k \phi^b). \quad (1.45)$$

Since α is small,

$$G_{ab}^k \phi^b \frac{\partial}{\partial \phi^a} V(\phi) = 0. \quad (1.46)$$

Deriving respect to ϕ^c and evaluating this expression at $\phi = \phi_0$ where ϕ_0 is the minimum of the potential, we obtain

$$\left(\frac{\partial G_{ab}^k \phi^b(\phi)}{\partial \phi^c} \right)_{\phi=\phi_0} \left(\frac{\partial V(\phi)}{\partial \phi^a} \right)_{\phi=\phi_0} + \left(G_{ab}^k \phi^b \frac{\partial^2}{\partial \phi^a \partial \phi^c} V(\phi) \right)_{\phi=\phi_0} = 0. \quad (1.47)$$

The first term vanishes because ϕ_0 is the minimum. $G_{ab}^k \phi_0^b$ is non zero for the scalars which vev breaks the symmetry. Consequently, the second factor should also vanish. This factor is precisely one row of the scalar mass matrix. The fields associated with the spontaneously broken generators are thus massless.

1.2.5 Loops in effective field theories

If the expansion seems consistent at the tree-level, the validity of effective theories is questionable at the loop-level. The expansion may break down due to the large momenta in the loops. A generic effective Lagrangian can be written as

$$\mathcal{L} = \sum_{d,k} \frac{1}{\Lambda^{d-4}} c_k O_k^d \quad (1.48)$$

where d is the dimension of the operator. From this Lagrangian, we can compute the degree of divergence of an arbitrary amplitude. Only one-particle irreducible amplitudes, amplitudes that cannot be split into two by removing one propagator, need to be considered. All amplitudes can always be decomposed into products of irreducible ones.

In an amplitude, each vertex contribution goes like p^{d-e-i} where p is a generic label for the loop-momenta, d is the dimension of the operator from which the vertex comes from, e is the sum of the dimensions of the external legs and external momenta and i is the sum of the dimensions of the internal legs. If the diagram contains V vertices, their momenta dependence is given by p^{D-E-I} , where D , E and I are the sum of the d , e and i of each vertex. All those vertices need to be connected to form at least one-loop. To obtain exactly one-loop, we need V propagators. If the propagating particle is a fermion, adding its propagator gives a factor $\frac{1}{p}$ and I increases by 3. If the propagating particle is a boson, adding its propagator gives a factor $\frac{1}{p^2}$ and I increases by 2. The contribution of all propagators and vertices for a one-loop amplitude is thus given by p^{D-E-4V} . Each time a new propagator between two vertices (different or not) is added, one more loop is created. At the end, an amplitude with L loops goes

like³

$$\begin{aligned}
A(D, E, V, L) &\propto \left(\int d^4 p \right)^L p^{D-E-4V-4(L-1)} \\
&\sim \begin{cases} \Lambda^{D-E-4V+4} & \text{if } D - 4V \neq E - 4 \\ \log \left(\frac{\Lambda^2}{\mu^2} \right) & \text{if } D - 4V = E - 4 \end{cases} \quad (1.49)
\end{aligned}$$

where μ is the typical scale of the process. Each vertex coefficient brings a factor $\frac{1}{\Lambda^{d-4}}$. Consequently, the amplitude goes like Λ^{4-E} if $D - 4V \neq E - 4$ or like $\Lambda^{4-E} \log \left(\frac{\Lambda^2}{\mu^2} \right)$ otherwise. The dimensions of the operators that are corrected by this amplitude are at least equal to E . As a consequence, the loop corrections can be written as

$$\begin{aligned}
c_k \frac{1}{\Lambda^{d-4}} O_k^d &\rightarrow \frac{1}{\Lambda^{d-4}} \left(c_k + \left(\frac{w}{(4\pi)^2} + \frac{x}{(4\pi)^4} + \dots \right) \log \left(\frac{\Lambda^2}{\mu^2} \right) \right. \\
&\quad \left. + \left(\frac{y}{(4\pi)^2} + \frac{z}{(4\pi)^4} + \dots \right) + \mathcal{O}(\Lambda^{-2}) \right) O_k^d \quad (1.50)
\end{aligned}$$

where w , x , y and z are polynomials of the c_k and of the gauge couplings. If none of the c_k or the gauge couplings are large, the Lagrangian is perturbative and loop corrections are small. To sum up, the loops do not break the expansion in $\frac{1}{\Lambda}$ but renormalize the couplings and the fields. This result is known as the decoupling theorem [15]. In fact, all divergences from the $\mathcal{O} \left(\frac{1}{\Lambda^n} \right)$ amplitudes can be absorbed into the operators of dimension $n + 4$ as it can be seen from Eq. (1.49). The effective theories are usually called non renormalizable theories since an infinite number of counter terms are needed to absorb the divergences. However, at each order in the expansion, only a finite number of counter terms are needed. Consequently, effective theories are renormalizable not in the usual sense but order by order.

The logarithmic divergences in Eq. (1.50) can be absorbed in the definition of c_k at one scale μ_R only. Consequently, they also induce a physical running for the coefficients. For strongly coupled theories, those logarithmic divergences can generate large anomalous dimensions,

$$\left(1 + A \log \left(\frac{\Lambda^2}{\mu^2} \right) \right) = e^{A \log \left(\frac{\Lambda^2}{\mu^2} \right)} = \left(\frac{\Lambda^2}{\mu^2} \right)^A. \quad (1.51)$$

³If $D - E$ is odd, the integral of the largest power of p vanishes. Consequently, D should be replaced by $D - 1$ in the second line.

In this case, the usual power counting breaks down. However, the degrees of freedom at low energy are not anymore the elementary particles of the fundamental theory but bound states. Those anomalous dimensions are welcome in technicolor to alleviate the tension between the SM fermion masses and flavor violation. Technifermion anti-technifermion bound states have an anomalous dimension -2 (an example of walking technicolor model can be found in ref. [16]). The mass terms for the SM fermion originate from dimension-four operators with two SM fermions and two technifermions. On the contrary, flavor violation is induced by dimension-six operators with four SM fermions and is thus suppressed by the square of the heavy particles scale.

From Eq. (1.50), we can see that scalar masses receive corrections proportional to Λ because the dimension of the associated operator is two. Consequently, scalar masses and, in particular, the Higgs mass are expected to be of the order of the cut-off of the theory. New physics should thus appear at the LHC to avoid fine tuning. Another way out is to protect the Higgs mass by a symmetry. As we saw, its mass would remain small if the Higgs is a pseudo-Goldstone boson. This issue only happens for scalar. On the contrary, the fermions Dirac masses diverge at most logarithmically despite that they originate from a dimension-three operator. In fact, they are protected by chiral symmetry in gauge theories like the SM. Namely, the Lagrangian up to the mass term is invariant under a rephasing of either the left- or right-handed fermions since all the terms of the Lagrangian except the mass term contain only one of the two chiralities. As a consequence, the corrections to the fermion masses are proportional to the masses themselves⁴.

1.3 Top scenery

Top physics has already reached a high-level of sophistication and we already know a lot from the Tevatron which sets strong constraints on *top-philic* new physics [17–20]. Until recently, Tevatron was the only source of top quarks. However, LHC finally produced its first top quarks [21–24] in 2010 and started this year to get the first precise measurements [25].

This short review is not exhaustive but only focuses on the measurements needed in Chap. 4. The two experiments of the Tevatron actually measured several other important quantities like the top mass, single top cross-section and so on.

⁴In supersymmetry, the corrections to the scalar masses diverge also logarithmically since fermions and scalars belong to the same supermultiplets.

1.3.1 $t\bar{t}$ total cross-section and invariant mass distribution

Total $t\bar{t}$ cross-section was measured at the Tevatron and already at the LHC with a precision comparable to the theoretical one. The most precise measurement at the Tevatron is the CDF combination of all channel at 4.6 fb^{-1} [26],

$$\sigma_{\text{obs}}^{1.96 \text{ TeV}} = 7.5 \pm 0.31(\text{stat}) \pm 0.34(\text{syst}) \pm 0.15(\text{lumi}) \text{ pb.} \quad (1.52)$$

Their analysis combines both dileptonic, semileptonic and fully hadronic channels. CMS combination of the semileptonic and dileptonic channels with 36 pb^{-1} [25],

$$\sigma_{\text{obs}}^{7 \text{ TeV}} = 158 \pm 10(\text{stat}) \pm 15(\text{syst}) \pm 6(\text{lumi}) \text{ pb,} \quad (1.53)$$

is about one sigma below the Atlas one with 35 pb^{-1} [27]

$$\sigma_{\text{obs}}^{7 \text{ TeV}} = 180 \pm 9(\text{stat}) \pm 15(\text{syst}) \pm 6(\text{lumi}) \text{ pb.} \quad (1.54)$$

All those experimental results agree with the NLO+NLL predictions [28] for the SM cross-sections at the Tevatron ($m_t = 174.3 \text{ GeV}$)

$$\sigma_{\text{th}}^{1.96 \text{ TeV}} = 6.87_{-0.48}^{+0.26}(\text{scale})_{-0.33}^{+0.47}(\text{pdf}) \text{ pb,} \quad (1.55)$$

and at the LHC

$$\sigma_{\text{th}}^{7 \text{ TeV}} = 146_{-13}^{+12}(\text{scale})_{-11}^{+11}(\text{pdf}) \text{ pb.} \quad (1.56)$$

The experimental and theoretical results for the total $t\bar{t}$ cross-sections are summarized in Fig. 1.2.

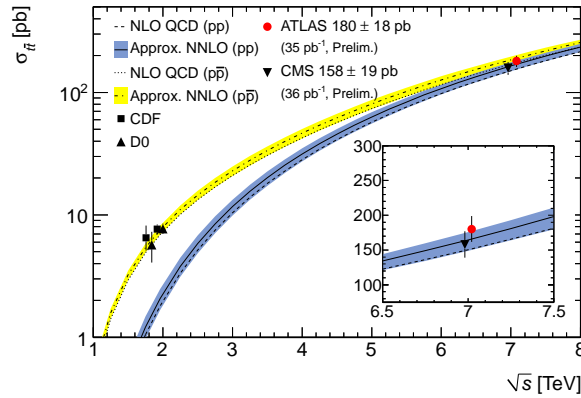


Figure 1.2: Summary of the $t\bar{t}$ cross-sections measurements and SM predictions [27].

The first measurement of the $t\bar{t}$ invariant mass distribution was done at CDF [29] with 2.7 fb^{-1} in the semileptonic channel and showed no deviation from the SM. The updated measurement with 4.8 fb^{-1} [30] confirms this conclusion (see Fig. 1.3) as well as D0 analysis with 3.6 fb^{-1} [31]. At the LHC, CMS has already started to constrain the presence of new resonances with the $t\bar{t}$ invariant mass distribution [32].

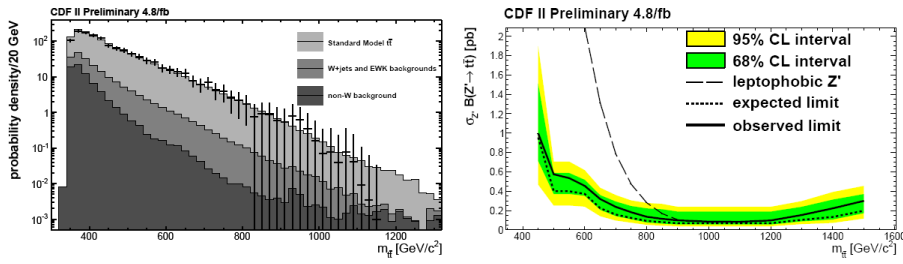


Figure 1.3: $t\bar{t}$ invariant mass distribution measurement by CDF [30] and the corresponding limit on narrow resonances.

1.3.2 Forward-backward Asymmetry

The forward-backward asymmetry in $t\bar{t}$ production is defined as

$$A_{FB} \equiv \frac{\sigma(\cos\theta_t > 0) - \sigma(\cos\theta_t < 0)}{\sigma(\cos\theta_t > 0) + \sigma(\cos\theta_t < 0)} \quad (1.57)$$

where θ_t is the angle between the momenta of the incoming parton in the proton and the outgoing top quark in the laboratory or $t\bar{t}$ rest frame. In the Standard Model, there are no preferred directions for the top and antitop quarks at the lowest order. A positive asymmetry is generated at NLO, *i.e.*, the top quark prefers to go in the direction of the incoming quark and the antitop quark in the direction of the incoming antiquark [33]:

$$A_{FB}^{\text{SM,lab}} = 0.05 \pm 0.015 \quad (1.58)$$

in the laboratory frame. The recent measurements of A_{FB} at the Tevatron show an intriguing deviation from the SM prediction [34–36]. The most precise CDF result (semileptonic channel with 5.3 fb^{-1}) [37]

$$A_{FB}^{\text{EXP,lab}} = 0.15 \pm 0.05(\text{stat}) \pm 0.024(\text{syst}), \quad (1.59)$$

is larger by about 2σ than the SM prediction. Moreover, the discrepancy seems to increase with the energy. As a matter of fact, CDF measurements above 450 GeV [38]

$$A_{FB}^{\text{EXP},t\bar{t}}(M_{t\bar{t}} \geq 450 \text{ GeV}) = 0.475 \pm 0.114 \quad (1.60)$$

$$A_{FB}^{\text{EXP},t\bar{t}}(M_{t\bar{t}} < 450 \text{ GeV}) = -0.116 \pm 0.153 \quad (1.61)$$

is more than 3σ away from the SM prediction

$$A_{FB}^{\text{SM},t\bar{t}}(M_{t\bar{t}} \geq 450 \text{ GeV}) = 0.088 \pm 0.013 \quad (1.62)$$

$$A_{FB}^{\text{SM},t\bar{t}}(M_{t\bar{t}} < 450 \text{ GeV}) = 0.040 \pm 0.006 \quad (1.63)$$

while the low mass asymmetry measurement is only about 1σ below the theoretical value. The bins with a measured asymmetry below and above the SM predictions are split by the cut at 450 GeV as shown on Fig. 1.4. Contrary to the total forward-backward asymmetry, the enhancement at high invariant mass is not observed by D0 [39]. The excess on the total asymmetry is also confirmed in the dileptonic channel

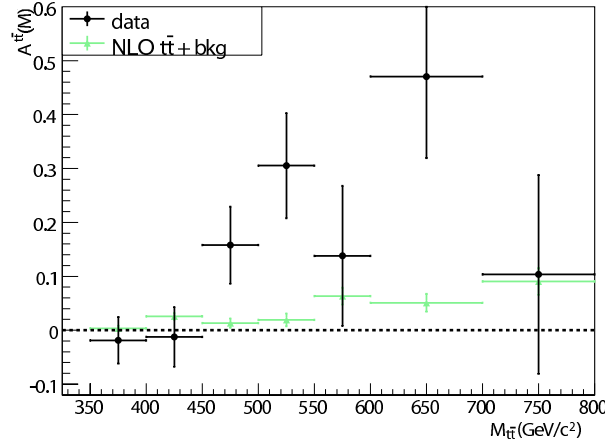


Figure 1.4: Forward-backward asymmetry as a function of the invariant mass from CDF [38].

($t\bar{t}$ rest frame with 5.1 fb^{-1}) [40]:

$$A_{FB}^{\text{EXP},t\bar{t}} = 0.42 \pm 0.15(\text{stat}) \pm 0.05(\text{syst}) \quad (1.64)$$

to be compared to $A_{FB}^{\text{SM},t\bar{t}} = 0.06 \pm 0.01$ from QCD.

At the LHC, CMS rather uses the charge asymmetry as defined by [41]

$$A_C = \frac{N^+ - N^-}{N^+ + N^-} \quad (1.65)$$

where N^+ and N^- are the numbers of events with positive or negative values of $|\eta_t| - |\eta_{\bar{t}}|$ respectively. With 1.09fb^{-1} , they observe

$$A_C^{\text{EXP}} = -0.016 \pm 0.030(\text{stat})_{-0.019}^{+0.010}(\text{syst}) \quad (1.66)$$

consistently with the SM prediction

$$A_C^{\text{SM}} = 0.0130 \pm 0.0011. \quad (1.67)$$

1.3.3 Spin correlations

Due to the V-A structure of the weak interaction, the directions of the decay products are correlated with the direction of the spin of the weakly decaying fermion, the top quark in our case,

$$\frac{\Gamma_{\uparrow}}{\Gamma} = \frac{1 + A_i \cos \theta}{2}, \quad \frac{\Gamma_{\downarrow}}{\Gamma} = \frac{1 - A_i \cos \theta}{2}, \quad (1.68)$$

where θ is the angle between the decay product i and the spin of the top quark, the arrows denote the different projections of the top spin, A_i is the correlation coefficient for the decay product i . Numerically, $A_l = A_d = 1$, $A_u = A_{\nu} = -0.31$ and $A_b = -0.41$ [42, 43]. Leptons and down type quarks have a maximal spin analysing power. However, light down type quarks can hardly be distinguished from light up type quarks. Their correlation is then effectively smaller. Despite existing for all the fermions, this correlation is destroyed by hadronization for all quarks but top quark. In fact, the top is so heavy that it decays before hadronization. Consequently, the general form of the normalized differential $t\bar{t}$ cross-section is given by

$$\frac{1}{\sigma} \frac{d\sigma}{d \cos \theta_+ d \cos \theta_-} = \frac{1}{4} (1 + C A_i A_j \cos \theta_+ \cos \theta_- + b_+ A_i \cos \theta_+ + b_- A_j \cos \theta_-), \quad (1.69)$$

where θ_+ (θ_-) is the angle between the particle i (j) resulting from the top (antitop) decay in the top (antitop) rest frame and some reference direction \vec{a} (\vec{b}). For dileptonic events, the differential cross-section reduces to

$$\frac{1}{\sigma} \frac{d\sigma}{d \cos \theta_+ d \cos \theta_-} = \frac{1}{4} (1 + C \cos \theta_+ \cos \theta_- + b_+ \cos \theta_+ + b_- \cos \theta_-). \quad (1.70)$$

D0 measurement (5.4 fb^{-1}) in the dileptonic channel from the differential distribution in the beam basis [44], $\vec{a} = -\vec{b} = \vec{k}_1$ where \vec{k}_1 is the proton momentum in the $t\bar{t}$ rest frame,

$$C = -0.1 \pm 0.45 \quad (1.71)$$

is in agreement with the SM NLO prediction $C = -0.777^{+0.042}_{-0.027}$ [45]. However, this result is also in agreement with the no correlation hypothesis, $C = 0$. Last measurement with the same data set but based on matrix element method,

$$C = -0.57 \pm 0.31 \quad (1.72)$$

excludes the no correlation hypothesis at 97.7% C.L.. In this case, the fraction of events with no correlation and with a SM correlation ($C = -0.777$) is fitted. As a consequence, C is assumed to vary only between the SM value and zero.

CDF also measured spin correlation in $t\bar{t}$ but in the helicity basis, *i.e.* $\vec{a} = -\vec{b} = \vec{p}_1$ where \vec{p}_1 is the top momentum in the $t\bar{t}$ rest frame. They obtain

$$C = 0.50 \pm 0.60 \text{ (stat)} \pm 0.16 \text{ (syst)} \quad (1.73)$$

in the semi-leptonic channel with 4.3 fb^{-1} (~ 1000 events) [46]. With 15 fb^{-1} , the statistical error is expected to go down to 0.26.

1.3.4 Beyond $t\bar{t}$

Same sign top pair production

Same sign top pair production can be probed in same sign dilepton events. Moreover, the events should have a large missing transverse energy and should contain b-jets. Consequently, the background is quite low. The expected background is 2.1 ± 1.8 events at the Tevatron with 2 fb^{-1} . The 3 events observed by CDF were used to constrain the coupling of light ($\leq 300 \text{ GeV}$) flavor violating scalars to be at most of order one [47]⁵. Despite the quite large cross-section ($\sim 1 \text{ pb}$) of this model for $tt + \bar{t}\bar{t}$, the low acceptance (0.5%) strongly reduces the sensitivity.

Recently, CDF updated these results with a new data set of 6.1 fb^{-1} . Again, the number of observed events (27) is in agreement with the expected background (28 ± 7.5).

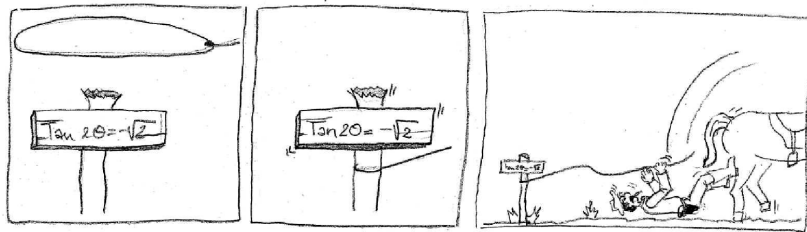
⁵The model will be discussed in Sect. 3.2.2

Dijets

If the new physics does not only affect the top sector, the dijets spectrum might show deviation from the QCD prediction. In fact, the dijet invariant mass distribution puts strong constraints on many models [48]. Moreover, CMS used dijet angular distributions to constrain four-fermion operators [49]. However, a flavor structure is needed to go from the dijet production to the top sector.

Chapter 2

A Theoretical determination of the $\eta - \eta'$ mixing



Based on

Degrade, C. and Gerard, J. -M., "A theoretical determination of the eta-eta' mixing", *JHEP*, vol. 05, p. 043, 0901.2860.

A vast literature on phenomenological descriptions of the $\eta - \eta'$ system was published in the past ten years [50, 51]. Yet, the $\eta - \eta'$ mixing angle alone is more than an effective parameter to be extracted from low energy data. Its peculiar value may actually shed some light on the non-perturbative dynamics of the fundamental QCD theory and in particular on the axial $U(1)$ anomaly. Needless to recall here why the subsequent parity (P) and time-reversal (T) violations constitute a major puzzle in the Standard Model for electroweak and strong interactions (see, for example, [52]).

To link this axial anomaly with the observed mass spectrum for the pseudoscalar meson nonet, alternative paths based on the chiral perturbation theory or the large

number of colours limit were proposed. Among them, the chiral perturbation theory at leading order in p^2 and $1/N_c$ is efficient once the typical 20% corrections expected from the flavour symmetry breaking are duly acknowledged.

Within this rather simple framework, the η and η' masses are functions of the mixing angle θ . In particular, the $\eta - \eta'$ mass ratio is not fixed by the theory but can only be optimized with respect to its experimental value for $\theta \approx -27^\circ$. However, the corrections requisite to reproduce the measured value of this ratio raise the question of the systematic expansion to adopt. It appears that including the next to leading order in p^2 in the large N_c limit is quite predictive and compatible with the data. Consequently, this approach requires the $1/N_c$ -suppressed one-loop contributions to be small. In this chapter, we emphasize that the optimal value of the $\eta - \eta'$ mixing angle at leading order turns out to consistently damp out the quadratically divergent one-loop corrections to the $\eta - \eta'$ inverse propagator matrix and the $\eta' \rightarrow \eta\pi\pi$ decay amplitude.

2.1 An effective theory at leading order in p^2 and $\frac{1}{N_c}$

If n quark flavours are massless, the fundamental Lagrangian of QCD displays a global $U(n)_L \otimes U(n)_R$ invariance. The symmetry is broken by the mass matrix of the quarks m and is thus only approximate. However, it can be restored if m is treated like a spurion transforming as $m \rightarrow g_L m g_R^\dagger$. In the large N_c limit, N_c being the number of colours, the effective Lagrangian which features this chiral symmetry at lowest order in p^2 reads [53]

$$\mathcal{L}^{(p^2,0)} = \frac{f^2}{8} [\langle \partial_\mu U \partial^\mu U^\dagger \rangle + r \langle m U^\dagger + U m^\dagger \rangle] \quad (2.1)$$

where U is a n -by- n unitary matrix transforming as $U \rightarrow g_L U g_R^\dagger$. The determinant of m is assumed to be real to ensure P and T invariance. In Eq.(2.1), the parameters with dimensions of mass scale respectively as¹

$$f \propto N_c^{1/2}, \quad r \propto N_c^0. \quad (2.2)$$

In the large N_c limit, $U(n)_L \otimes U(n)_R$ has to be spontaneously broken into the maximal vectorial subgroup $U(n)_V$ if $n \geq 3$ [54]. Consequently, U is a unitary field which

¹One trace at the effective level corresponds to one-loop at the fundamental level which scales like N_c .

can be expanded around its vacuum expectation value as a function of the Goldstone bosons,

$$U = \mathbb{1} + i\sqrt{2}\frac{\pi}{f} - \frac{\pi^2}{f^2} + \mathcal{O}\left(\frac{\pi^3}{f^3}\right). \quad (2.3)$$

In the case of three light flavours, the Goldstone bosons nonet can be written as

$$\pi = \begin{pmatrix} \pi^3 + \frac{1}{\sqrt{3}}\eta^8 + \sqrt{\frac{2}{3}}\eta^0 & \sqrt{2}\pi^+ & \sqrt{2}K^+ \\ \sqrt{2}\pi^- & -\pi^3 + \frac{1}{\sqrt{3}}\eta^8 + \sqrt{\frac{2}{3}}\eta^0 & \sqrt{2}K^0 \\ \sqrt{2}K^- & \sqrt{2}\bar{K}^0 & -\frac{2}{\sqrt{3}}\eta^8 + \sqrt{\frac{2}{3}}\eta^0 \end{pmatrix} \quad (2.4)$$

and the masses of the pseudoscalars can be easily extracted once m is diagonalized. Working from now in the isospin limit $m_u = m_d = \tilde{m}$, we obtain

$$m_\pi^2 = r\tilde{m} \quad (2.5)$$

$$m_K^2 = \frac{r}{2}(\tilde{m} + m_s) \quad (2.6)$$

and

$$m_{8-0}^2 = \frac{1}{3} \begin{pmatrix} 4m_K^2 - m_\pi^2 & -2\sqrt{2}(m_K^2 - m_\pi^2) \\ -2\sqrt{2}(m_K^2 - m_\pi^2) & 2m_K^2 + m_\pi^2 \end{pmatrix} \quad (2.7)$$

with the octet-singlet flavour basis conventionally characterized by the amount of strange/non-strange quarks in the meson wave function

$$\eta^8 \sim \frac{1}{\sqrt{6}}(u\bar{u} + d\bar{d} - 2s\bar{s}) \quad (2.8)$$

$$\eta^0 \sim \frac{1}{\sqrt{3}}(u\bar{u} + d\bar{d} + s\bar{s}). \quad (2.9)$$

At this level, the masses of the physical pseudoscalar fields

$$\begin{pmatrix} \eta \\ \eta' \end{pmatrix} = \begin{pmatrix} \cos\theta & -\sin\theta \\ \sin\theta & \cos\theta \end{pmatrix} \begin{pmatrix} \eta^8 \\ \eta^0 \end{pmatrix} \quad (2.10)$$

are only functions of the π and K ones and vanish in the chiral limit $\tilde{m} = m_s = 0$. However, the measured mass of the η' around 1 GeV tells us that the axial $U(1)$ is broken by the dynamics of QCD itself [55]. In the limit of a large number of colours

within chiral perturbation, this explicit breaking is implemented through the one and only term [53]

$$\mathcal{L}(p^0, 1/N_c) = \frac{f^2}{8} \frac{m_0^2}{4N_c} \langle \ln U - \ln U^\dagger \rangle^2 = -\frac{1}{2} m_0^2 \eta_0^2 + \mathcal{O}(\pi^4) \quad (2.11)$$

which is $1/N_c$ -suppressed but p^0 -enhanced with regard to the effective Lagrangian (2.1). Accordingly, the $\eta_0 - \eta_0$ element m_{00}^2 of the mass matrix (2.7) is corrected by the parameter m_0^2 so that the η , η' masses are not anymore fixed in terms of the π and K masses but are functions of the mixing angle θ , as displayed in Fig.2.1:

$$m_\eta^2 = \frac{1}{3} \left[4m_K^2 - m_\pi^2 + 2\sqrt{2} (m_K^2 - m_\pi^2) \tan \theta \right] \quad (2.12)$$

$$m_{\eta'}^2 = \frac{1}{3} \left[4m_K^2 - m_\pi^2 - 2\sqrt{2} (m_K^2 - m_\pi^2) \cot \theta \right]. \quad (2.13)$$

The resulting relation between physical quantities defined at lowest order

$$\tan^2 \theta = \frac{m_\eta^2 - \frac{1}{3} (4m_K^2 - m_\pi^2)}{\frac{1}{3} (4m_K^2 - m_\pi^2) - m_{\eta'}^2} \quad (|\theta| = 11.4^\circ) \quad (2.14)$$

is analogous to

$$\tan^2 \theta_W = \frac{m_Z^2 - m_W^2}{m_W^2 - m_\gamma^2} \quad (|\theta_W| = 28.2^\circ) \quad (2.15)$$

where the mixing angles have been obtained using the physical masses. In other words, the Gell-Mann-Okubo (GMO) mass relation $m_{88}^2 = \frac{1}{3} (4m_K^2 - m_\pi^2)$ in the $\eta_8 - \eta_0$ mass matrix (2.7) plays here the role of the isospin mass relation $m_{W_3}^2 = m_{W^\pm}^2$ in the $W_3 - B_0$ mass matrix of the Standard Model for electroweak interactions. The latter relation is known to be invariant under the unbroken custodial $SU(2)_V$ of the Higgs potential; the former is invariant under the unbroken vectorial $SU(2)_I \otimes U(1)_Y$ since the quark mass matrix m in Eq.(2.1) transforms at most as a singlet and an octet of $SU(3)_V$. A breaking of the GMO relation for m_{88}^2 would require $\mathcal{O}(p^4, 0)$ terms like $\langle m U^\dagger m U^\dagger \rangle$ with $m \otimes m$ also transforming as a $\underline{27}$ under the vectorial flavour group.

Surprisingly, even with the additional parameter m_0^2 , the masses of η and η' cannot be fitted simultaneously [56]. Taking away m_K^2 from Eqs.(2.12-2.13), we easily obtain

$$\begin{aligned} \frac{m_\eta^2 - m_\pi^2}{m_{\eta'}^2 - m_\pi^2} &= \tan(2\theta_{th} - \theta) \tan \theta \quad \left(\tan 2\theta_{th} \equiv -\sqrt{2} \right) \\ &\leq \tan^2 \theta_{th} = 2 - \sqrt{3}. \end{aligned} \quad (2.16)$$

In the safe $m_\pi^2 \rightarrow 0$ limit, the resulting upper bound of 0.27 for the $\eta - \eta'$ squared mass ratio is clearly at variance with the corresponding experimental value of about 0.33.

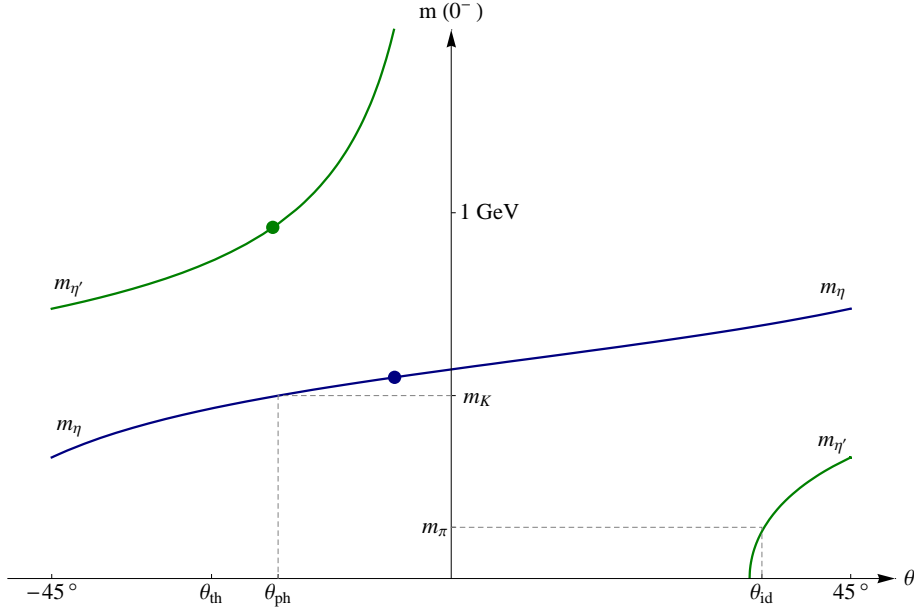


Figure 2.1: The η and η' masses as a function of their mixing angle from Eqs (2.12) and (2.13). We choose to work with $\theta \in [-\frac{\pi}{4}, +\frac{\pi}{4}]$ to avoid the renaming $\eta \rightarrow \eta'$, $\eta' \rightarrow -\eta$ at $\theta = -\frac{\pi}{4}$. If $m_{\pi,K}$ are fixed at their experimental values, the measured η and η' masses denoted by dots cannot simultaneously be reproduced at lowest order.

Mass corrections of about 20%, as requested by Eq.(2.16) to reproduce the observed $\eta - \eta'$ spectrum, drastically change the absolute value of the mixing angle derived in Eq.(2.14). In fact, the physical mass of the η and the octet mass m_{88} turn out to be numerically close, within a few percent. Therefore, any departure of lowest order η mass from its physical value is enough to produce a major modification of the angle θ extracted with the help of Eq.(2.12), as illustrated in Fig.2.1. So, a determination of the mixing angle at lowest order is sensible only if its value is stable with regard to $1/N_c$ and chiral corrections. In this respect, any enlarged symmetry beyond the custodial one is welcome to tame the quantum corrections. For example, a parity-conserving local $SU(3)_L \otimes SU(3)_R$ extension of the $SU(2)_L \otimes U(1)_Y$ electroweak

gauge symmetry [57] covers the custodial $SU(2)_V$ and would imply

$$\tan \theta_W = -\frac{1}{\sqrt{3}} \quad (\theta_W = -30^\circ) \quad (2.17)$$

in pretty good agreement with the on-shell absolute value of the weak mixing angle already introduced in Eq.(2.15).

In Eq.(2.1), the canonical kinetic term for the π field has a global $SO(9)$ invariance. Both the vectorial $SU(3)$ -breaking in Eq.(2.1) and the axial $U(1)$ -breaking in Eq.(2.11) already violate this symmetry at the level of the terms quadratic in the meson fields. Yet, for particular values of the angle θ , remnants of $SO(9)$ may survive at this level; they correspond to the two mass degeneracies displayed with dashes in Fig.2.1:

- If $\theta = \theta_{id}$ with

$$\tan \theta_{id} \equiv \frac{1}{\sqrt{2}} \quad (\theta_{id} = +35.3^\circ), \quad (2.18)$$

the physical $\eta' \sim \frac{1}{\sqrt{2}}(u\bar{u} + d\bar{d})$ is degenerate in mass with the pions [58] while $\eta \sim -s\bar{s}$. Note that the negative value $\theta_{id} = -54.7^\circ$ corresponding to the other convention with the $s\bar{s}$ component singled out, namely $\eta \sim \frac{1}{\sqrt{2}}(u\bar{u} + d\bar{d})$ and $\eta' \sim +s\bar{s}$, is outside the interval $[-\frac{\pi}{4}, +\frac{\pi}{4}]$ (see Fig.2.1). The ideal mixing obtained from Eq.(2.7), *i.e.*, for $m_0^2 = 0$, is relevant for the vector meson mass spectrum on which the axial $U(1)$ anomaly has no effect, but totally unrealistic for the pseudoscalar one.

- If $\theta = \theta_{ph}$ with

$$\tan \theta_{ph} \equiv \frac{-1}{2\sqrt{2}} \quad (\theta_{ph} = -19.5^\circ), \quad (2.19)$$

the physical $\eta \sim \frac{1}{\sqrt{3}}(u\bar{u} + d\bar{d} - s\bar{s})$ is degenerate in mass with the kaons while $\eta' \sim \frac{1}{\sqrt{6}}(u\bar{u} + d\bar{d} + 2s\bar{s})$. Here, this sensible value for the mixing angle has been called phenomenological since it was extensively used to study hadronic B decays and, in particular, to explain the striking suppression of $B \rightarrow K\eta$ with respect to $B \rightarrow K\eta'$ [59] if penguin diagrams dominate these processes [60]. It is also quite popular because the associated quark components are easy to remember and to handle in a phenomenological quark-diagram description of the decay amplitudes according to their $SU(3)$ properties.

We have no simple mass degeneracy for the case of θ_{th} already introduced in Eq.(2.16) but note that the three angles of peculiar interest are related through

$$\tan 2\theta_{th} = \tan(\theta_{ph} - \theta_{id}) \quad (\theta_{th} = -27.4^\circ) \quad (2.20)$$

with, quite incidentally, $\theta_{th} \approx \theta_W$ if the weak mixing angle turns out to be negative as predicted by some unification theory.

With respect to possible enlarged symmetries covering the custodial $SU(2)_I \otimes U(1)_Y$, we observe that the mass degeneracies $m_{\eta'} = m_\pi$ and $m_\eta = m_K$ correspond to the breaking patterns $SO(9) \rightarrow SO(4) \otimes SO(4)$ and $SO(9) \rightarrow SO(3) \otimes SO(5)$, respectively. These patterns for θ_{id} and θ_{ph} can be understood from the fact that $SO(9)$ group admits $SU(2) \otimes SU(2) \otimes Sp(4)$ or, equivalently, $SO(4) \otimes SO(5)$ as a maximal subgroup [61]. However, such enlarged symmetries are explicitly broken at the level of the full effective theory expressed in terms of the $U(\pi)$ field and thus accidental. Consequently, the finite value of the θ_{id} and θ_{ph} mixing angles should not be protected against (quadratically) divergent quantum corrections. The fact that the relations (2.18) and (2.19) are not natural can easily be confirmed through the following one-loop computation.

2.2 One-loop corrections to the $\eta - \eta'$ inverse propagator matrix

The unification value (2.17) for the observable weak mixing angle θ_W can most easily be derived by requiring the one-loop fermionic contribution to the $Z - \gamma$ mixing diagram to be finite [62]. In the same spirit, let us impose the cancellation of the quadratically divergent one-loop corrections to the $\eta - \eta'$ mixing angle θ .

In order to compute these corrections, we need now to expand U up to the order π^4 ,

$$U = \mathbb{1} + \sum_{k=1}^{\infty} a_k \left(i\sqrt{2}\frac{\pi}{f} \right)^k. \quad (2.21)$$

The parameter a_1 may be absorbed into the definition of f while the even coefficients are fixed by the unitarity condition [63]

$$a_1 = 1, \quad a_2 = \frac{1}{2}, \quad a_3 = b, \quad a_4 = b - \frac{1}{8}, \quad \dots \quad (2.22)$$

with b an arbitrary parameter. For $b = \frac{1}{6}$, we recover the standard form

$$U = \exp\left(i \frac{\sqrt{2}\pi}{f}\right) \quad (2.23)$$

also suited for an octet of pseudoscalars (for a review, see [64]). But as shown in ref. [65, 66], any other value of b gives rise to the same T matrix when all external lines are put on the mass shell. Yet, one-loop corrections from the kinetic part of the Lagrangian (2.1) induce in principle a momentum-dependent $\eta - \eta'$ mixing term which thus has to be taken off-shell. Again by analogy with the scale dependent $Z^0 - \gamma$ mixing induced at one-loop in the Standard Model, let us therefore introduce the propagator formalism [67, 68].

If we denote by $-iA_{\chi_1\chi_2}(p^2)$ with $\chi_1, \chi_2 = \eta, \eta'$ the one-loop contributions to the corresponding two point functions, the inverse propagator matrix Σ can be parametrized as follows

$$\begin{aligned} \Sigma_{\eta\eta} &= (1 + Z_\eta)(p^2 - m_\eta^2) + \delta m_\eta^2 - A_{\eta\eta}(p^2) \\ \Sigma_{\eta'\eta'} &= (1 + Z_{\eta'})(p^2 - m_{\eta'}^2) + \delta m_{\eta'}^2 - A_{\eta'\eta'}(p^2) \\ \Sigma_{\eta\eta'} &= \delta m_{\eta\eta'}^2 - A_{\eta\eta'}(p^2). \end{aligned} \quad (2.24)$$

The last relation in Eq.(2.24) takes into account the fact that η and η' are decoupled at tree-level, but leaves open the possibility for the one-loop induced mixing to depend on p^2 . Imposing the normalization of the kinetic part of $\Sigma_{\chi_i\chi_i}$ to be canonical and the physical masses m_{χ_i} to be the poles of the propagators, we identify

$$Z_{\chi_i} = A'_{\chi_i\chi_i}(m_{\chi_i}^2) \quad (2.25)$$

and

$$\delta m_{\chi_i}^2 = A_{\chi_i\chi_i}(m_{\chi_i}^2) \quad (2.26)$$

where the prime denotes the derivative with respect to p^2 . From a one-loop computation, we obtain the following quadratic dependences on the ultraviolet momentum cut-off Λ :

$$\begin{aligned} Z_\eta &= 3[(3 - 20b) + (4b - 1)\cos 2\theta] \frac{\Lambda^2}{(4\pi f)^2} \\ Z_{\eta'} &= 3[(3 - 20b) - (4b - 1)\cos 2\theta] \frac{\Lambda^2}{(4\pi f)^2} \end{aligned} \quad (2.27)$$

and

$$\begin{aligned}\delta(m_\eta^2 + m_{\eta'}^2) &= -2(2m_K^2 + m_\pi^2) \frac{\Lambda^2}{(4\pi f)^2} \\ \delta(m_\eta^2 m_{\eta'}^2) &= -6m_\pi^2(2m_K^2 - m_\pi^2) \frac{\Lambda^2}{(4\pi f)^2}\end{aligned}\quad (2.28)$$

with

$$\begin{aligned}A_{\eta\eta'}(p^2) &= \left\{ [3(4b-1)p^2 + 2(1-8b)m_K^2 + 2(2b-1)m_\pi^2] \sin 2\theta \right. \\ &\quad \left. + 4\sqrt{2}(2b-1)(m_K^2 - m_\pi^2) \cos 2\theta \right\} \frac{\Lambda^2}{(4\pi f)^2}.\end{aligned}\quad (2.29)$$

Here, the pseudoscalar masses $m_{K,\pi}$ and the mixing angle θ are parameters associated with the lowest order Lagrangian defined by Eqs (2.1) and (2.11). In particular, m_0^2 has been taken away with the help of the relation

$$m_0^2 = \frac{2}{3} \left(1 - 2\sqrt{2} \cot 2\theta \right) (m_K^2 - m_\pi^2). \quad (2.30)$$

In general, the one-loop quadratic divergences can be absorbed by a redefinition of the parameters in the $\mathcal{O}(p^2)$ Lagrangian. In fact, the corrections quadratic in the cut-off can be identified with the $d = 2$ pole in dimensional regularization. Here, a full cancellation of the $\mathcal{O}(p^2, 1/N_c)$ divergent correction (2.29) to the mixing requires

$$\tan 2\theta(p^2) = \frac{4\sqrt{2}(2b-1)(m_K^2 - m_\pi^2)}{3(1-4b)p^2 + 2(8b-1)m_K^2 + 2(1-2b)m_\pi^2}. \quad (2.31)$$

Depending on the parameter b , the mixing angle defined in Eq.(2.31) is not a physical quantity. The only way to get rid of the b -dependence is to choose $p^2 = 2m_K^2$. At such a momentum consistently located between the η and η' masses, Eq.(2.31) then provides us with an effective mixing angle $\hat{\theta}$ defined at the QCD scale m_0^2 :

$$\tan 2\hat{\theta}(m_0^2) = \frac{-2\sqrt{2}(m_K^2 - m_\pi^2)}{(2m_K^2 + m_\pi^2)} \quad \left(\hat{\theta} = -25.8^\circ \right). \quad (2.32)$$

We note that the same expression for an on-shell mixing angle θ can be obtained by simply fixing $b = \frac{1}{4}$ to cancel the momentum dependence in Eq.(2.29). This value of the parameter b , which suggests the other significant form

$$U = \frac{\mathbb{1} + \frac{i\pi}{\sqrt{2}f}}{\mathbb{1} - \frac{i\pi}{\sqrt{2}f}} \quad (2.33)$$

only suited for a whole nonet of pseudoscalars [63], ensures θ -independent wave-function renormalizations, *i.e.*, $Z_\eta = Z_{\eta'}$ in Eq.(2.27). As a consequence, the only chiral invariant mass operator that would absorb any divergent $\eta_8 - \eta_0$ rotation at $\mathcal{O}(p^2, 1/N_c)$ is proportional to

$$\begin{aligned} \frac{f^2}{16} r \langle mU^\dagger - Um^\dagger \rangle \langle \ln U - \ln U^\dagger \rangle &= (2m_K^2 + m_\pi^2) \eta_0^2 \\ &\quad - 2\sqrt{2} (m_K^2 - m_\pi^2) \eta_0 \eta_8 + \mathcal{O}(\pi^4) \end{aligned} \quad (2.34)$$

in full agreement with Eq.(2.28) and Eq.(2.32). So, the parity-conserving global $SU(3)_L \otimes SU(3)_R$ plays here the role of the enlarged symmetry which covers the custodial $SU(2)_I \otimes U(1)_Y$. Eq.(2.34) actually tells us that the chiral symmetry of the full effective theory selects in a natural way one negative value ($\hat{\theta}$) for the $\eta - \eta'$ mixing angle, without spoiling the GMO mass relation for m_{88}^2 .

As already anticipated from the explicit breaking of the accidental symmetries $SO(4) \otimes SO(4)$ or $SO(3) \otimes SO(5)$ at the level of terms quartic in the meson fields, neither θ_{id} nor θ_{ph} are protected against Λ^2 quantum corrections. On the contrary, Eq.(2.32) tells us that the angle θ_{th} which optimizes the $\eta - \eta'$ mass ratio at lowest order might be natural in the safe limit $m_\pi^2 \rightarrow 0$. In the fundamental theory (*i.e.*, QCD), the corresponding limit $m_{u,d} \rightarrow 0$ would, in principle, solve the so-called strong CP problem. This rather intriguing link evidently calls for further investigations.

2.3 One-loop corrections to the $\eta' \rightarrow \eta\pi\pi$ decay amplitude

For the purpose of computing a b -independent one-loop correction involving the $\eta - \eta'$ mixing, let us now consider a physical process with on-shell η and η' states.

2.3.1 Tree-level amplitude

The tree-level amplitude for the $\eta' \rightarrow \eta\pi\pi$ decay reads

$$\begin{aligned}
 A(\eta' \rightarrow \eta\pi\pi) = & \frac{1}{f^2} \left[2 \left(2\sqrt{2} \cos 2\theta - \sin 2\theta \right) \left(\frac{1}{6} - b \right) (m_\eta^2 + m_{\eta'}^2 + 2m_\pi^2) \right. \\
 & + 8 \left(2\sqrt{2} \cos 2\theta - \sin 2\theta \right) \left(b - \frac{1}{8} \right) r\tilde{m} \\
 & \left. + 4\sqrt{2} \left(\cos 2\theta - \sqrt{2} \sin 2\theta \right) \left(b - \frac{1}{6} \right) m_0^2 \right] \quad (2.35)
 \end{aligned}$$

where m_η , $m_{\eta'}$ and m_π stand now for the physical masses since they come from the momentum dependence induced by the kinetic term in (2.1). In Eq.(2.35), the second term proportional to r is due to the mass term in Eq.(2.1) and the third one arises from the anomalous part given in Eq.(2.11). With the help of Eq.(2.30), we eventually recover the well-known result that the tree-level amplitude

$$A(\eta' \rightarrow \eta\pi\pi) = \frac{m_\pi^2}{3f^2} \left(2\sqrt{2} \cos 2\theta - \sin 2\theta \right) \quad (2.36)$$

vanishes if $\theta = \theta_{id}$ and is by far too small to reproduce the measured decay width.

2.3.2 One-loop amplitude

The one-loop corrections to the process $\eta' \rightarrow \eta\pi\pi$ are associated with the diagrams given in Fig.2.2.

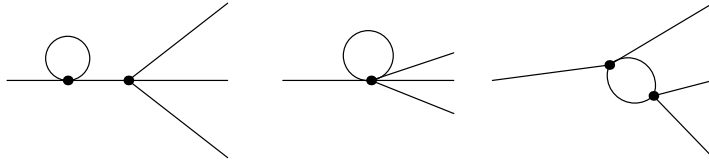


Figure 2.2: One-loop topologies for the $\eta' \rightarrow \eta\pi\pi$ decay amplitude.

The first topology corresponds to the corrections of the inverse propagator given in section 2.2. The second one involves π^6 vertices and thus requires the introduction of

the next two coefficients in the development (2.21), namely

$$\begin{aligned} a_5 &= c \\ a_6 &= c + \frac{b^2}{2} - \frac{b}{2} + \frac{1}{16}. \end{aligned} \quad (2.37)$$

As a result, the Λ^2 -correction to the decay amplitude is given by

$$\begin{aligned} \delta A(\eta' \rightarrow \eta\pi\pi) &= 4 \frac{m_\pi^2}{f^2} \cos^3 2\theta \left[(\tan 2\theta + \sqrt{2}) \left(\tan^2 2\theta + \frac{1}{4\sqrt{2}} \tan 2\theta + \frac{1}{2} \right) \right. \\ &\quad \left. + \frac{3}{4} \frac{m_\pi^2}{m_K^2 - m_\pi^2} \left(\tan 2\theta + \frac{1}{2\sqrt{2}} \right) \tan^2 2\theta \right] \frac{\Lambda^2}{(4\pi f)^2}. \end{aligned} \quad (2.38)$$

This correction is independent of b and c , as it should for any physical quantity, and has been reproduced using the output of FeynRules [69] and Feynarts [70].

If we consider again the limit $m_\pi^2 \ll m_K^2$, we conclude from Eq.(2.38) that the optimal value θ_{th} given in Eq.(2.20) for the $\eta - \eta'$ mixing angle actually damps out the quadratic dependence on the ultra-violet momentum cut-off Λ , as anticipated from Eq.(2.32).

2.4 Concluding remarks

In the past, alternative ways to merge the large number of colours limit into the chiral perturbation theory have been used to study the $\eta - \eta'$ system. In particular, the combined expansion

$$p^2 = \mathcal{O}(\delta), \quad \frac{1}{N_c} = \mathcal{O}(\delta) \quad (2.39)$$

advocated in ref. [71, 72] is quite standard nowadays. In this chapter, inspired by the pseudoscalar mass spectrum, we rather follow the approach of ref. [73] where the leading term in the $1/N_c$ expansion is retained at each order in p^2 . At the effective level, this implies the hierarchy

$$\mathcal{O}(p^0, 1/N_c) > \mathcal{O}(p^2, 0) > \mathcal{O}(p^4, 0), \quad (2.40)$$

namely

$$\mathcal{O}(p^2, 1/N_c) \ll \mathcal{O}(p^4, 0) \quad (2.41)$$

with the large N_c limit denoted by a zero as in Eqs.(2.1) and (2.11). It amounts to remove the double trace term (2.34) as well as $\langle \partial_\mu U U^\dagger \rangle \langle \partial^\mu U^\dagger U \rangle$ in the Lagrangian, *and* to neglect the quadratic one-loop divergences which would renormalize them. The $\eta' \rightarrow \eta \pi \pi$ decay amplitude and the $\eta - \eta'$ mass ratio are known to require sizeable corrections beyond the $\mathcal{O}(p^2, 0)$ approximation and can thus distinguish between the two working hypothesis (2.39) and (2.41). In ref. [74] and ref. [56], the $\mathcal{O}(p^2, 1/N_c)$ contributions were invoked for the decay amplitude and the mass ratio, respectively. On the contrary, in ref. [75] and ref. [73] the $\mathcal{O}(p^4, 0)$ contributions were favoured for these physical quantities, respectively.

At $\mathcal{O}(p^4, 0)$, the full set of corrections allows us to naturally reproduce the observed $\eta - \eta'$ mass spectrum. They do not fix by themselves the value of the mixing angle θ but imply a splitting among the pseudoscalar decay constants [73]. In particular, the measured $SU(3)$ -splitting between π and K decay constants,

$$\frac{f_K}{f_\pi} \equiv 1 + \epsilon \quad (2.42)$$

with $\epsilon = 0.22 \pm 0.01$ of the order of $(m_K^2 - m_\pi^2)/1\text{GeV}^2$, provides a rather interesting link between our present work on the $\eta - \eta'$ mixing and the so-called two-mixing-angle scheme high-lighted in ref. [50, 51]. The equations

$$\begin{aligned} \theta_8 &= \theta - \frac{2\sqrt{2}}{3}\epsilon \\ \theta_0 &= \theta + \frac{2\sqrt{2}}{3}\epsilon \end{aligned} \quad (2.43)$$

relate the universal mixing angle θ which diagonalizes the octet-singlet mass matrix (after renormalizing the meson fields) to the $\theta_{8,0}$ angles associated with the octet-singlet decay constants

$$\begin{aligned} f_8 &= \left(1 + \frac{\epsilon}{3}\right) f_K \\ f_0 &= \left(1 - \frac{\epsilon}{3}\right) f_K. \end{aligned} \quad (2.44)$$

At $\mathcal{O}(p^2, 0)$, $\epsilon = 0$ and $\theta_8 = \theta_0$ but θ cannot be determined. Yet, in this chapter, we have explicitly checked that the mixing angle

$$\theta_{th} \equiv -\frac{1}{2} \tan^{-1} \sqrt{2} \approx -27^\circ \quad (2.45)$$

which optimizes the $\eta - \eta'$ mass spectrum at lowest order is protected against quadratic one-loop divergences in the safe $m_\pi^2 \rightarrow 0$ limit. This result vindicates the approach

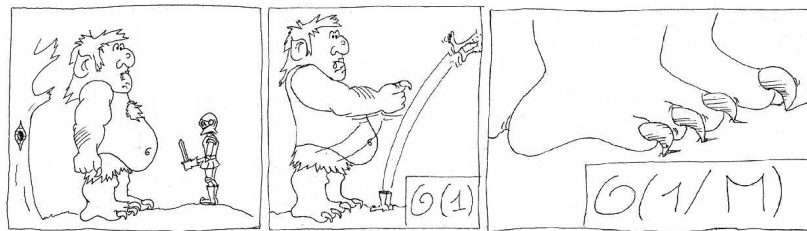
based on Eq.(2.40) since θ_{th} is quite consistent with the physical mixing angle

$$\theta \approx -(22 \pm 1)^\circ \quad (2.46)$$

directly extracted from the anomalous $J/\Psi \rightarrow \eta(\eta')\gamma$ decays [73]. In fact, higher order corrections are typically of the order of 20%, as nicely illustrated in Eq.(2.42). In consequence, $\theta_8 \approx -34^\circ$ and $\theta_0 \approx -10^\circ$ within our specific momentum expansion supplemented by a large N_c limit. However, any physical process only evaluated at the lowest order in the chiral expansion should rely on Eq.(2.45) if it involves on-shell or off-shell $\eta(\eta')$, as it is the case in $\eta(\eta') \rightarrow \gamma\gamma$ or in $K_L \rightarrow (\eta, \eta') \rightarrow \gamma\gamma$ decays, respectively.

Chapter 3

Effective theory for the top pair productions



Based on

C. Degrande, J.-M. Gerard, C. Grojean, F. Maltoni, and G. Servant, "Non-resonant New Physics in Top Pair Production at Hadron Colliders", *JHEP*, vol. 03, p. 125, 2011, 1010.6304.

C. Degrande, J.-M. Gerard, C. Grojean, F. Maltoni, and G. Servant, "An effective approach to same sign top pair production at the LHC and the forward-backward asymmetry at the Tevatron", 2011, 1104.1798.

Top quark physics is among the central physics topics at the Tevatron and at the LHC. The top being the only quark with a coupling to the Higgs of order one, it is expected to play a special role in electroweak symmetry breaking and as a result its coupling to new physics could be large. Searching for beyond the SM physics in observables involving the top quark is, therefore, strongly motivated. Moreover, the discrepancy between the measured forward-backward asymmetry and its SM prediction tends to confirm this theoretical presumption.

A large effort has been devoted to search for new physics in $t\bar{t}$ resonances [76–78]. While the current existing bounds do not forbid the existence of new degrees of freedom that are within the kinematical reach of the Tevatron and the LHC, electroweak precision data [79] together with constraints from flavor physics make plausible if not likely that there exists a mass gap between the SM degrees of freedom and any new physics threshold. In this case, the effects of new physics on a SM process like top pair production can be well captured by higher dimensional interactions among the SM particles. These new interactions are assumed to respect all the symmetries of the SM. Here, we follow this low-energy effective field theory approach. Our study concentrates on testing non-resonant *top-philic* new physics. The study of some dimension-six operators on $t\bar{t}$ production at the Tevatron was initiated in Refs. [80–84] and further explored in Refs [85–89]. In addition, the effects of higher dimensional operators on top anomalous couplings have already been discussed in Refs. [90–92].

In this chapter, we construct the effective Lagrangians for both opposite and same sign top pair productions. Our analysis aims at identifying the effects of the new physics on top pair productions, so it ignores the operators which affect the decay of the top [90, 93, 94]. Secondly, we link the main classes of models and our effective approach. The effects of the new physics on the Higgs-gluon-gluon vertex are then computed. As a matter of fact, any modification of the interaction between the top and the gluons might strongly affect the Higgs production at the LHC since Higgs production by gluon fusion is due to a top loop. Finally, we look at the most stringent LEP constraints on our effective Lagrangian, *i.e.* the Z decay widths.

3.1 Effective Lagrangians

When working with an effective field theory, the starting point is to consider the underlying symmetries. Here, we assume that the symmetries of the SM, including baryon number conservation, are unbroken by the new physics. The gauge invariant operators of dimension-six built from the SM degrees of freedom were classified many years ago in Ref. [95] and they have been reconsidered recently in Ref. [96]. We shall focus our analysis on *top-philic* new physics, *i.e.*, new physics that manifests itself in the top sector, as well-motivated in a large class of theories to be discussed in Section 3.2. The additional operators that affect top pair production without involving the top will be mentioned briefly at the end of section 3.1.1.

3.1.1 Dimension-six operators for opposite sign top pair production

In this section, we consider the set of operators which affect $t\bar{t}$ production at tree-level by interference with the SM amplitudes. Both at the Tevatron and at the LHC, the dominant SM amplitudes are those involving QCD in quark-antiquark annihilation or gluon fusion. Therefore, we shall neglect all new interactions that could interfere only with SM weak processes like $q\bar{q} \rightarrow Z(\gamma) \rightarrow t\bar{t}$. We are then left with only two classes of dimension-six gauge-invariant operators [95]:

- operators with a top and an antitop and one or two gluons, namely

$$\begin{aligned}
\mathcal{O}_{gt} &= [\bar{t}_R \gamma^\mu T^A D^\nu t_R] G_{\mu\nu}^A, \\
\mathcal{O}_{gQ} &= [\bar{Q}_L \gamma^\mu T^A D^\nu Q_L] G_{\mu\nu}^A, \\
\mathcal{O}_{hg} &= [(H \bar{Q}_L) \sigma^{\mu\nu} T^A t_R] G_{\mu\nu}^A,
\end{aligned} \tag{3.1}$$

where $Q_L = (t_L, b_L)$ denotes the left-handed weak doublet of the third quark generation, t_R is the right-handed top quark.

- four-fermion operators with a top and an antitop together with a pair of light quark and antiquark that can be organized following their chiral structures:

$\bar{L}L\bar{L}L$:

$$\begin{aligned}
\mathcal{O}_{Qq}^{(8,1)} &= (\bar{Q}_L \gamma^\mu T^A Q_L) (\bar{q}_L \gamma_\mu T^A q_L), \\
\mathcal{O}_{Qq}^{(8,3)} &= (\bar{Q}_L \gamma^\mu T^A \sigma^I Q_L) (\bar{q}_L \gamma_\mu T^A \sigma^I q_L),
\end{aligned} \tag{3.2}$$

$\bar{R}R\bar{R}R$:

$$\begin{aligned}
\mathcal{O}_{tu}^{(8)} &= (\bar{t}_R \gamma^\mu T^A t_R) (\bar{u}_R \gamma_\mu T^A u_R), \\
\mathcal{O}_{td}^{(8)} &= (\bar{t}_R \gamma^\mu T^A t_R) (\bar{d}_R \gamma_\mu T^A d_R),
\end{aligned} \tag{3.3}$$

$\bar{L}L\bar{R}R$:

$$\begin{aligned}
\mathcal{O}_{Qu}^{(8)} &= (\bar{Q}_L \gamma^\mu T^A Q_L) (\bar{u}_R \gamma_\mu T^A u_R), \\
\mathcal{O}_{Qd}^{(8)} &= (\bar{Q}_L \gamma^\mu T^A Q_L) (\bar{d}_R \gamma_\mu T^A d_R), \\
\mathcal{O}_{tq}^{(8)} &= (\bar{q}_L \gamma^\mu T^A q_L) (\bar{t}_R \gamma_\mu T^A t_R),
\end{aligned} \tag{3.4}$$

$\bar{L}R\bar{L}R$:

$$\mathcal{O}_d^{(8)} = (\bar{Q}_L T^A t_R) (\bar{q}_L T^A d_R), \tag{3.5}$$

where q_L and u_R and d_R are respectively the left- and right-handed components of the two lightest generations.

Note that there also exist some color-singlet analogues of all these operators but they do not interfere with the SM QCD amplitudes and therefore are not considered here (such operators can be generated by a Z' for example). All the four-fermion operators are written in the mass-eigenstates basis and no CKM mixing will enter in our analysis since we are neglecting weak corrections. Note also that operators with a different Lorentz or gauge structure, like for instance $(\bar{Q}_L \gamma^\mu T^A q_L) (\bar{q}_L \gamma^\mu T^A Q_L)$ or $(\bar{t}_R \gamma^\mu T^A u_R) (\bar{u}_R \gamma_\mu T^A t_R)$, can be transformed (using Fierz identities, see App. A.1) into linear combinations of the four-fermion operators listed above and their color-singlet partners.

The $\bar{L}R\bar{L}R$ operator $\mathcal{O}_d^{(8)}$ involves both the left- and the right-handed components of the down quark. So, given the fact that QCD interactions are chirality-diagonal, it can only interfere with the SM amplitude after a mass insertion and therefore its contribution to the $t\bar{t}$ production cross-section is negligible and we shall not consider it further in our analysis.

It is rather natural to assume the universality of new physics with respect to the light generations. In that limit, the contribution to the cross-section from the second generation is more than two orders of magnitude smaller than the one from the first generation due to the different parton distribution functions (pdf). We shall therefore concentrate on the contribution from the lightest generation only.

Our list (3.1)–(3.5) of top-philic operators contains eleven operators. However, they are still not all independent. Using the equation of motion for the gluons,

$$D^\nu G_{\mu\nu}^A = g_s \sum_f \bar{q}_f \gamma_\mu T^A q_f, \tag{3.6}$$

we obtain the following two relations :

$$\mathcal{O}_{gt} + \mathcal{O}_{gt}^\dagger = -g_s \sum_{\text{generations}} \left(\mathcal{O}_{tq}^{(8)} + \mathcal{O}_{tu}^{(8)} + \mathcal{O}_{td}^{(8)} \right), \quad (3.7)$$

$$\mathcal{O}_{gQ} + \mathcal{O}_{gQ}^\dagger = -g_s \sum_{\text{generations}} \left(\mathcal{O}_{Qq}^{(8,1)} + \mathcal{O}_{Qu}^{(8)} + \mathcal{O}_{Qd}^{(8)} \right). \quad (3.8)$$

The linear combinations $\mathcal{O}_{gt} - \mathcal{O}_{gt}^\dagger$ and $\mathcal{O}_{gQ} - \mathcal{O}_{gQ}^\dagger$ do not interfere with the SM amplitudes because the associated vertices are CP-odd and we are not concerned about CP violating observables (see Ref. [93] for a discussion on possible observables sensitive to CP violation). Consequently, the two operators \mathcal{O}_{gt} and \mathcal{O}_{gQ} can be dropped in our analysis and only one two-fermion operator, namely \mathcal{O}_{hg} , interferes with the SM gluon fusion process!

In conclusion, the most general top-philic Lagrangian that can affect the $t\bar{t}$ production involves eight dimension-six operators

$$\mathcal{L}_{t\bar{t}}(\Lambda^{-2}) = \frac{1}{\Lambda^2} \left((c_{hg}\mathcal{O}_{hg} + h.c.) + \sum_i c_i \mathcal{O}_i \right), \quad (3.9)$$

where i runs over the seven self-hermitian four-fermion operators of Eqs. (3.2)–(3.4).

In Eq. (3.9), the coefficient c_{hg} might be complex. However, since we are concerned with CP-invariant observables, only its real part enters in the interference with the SM processes and therefore we shall assume in our analysis that c_{hg} is real. This coefficient corresponds to a chromomagnetic moment for the top.

The phenomenological basis

In Eq. (3.9), we have identified eight independent top-philic operators. Yet, additional simple considerations are going to show that physical observables like the $t\bar{t}$ production total cross-section, the invariant mass distribution or the forward-backward asymmetry only depends on specific linear combinations of these operators.

The seven four-fermion operators can be combined to form linear combinations with definite $SU(2)$ isospin quantum numbers. In the isospin-0 sector, it is further convenient to define axial and vector combinations of the light quarks:

$$\mathcal{O}_{Rv} = \mathcal{O}_{tu}^{(8)} + \mathcal{O}_{td}^{(8)} + \mathcal{O}_{tq}^{(8)}, \quad \mathcal{O}_{Ra} = \mathcal{O}_{tu}^{(8)} + \mathcal{O}_{td}^{(8)} - \mathcal{O}_{tq}^{(8)}, \quad (3.10)$$

and similar operators involving the left-handed top quarks:

$$\mathcal{O}_{Lv} = \mathcal{O}_{Qu}^{(8)} + \mathcal{O}_{Qd}^{(8)} + \mathcal{O}_{Qq}^{(8,1)}, \quad \mathcal{O}_{La} = \mathcal{O}_{Qu}^{(8)} + \mathcal{O}_{Qd}^{(8)} - \mathcal{O}_{Qq}^{(8,1)}. \quad (3.11)$$

The reason is that the axial operators are asymmetric under the exchange of the quark and antiquark while the vector operators are symmetric¹:

$$\begin{aligned} [\bar{\psi}(k_1) \gamma^\mu \gamma^5 T^A \psi(k_2)] &= - [\bar{\psi}^c(k_2) \gamma^\mu \gamma^5 T^A \psi^c(k_1)], \\ [\bar{\psi}(k_1) \gamma^\mu T^A \psi(k_2)] &= [\bar{\psi}^c(k_2) \gamma^\mu T^A \psi^c(k_1)]. \end{aligned} \quad (3.12)$$

Therefore, the interferences of \mathcal{O}_{Ra} and \mathcal{O}_{La} with the SM will be odd under the exchange of the momenta of the initial partons and these axial operators can only contribute to observables that are odd functions of the scattering angle and certainly not to the total cross-section. On the contrary, the operators \mathcal{O}_{Rv} and \mathcal{O}_{Lv} are even functions of the scattering angle and can contribute to $\sigma_{t\bar{t}}$.

In addition, the operators \mathcal{O}_{Rv} and \mathcal{O}_{Lv} will obviously produce the same amount of top pairs but with opposite chirality. Consequently, the spin-independent observables associated to the $t\bar{t}$ production are expected to only depend on the sum $\mathcal{O}_{Rv} + \mathcal{O}_{Lv}$ while the difference $\mathcal{O}_{Rv} - \mathcal{O}_{Lv}$ will only contribute to spin-dependent observables. Similarly, but with a sign flip, only their difference, $\mathcal{O}_{Ra} - \mathcal{O}_{La}$, can contribute to spin-independent observables and in particular to the $t\bar{t}$ differential cross-section after summing over the spins. The orthogonal combination $\mathcal{O}_{Ra} + \mathcal{O}_{La}$ could contribute to spin-dependent observables which are odd functions of the scattering angle, but we shall not consider any observable of this type in our analysis.

Therefore, we expect a dependence of the total $t\bar{t}$ production cross-section on the sum

$$c_{Vv} = c_{Rv} + c_{Lv} \quad \text{with} \quad \begin{cases} c_{Rv} = c_{tq}/2 + (c_{tu} + c_{td})/4 \\ c_{Lv} = c_{Qq}^{(8,1)}/2 + (c_{Qu} + c_{Qd})/4 \end{cases} \quad (3.13)$$

and the forward-backward asymmetry will depend on the combination

$$c_{Aa} = c_{Ra} - c_{La} \quad \text{with} \quad \begin{cases} c_{Ra} = -c_{tq}/2 + (c_{tu} + c_{td})/4 \\ c_{La} = -c_{Qq}^{(8,1)}/2 + (c_{Qu} + c_{Qd})/4. \end{cases} \quad (3.14)$$

The difference

$$c_{Av} = c_{Rv} - c_{Lv} \quad (3.15)$$

can only contribute to spin-dependent observables (see Section 4.1.5).

The isospin-1 sector is spanned by the three combinations:

$$\mathcal{O}_{Rr} = \mathcal{O}_{tu}^{(8)} - \mathcal{O}_{td}^{(8)}, \quad \mathcal{O}_{Lr} = \mathcal{O}_{Qu}^{(8)} - \mathcal{O}_{Qd}^{(8)} \quad \text{and} \quad \mathcal{O}_{Qq}^{(8,3)}. \quad (3.16)$$

¹The matrices $C\gamma^\mu\gamma^5$ are antisymmetric but the matrices $C\gamma^\mu$ are symmetric, C being the charge conjugation matrix.

Again, parity arguments lead to the conclusion that the total cross-section can only depend on the combination

$$c'_{Vv} = (c_{tu} - c_{td})/2 + (c_{Qu} - c_{Qd})/2 + c_{Qq}^{(8,3)}, \quad (3.17)$$

while the forward-backward asymmetry will only receive a contribution proportional to

$$c'_{Aa} = (c_{tu} - c_{td})/2 - (c_{Qu} - c_{Qd})/2 + c_{Qq}^{(8,3)}. \quad (3.18)$$

As we shall see in Section 4.1.2, the isospin-0 sector gives a numerically larger contribution to the observables we are considering than the isospin-1 sector. This is due to the fact that the up and down quarks contributions add to each other in the first case while they subtract to each other in the second case.

It is interesting to note that, in composite models where the strong sector is usually invariant under the weak-custodial symmetry $SO(4) \rightarrow SO(3)$ [97], the right-handed up and down quarks certainly transform as a doublet of the $SU(2)_R$ symmetry, and therefore $c_{Qu} = c_{Qd}$. There are however various ways to embed the right-handed top quarks into a $SO(4)$ representation [98]: if it is a singlet, then $c_{tu} = c_{td}$ also and the isospin-1 sector reduces to the operator $\mathcal{O}_{Qq}^{(8,3)}$ only.

In summary, the relevant effective Lagrangian for $t\bar{t}$ production contains a single two-fermion operator and seven four-fermion operators conveniently written as:

$$\begin{aligned} \mathcal{L}_{t\bar{t}} = & + \frac{1}{\Lambda^2} \left((c_{hg} \mathcal{O}_{hg} + h.c.) + (c_{Rv} \mathcal{O}_{Rv} + c_{Ra} \mathcal{O}_{Ra} + c'_{Rr} \mathcal{O}'_{Rr} + R \leftrightarrow L) \right. \\ & \left. + c_{Qq}^{(8,3)} \mathcal{O}_{Qq}^{(8,3)} \right). \end{aligned} \quad (3.19)$$

The vertices arising from the dimension-six operators given in Eq. (3.19) relevant for opposite sign top pair production at hadron colliders are depicted in Fig. 3.1.

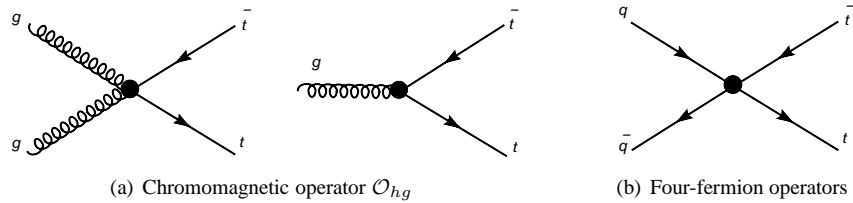


Figure 3.1: A Feynman representation of the relevant operators for $t\bar{t}$ production at hadron colliders.

Non top-philic operators

As mentioned, we have only considered so far operators that modify the top interactions. However, two additional operators can change the $t\bar{t}$ production. Namely,

$$\mathcal{O}_G = f_{ABC} G_{\mu\nu}^A G^{B\nu\rho} G_\rho^{C\mu} \quad (3.20)$$

modifies the three (and four) gluons vertex. All the quarks pair productions are identically affected by this operator. However, its contribution becomes sizeable only at high energy. So, even if it can be seen in processes with much larger cross-sections, they cannot necessary put stronger constraints on its coefficient. Moreover, this operator changes the jets production for various multiplicities since this operator also gives rise to five and six gluons vertices. Its effects on opposite sign top pair production were studied in Refs. [93, 99–101]. The second operator [93],

$$\mathcal{O}_{hG} = H^\dagger H G_{\mu\nu}^A G^{A\mu\nu}, \quad (3.21)$$

induces the production of a virtual Higgs by gluon fusion which then decay into two top quarks. On the contrary, this operator affects only top pair production due to the hierarchy of the Yukawa couplings.

3.1.2 Dimension-six operators for same sign top pair production

At the LHC, the forward-backward asymmetry can hardly be measured. On the one hand, the asymmetry, due to quark antiquark annihilation, is small since the dominant process at the LHC is gluon fusion. On the other hand, the LHC is a symmetric machine. Consequently, the asymmetry can only be measured on a statistical basis. However, some explanations of the forward-backward asymmetry imply same sign top pair production. The main advantage of this process at the LHC is that its initial state, quark-quark, is more likely in proton-proton collisions.

Only four-fermion operators can induce same sign top pair production because it is a $\Delta F = 2$ process. As a consequence, it is possible to avoid (suppress) any new physics contribution to this process with the help of (approximate) flavor symmetries. Any operator contributing to same sign top pair production can be expressed as a linear

combination of

$$\begin{aligned}
\mathcal{O}_{RR} &= [\bar{t}_R \gamma^\mu u_R] [\bar{t}_R \gamma_\mu u_R] \\
\mathcal{O}_{LL}^{(1)} &= [\bar{Q}_L \gamma^\mu q_L] [\bar{Q}_L \gamma_\mu q_L] \\
\mathcal{O}_{LL}^{(3)} &= [\bar{Q}_L \gamma^\mu \sigma^I q_L] [\bar{Q}_L \gamma_\mu \sigma^I q_L] \\
\mathcal{O}_{LR}^{(1)} &= [\bar{Q}_L \gamma^\mu q_L] [\bar{t}_R \gamma_\mu u_R] \\
\mathcal{O}_{LR}^{(8)} &= [\bar{Q}_L \gamma^\mu T^A q_L] [\bar{t}_R \gamma_\mu T^A u_R].
\end{aligned} \tag{3.22}$$

The relevant effective Lagrangian is then given by

$$\mathcal{L}_{\text{dim}=6}^{qq \rightarrow tt} = \frac{1}{\Lambda^2} \left(c_{RR} \mathcal{O}_{RR} + c_{LL}^{(1)} \mathcal{O}_{LL}^{(1)} + c_{LL}^{(3)} \mathcal{O}_{LL}^{(3)} + c_{LR}^{(1)} \mathcal{O}_{LR}^{(1)} + c_{LR}^{(8)} \mathcal{O}_{LR}^{(8)} \right) + h.c.. \tag{3.23}$$

$\mathcal{O}_{LL}^{(1)}$ and $\mathcal{O}_{LL}^{(3)}$ contain the same product of neutral currents $[\bar{t}_L \gamma^\mu u_L] [\bar{t}_L \gamma_\mu u_L]$, which are relevant for $uu \rightarrow tt$. In addition, they contain $[\bar{b}_L \gamma^\mu d_L] [\bar{b}_L \gamma_\mu d_L]$ which can contribute to the B_d mixing and to di-jet production. For example, the linear combination $c_{LL} = c_{LL}^{(1)} + c_{LL}^{(3)}$ can be strongly constrained from the former [102]

$$|c_{LL}| \left(\frac{1 \text{ TeV}}{\Lambda} \right)^2 < 2.3 \times 10^{-5}. \tag{3.24}$$

The difference between the two LL operators in Eq. (3.23) is thus in the product of charged currents $[\bar{t}_L \gamma^\mu d_L] [\bar{b}_L \gamma_\mu u_L]$ present only in $\mathcal{O}_{LL}^{(3)}$ and affecting the top decay as well as single top production [93].

3.2 Connection with composite top and heavy boson exchange models

3.2.1 Composite models

The effects of a composite top were first studied in Ref. [103]. The construction of an effective Lagrangian for the fermionic sector was discussed in details in Ref. [98]. It relies on the assumption of partial compositeness, meaning that SM fermions are assumed to be linearly coupled to the resonances of the strong sector through mass mixing terms. The composite models are characterized by a new strong interaction responsible for the breaking of the electroweak symmetry and broadly parametrized by two parameters [104]: a dimensionless coupling g_ρ and a mass scale m_ρ . The latter,

associated with the heavy physical states, was generically denoted Λ in Eqs. (3.9) and (3.23). In order to alleviate the tension with EW precision data, we assume that in the limit where all the gauge and Yukawa interactions of the SM are switched off, the full Higgs doublet is an exact Goldstone boson living in the G/H coset space of a spontaneously broken symmetry of the strong sector. In such a case, f , the decay constant of the Goldstones, is related to g_ρ and m_ρ by

$$m_\rho = g_\rho f \quad (3.25)$$

with $1 \lesssim g_\rho \lesssim 4\pi$. The effective Lagrangian of the gauge and Higgs sectors was constructed in Ref. [104].

At energies below the resonances masses, the dynamics of the top sector is described by the usual SM Lagrangian supplemented by a few higher dimensional operators. Simple rules control the size of these different operators, referred as Naive Dimensional Analysis (NDA) [105, 106]. Inspired by the rather successful chiral perturbation approach to QCD at low scale (seen Chap. 2), NDA provides the following rules for the effective operators beyond \mathcal{L}_{SM} :

1. first, multiply by an overall factor f^2 ;
2. then, multiply by a factor $\frac{1}{f}$ for each strongly interacting field;
3. finally, multiply by powers of m_ρ (instead of Λ) to get the right dimension.

Hereafter, we may consider two classes of gauge-invariant operators for the top pair production:

- Operators that contain only fields from the strong sector are called dominant because their coefficients scale like g_ρ^2 . In most composite top models, only its right component is composite to avoid experimental constraints (see Sect. 3.4). In this case, there is only one such operator since the color octet equivalent is related to the color singlet by a Fierz transformation ($\mathcal{O}_R^{(8)} = 1/3 \mathcal{O}_R$),

$$\mathcal{O}_R = (\bar{t}_R \gamma^\mu t_R)(\bar{t}_R \gamma_\mu t_R). \quad (3.26)$$

If only the left handed top is composite, there are two independent dominant operators,

$$\mathcal{O}_L^{(1)} = (\bar{Q}_L \gamma^\mu Q_L)(\bar{Q}_L \gamma_\mu Q_L), \quad \mathcal{O}_L^{(8)} = (\bar{Q}_L \gamma^\mu T^A Q_L)(\bar{Q}_L \gamma_\mu T^A Q_L). \quad (3.27)$$

In the most general scenario where both chiralities are composite, two additional operators should also be considered,

$$\mathcal{O}_B^{(1)} = (\bar{Q}_L \gamma_\mu Q_L) (\bar{t}_R \gamma_\mu t_R), \quad \mathcal{O}_B^{(8)} = (\bar{Q}_L \gamma_\mu T^A Q_L) (\bar{t}_R \gamma_\mu T^A t_R). \quad (3.28)$$

Needless to say that none of these operators contribute at tree-level to $t\bar{t}$ or tt production. Yet they are relevant for direct production of four top-quarks (see Section 4.3.1).

- Operators which contribute directly to $t\bar{t}$ and tt productions are subdominant. On the one hand, the four-fermion operators given in Eqs. (3.19) and (3.23) contain at most two fields from the strong sector and their coefficients ($c_{R/Lv}$, $c_{R/La}$, $c_{R/Lr}$ and $c_{Qq}^{(8,3)}$) scale like g_ρ^0 at best. On the other hand, the coefficient c_{hg} associated with the operator \mathcal{O}_{hg} scales as g_ρ^{-1} (if only one field is composite), g_ρ^0 (if only two fields are composite) or g_ρ (if the three fields are composite)

In the limit $g_\rho \sim 4\pi$, the one-loop contributions of the dominant operators (3.26)–(3.28) to opposite sign top pair production may be as large as the tree-level contributions of the subdominant ones given in Section 3.1.1. However, the chiral structure of the dominant operators are such that their one-loop corrections (see Fig. 3.2 a and 3.2 b) simply amount to redefining the coefficients c_{Rv} and c_{Lv} in the Lagrangian (3.19) [107]:

$$\begin{aligned} \frac{\delta c_{Rv}}{g_s^2} &= \frac{c_B^{(8)} - 4c_R}{3(4\pi)^2} \log\left(\frac{\Lambda^2}{m_t^2}\right) + \frac{c_B^{(8)}}{3(4\pi)^2} \log\left(\frac{\Lambda^2}{m_b^2}\right) \\ \frac{\delta c_{Lv}}{g_s^2} &= \frac{c_B^{(8)} - 4c_L^{(1)} + 8c_L^{(8)}/3}{3(4\pi)^2} \log\left(\frac{\Lambda^2}{m_t^2}\right) + \frac{2c_L^{(8)}}{3(4\pi)^2} \log\left(\frac{\Lambda^2}{m_b^2}\right) \end{aligned} \quad (3.29)$$

where c_R , $c_L^{(i)}$ and $c_B^{(i)}$ are the coefficients of the operator \mathcal{O}_R , $\mathcal{O}_L^{(i)}$ and $\mathcal{O}_B^{(i)}$ respectively. The operator $(\bar{t}_L t_R) (\bar{t}_L t_R)$ and $(\bar{t}_R t_L) (\bar{t}_R t_L)$ would induce a modification of c_{hg} at one-loop [107]. However, $SU(2)$ gauge invariance requires to consider loop corrections induced by a dimension-eight operator like $(H\bar{Q}t) (H\bar{Q}t)$ with the Higgs field H replaced by its $v\epsilon v$ (see Fig. 3.2b).

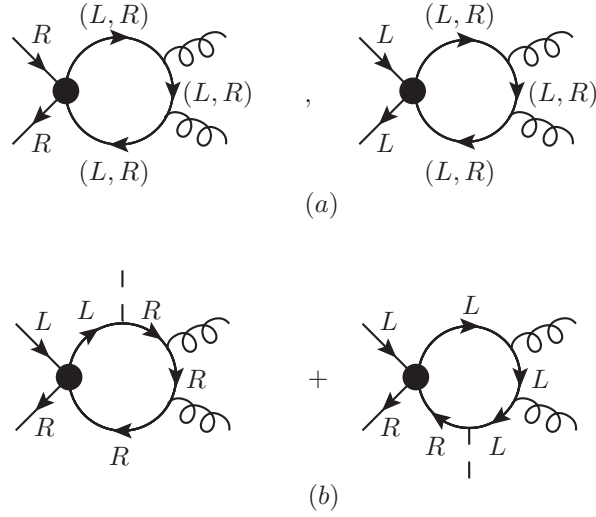


Figure 3.2: Typical one-loop contributions of (a) the dimension-six operators (3.26)–(3.28) leading to δc_{Rv} and δc_{Lv} respectively once the equation of motion (3.6) is used, and (b) the dimension-eight operator $(H\bar{Q}t)(H\bar{Q}t)$ leading to δc_{hg} if one chirality-flip is considered in the loop.

3.2.2 s - and t -channel exchanges

In this section, we focus on s - and t -channel exchanges because they can induce both same and opposite sign top pair productions. However, u -channel exchanges can also be advocated to explain the Tevatron forward-backward asymmetry [108–111]. While the exchanges of heavy vectors and scalars lead to four-fermion operators (see for instance Ref. [87]), they cannot contribute to the top chromomagnetic moment at tree-level as a consequence of $SU(3)_c$ gauge invariance (see Fig. 3.3a). Only higher-dimension effective operators quadratic in the gluon field-strength can be induced in this frame. For example, a heavy scalar or tensor induces at tree-level the operator $(H\bar{Q}t + h.c.) G_{\mu\nu}G^{\mu\nu}$ or $(H\bar{Q}t - h.c.) G_{\mu\nu}\tilde{G}^{\mu\nu}$ (see Fig. 3.3b). So, the operator \mathcal{O}_{hg} can only be generated at the loop-level and is suppressed in s - and t -channel exchange models.

In the following, we will consider model in which at least the up and top quarks are coupled to the new degree of freedom. Adding the right-handed down quark is irrelevant for same sign top pair production and is quite straightforward.

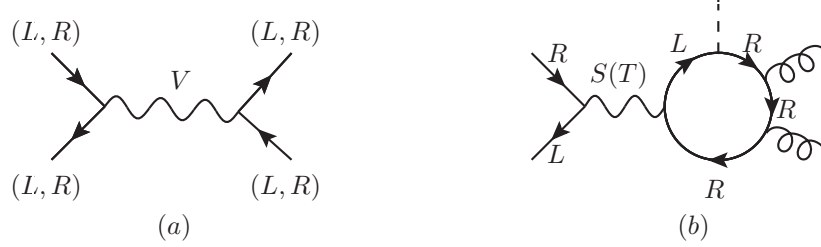


Figure 3.3: One particle exchange contributions to $\mathcal{L}_{t\bar{t}}$ in Eq. (3.19): (a) the five four-fermion operators can be directly associated with the exchange of a spin-1 resonance once Fierz transformations are used, (b) the single two-fermion operator \mathcal{O}_{hg} can be indirectly associated with the exchange of a spin-0 or spin-2 resonance coupled to two gluons via a fermion loop.

Link with a t -channel exchange

t -channel exchanges invoked to account for the Tevatron forward-backward asymmetry might imply a large same sign top pair production at the LHC [112, 113]. In the case of a t -channel exchange, the currents and the densities have to be flavor changing to generate top pair productions. The two possible currents are

$$J_R^\mu = \bar{t}_R^i \gamma^\mu u_R^j \times (\delta_{ij}/T_{ij}^A) \quad (3.30)$$

and

$$J_L^\mu = \bar{Q}_L^{i,\alpha} \gamma^\mu q_R^{j,\beta} \times (\delta_{ij}/T_{ij}^A) \times (\delta_{\alpha\beta}/\sigma_{\alpha\beta}^I). \quad (3.31)$$

Similarly, we have two densities, *i.e.*

$$d_R = \bar{t}_R^i q_L^j \times (\delta_{ij}/T_{ij}^A) \quad (3.32)$$

and

$$d_L = \bar{Q}_L^i u_R^j \times (\delta_{ij}/T_{ij}^A). \quad (3.33)$$

The color and the SU(2) structures have to be chosen accordingly to the quantum number of the exchanged particle. Tab. 3.1 shows the coefficients of the operators of Eq. (3.22) for any possible particle exchanged in the t -channel using the relations of Sect. 1.2. If the new physics is in the reach of the LHC, the left coupling of all vectors have to be very tiny to satisfy Eq. (3.24). In consequence, we will assume that $g_L = 0$ for the vectors in the following.

While no relation exists in general between same and opposite sign top pair production, in the special case of a flavor changing t -channel, each vertex can be replaced

Spin	SU(3)	SU(2)	Y	c_{RR}	$c_{LL}^{(1)}$	$c_{LL}^{(3)}$	$c_{LR}^{(1)}$	$c_{LR}^{(8)}$
1	1	1	0	$-\frac{1}{2}$	$-\frac{\xi^2}{2}$		$-\xi$	
1	8	1	0	$-\frac{1}{6}$	$-\frac{\xi^2}{24}$	$-\frac{\xi^2}{8}$		$-\xi$
0	1	2	$\frac{1}{2}$				$-\frac{1}{6}\xi$	$-\xi$
0	8	2	$\frac{1}{2}$				$-\frac{2}{9}\xi$	$\frac{1}{6}\xi$
1	1	3	0			$-\frac{\xi^2}{2}$		
1	8	3	0		$-\frac{3}{8}\xi^2$	$\frac{5}{24}\xi^2$		

Table 3.1: Coefficients of the operators up to a global factor g_R^2 for all possible t -channel exchanges (of mass $M = \Lambda$) identified by their quantum numbers ($Q = T_3 + Y$). $\xi = \frac{g_L}{g_R}$ with g_L (g_R) the coupling to the density d_L (d_R) or to the current J_L^μ (J_R^μ).

by its hermitian conjugate (see Fig. 3.4) if the exchanged particle is self-conjugate. The connection with the coefficients of the operators relevant for $t\bar{t}$ production in the allowed cases are displayed in Tab. 3.2.

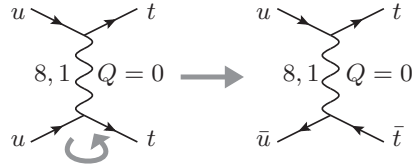


Figure 3.4: Possible connection between same and opposite sign top pair productions through a t -channel self-conjugate particle exchange.

Link with a s-channel exchange

The effects of any heavy qq-resonance relevant for $t\bar{t}$ production (listed in Ref. [114]) can be approximated by the four-fermion operators (3.22) at low energy (see Tab. 3.3). The associated current is

$$J_1^\mu = [\bar{u}_R^c]^i \gamma^\mu q_L^j \times (S_{ij}^A / A_{ij}^A) \quad (3.34)$$

Spin	SU(2)	Y	c_{Vv}	c'_{Vv}	c_{Aa}	c'_{Aa}
1	1	0	$-\frac{1}{2}$	-1	$-\frac{1}{2}$	-1
0	2	$\frac{1}{2}$	$-\frac{1}{2} \left(\xi ^2 + \frac{1}{2} \right)$	$-\frac{1}{2}$	$\frac{1}{2} \left(\xi ^2 + \frac{1}{2} \right)$	$\frac{1}{2}$

Table 3.2: Expressions of the parameters relevant for $t\bar{t}$ up to an overall factor $|g_R|^2$ for a color singlet particle of mass $M = \Lambda$ exchanged in the t -channel. The coefficients for the corresponding color octets are obtained by multiplying them all by $-\frac{1}{6}$.

where S^A and A^A are respectively the symmetric sextet and anti-symmetric anti-triplet representations of $SU(3)_c$ normalized as $\text{tr}(S^A S^{B\dagger}) = \text{tr}(A^A A^{B\dagger}) = \delta^{AB}/2$. The associated densities are given by

$$d_R^1 = \bar{u}_R^c S^A u_R \quad (3.35)$$

and

$$d_L^1 = \bar{q}_L^c S^A \varepsilon \sigma^I q_L \quad (3.36)$$

where $\varepsilon = i\sigma^2$. Similar current and densities can be defined for the top. A color anti-triplet scalar cannot contribute because its coupling is asymmetric under the exchange of the two fermions. It should also be noted that only axial (vector) couplings contribute to the $uu \rightarrow tt$ for the color sextet (anti-triplet) iso-doublet resonances. The cases of scalar and vector sextets were treated in Refs. [115, 116]. In general, same sign top pair production through an s -channel particle exchange cannot be related to opposite sign top pair production because of color and electric charges (see Fig. 3.5).

Spin	SU(3)	SU(2)	Y	c_{RR}	$c_{LL}^{(1)}$	$c_{LL}^{(3)}$	$c_{LR}^{(1)}$	$c_{LR}^{(8)}$
1	$\bar{3}$	2	$\frac{5}{6}$				$-\frac{1}{6}$	$\frac{1}{2}$
1	6	2	$\frac{5}{6}$				$-\frac{1}{3}$	$-\frac{1}{2}$
0	6	1	$\frac{4}{3}$	$\frac{1}{4}$				
0	6	3	$\frac{1}{3}$		$-\frac{3}{8}$	$-\frac{1}{8}$		

Table 3.3: Coefficients of the operators up to a global factor $g_1 g_3$ for all possible s -channel exchange (of mass $M = \Lambda$ and with a coupling g_1 (g_3) to the first (third) generation quarks) leading to tt production identified by their quantum numbers.

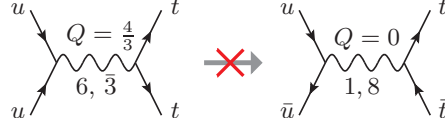


Figure 3.5: Diagrams for same and opposite sign top pair productions through an s -channel particle exchange.

As already mentioned in Sec. 3.1.1, only color octet s -channel exchange can interfere with the SM amplitude. Moreover, since the interference with the only product of densities (3.5) is suppressed by the light quarks mass, only vector exchanges remain. The associated currents can be read directly from Eqs. (3.2) to (3.4). The straightforward connections with the operators of Eqs. (3.3) to (3.4) is given in Tab. 3.4.

Spin	SU(3)	SU(2)	Y	$c_{tu}^{(8)}$	$c_{tq}^{(8)}$	$c_{Qu}^{(8)}$	$c_{Qq}^{(8,1)}$	$c_{Qq}^{(8,3)}$
1	8	1	0	$g_{R3}g_{R1}$	$g_{R3}g_{L1}$	$g_{L3}g_{R1}$	$g_{L3}g_{L1}$	
1	8	3	0					$g_{L3}g_{L1}$

Table 3.4: Coefficients of the operators up to a global factor -1 for all possible s -channel exchange (of mass $M = \Lambda$ and with a coupling g_{R1} (g_{R3}) and g_{L1} (g_{L3}) to the right- and left-handed first (third) generation quarks respectively) leading to $t\bar{t}$ production identified by their quantum numbers.

3.3 Corrections to the Higgs production

3.3.1 The chromomagnetic operator

The chromomagnetic operator \mathcal{O}_{hg} induces in addition to the vertices drawn in Fig. 3.1 similar vertices but with a Higgs leg added. The diagrams for Higgs production are depicted in Fig. 3.6

As in the SM, the leading correction from \mathcal{O}_{hg} leads to the operator \mathcal{O}_{hC} . Since both operators are of dimension-six, the one-loop amplitudes are logarithmically divergent. In the large top mass limit, the SM and chromomagnetic one-loop contributions can

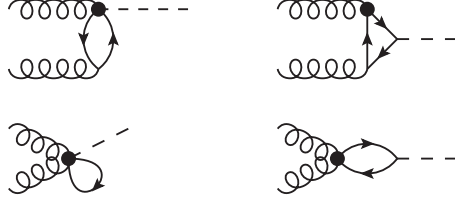


Figure 3.6: Chromomagnetic operator contribution to Higgs production by gluon fusion. In the first two diagrams, the two gluons can be interchanged. The amplitudes of the last two diagrams vanish due to color conservation.

be written as

$$\frac{\delta c_{hG}}{\Lambda^2} = \frac{\alpha_S}{3\pi} \frac{1}{v^2} \left(1 + 6\sqrt{2} \frac{\Re(c_{hg})}{g_s} \frac{m_t v}{\Lambda^2} \log \left(\frac{\Lambda_{cut}^2}{m^2} \right) \right) \quad (3.37)$$

where Λ_{cut} is the cut-off scale. Taking $\Lambda = \Lambda_{cut} = 1$ TeV, $m_t = 175$ GeV, $v = 246$ GeV and $g_s = 1.2$, we obtain

$$\delta c_{hG} \approx \frac{\alpha_S}{3\pi} \frac{1}{v^2} (1 + \Re(c_{hg})). \quad (3.38)$$

Consequently, the chromomagnetic operator can strongly enhance or suppress the Higgs production rate at the LHC. If the Higgs is not seen, $c_{hg} \approx -1$ may explain its absence. It is thus important to probe this region of the parameter space.

3.3.2 Composite Higgs

In most of the composite top models, the Higgs is also assumed to be composite [117]. For a right-handed composite top, there are then two additional dominant operators involving the top

$$\begin{aligned} \mathcal{O}_H &= H^\dagger H (H\bar{Q}_3) P_R t \\ \mathcal{O}_{HR} &= H^\dagger D_\mu H \bar{t} \gamma^\mu P_R t. \end{aligned} \quad (3.39)$$

In the case of a left-handed composite top, the additional dominant operators are \mathcal{O}_H and

$$\begin{aligned} \mathcal{O}_{HL} &= H^\dagger D_\mu H \bar{Q} \gamma^\mu P_L Q \\ \mathcal{O}_{HL}^3 &= H^\dagger \sigma^I D_\mu H \bar{Q} \sigma^I \gamma^\mu P_L Q. \end{aligned} \quad (3.40)$$

When both chiralities are composite, all the above operators need to be included. However, it should be noted that the operator \mathcal{O}_H is enhanced by a factor g_ρ in the latter case.

For all the above operators, their one-loop contributions to Higgs production come from the same diagram as in the SM. \mathcal{O}_H renormalizes both the top mass,

$$m_t = y_t \frac{v}{\sqrt{2}} + \frac{\Re(c_H)}{2\sqrt{2}} \frac{v^3}{\Lambda^2} \equiv y'_t \frac{v}{\sqrt{2}} \quad (3.41)$$

and the vertex $ht\bar{t}$,

$$\begin{aligned} \mathcal{L}^{ht\bar{t}} &= \bar{t}t \frac{h}{\sqrt{2}} \left(y_t + \frac{3}{2} \Re(c_H) \frac{v^2}{\Lambda^2} \right) \\ &= \bar{t}t h \frac{m_t}{v} \left(1 + \frac{\Re(c_H)}{\sqrt{2}} \frac{v}{m_t} \frac{v^2}{\Lambda^2} \right) + \mathcal{O}\left(\frac{1}{\Lambda^4}\right). \end{aligned} \quad (3.42)$$

The SM amplitude for Higgs production by gluon fusion can then be multiplied by this last factor to take the effect of \mathcal{O}_H into account.

The operators \mathcal{O}_{HR} , \mathcal{O}_{HL} and $\mathcal{O}_{HL}^{(3)}$ do not have any contribution to this process. The vertex $ht\bar{t}$ comes from the sum of those operators and of their hermitian conjugates². The relevant part of the operators can thus be written as

$$\partial_\mu (H^\dagger H) \bar{t} \gamma^\mu P_{R,L} t \propto (H^\dagger H) \partial_\mu \frac{(J^\mu \pm J_5^\mu)}{2} \propto (H^\dagger H) \partial_\mu J_5^\mu \quad (3.43)$$

because the vectorial current is conserved. Their contributions to Higgs production through the effective operator $H^\dagger H G^{\mu\nu} \tilde{G}_{\mu\nu}$, generated by the anomaly, vanish due to parity.

3.4 Z decay constraints

The operators introduced so far are not constrained at the tree-level by the precise LEP measurements. In particular, they are not constrained by the oblique parameters since they do not involve the electroweak bosons. However, four-fermion operators can modify the Z couplings at one-loop. Since all relevant four-fermion operators can be

²This combination is invariant under custodial symmetry and can thus not be constrained by the ρ parameter.

written as a product of two currents, the amplitude of the diagram depicted in Fig. 3.7 can be written as

$$M = c_i g_{R/L} J_\mu^q \epsilon_\nu(q) \int \frac{d^4 k}{(2\pi)^2} \text{Tr} \left[i\gamma^\nu \gamma_\pm \frac{i}{\not{k} - m} i\gamma^\mu \gamma_\pm \frac{i}{\not{k} - \not{q} - m} \right] \quad (3.44)$$

where $g_{R/L}$ is the Z coupling to the right/left-handed top which should be chosen accordingly to the first chirality projector in the integral. The second chirality projector comes from the top current in the considered operator. The amplitude for a color octet current vanishes due to color conservation. If the two projectors are identical,

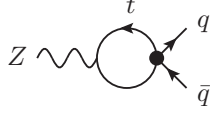


Figure 3.7: One-loop correction to the Z couplings to the quark q from the four-fermion operators.

the integral is

$$\begin{aligned} I_1 &= 2 \int \frac{d^4 k}{(2\pi)^2} \frac{k^\mu (k-q)^\nu + k^\nu (k-q)^\mu - k(k-q)\eta^{\mu\nu}}{(k^2 - m_t^2) \left((k-q)^2 - m_t^2 \right)} \\ &= 2 \int_0^1 dx \int \frac{d^4 p}{(2\pi)^2} \frac{2p^\mu p^\nu - p^2 \eta^{\mu\nu} + (2q^\nu q^\mu - \eta^{\mu\nu} q^2) x(x-1)}{(p^2 - \Delta)^2} \\ &= \frac{i}{(4\pi)^2} \int_0^1 dx \ln \left(\frac{\Lambda_{cut}^2}{\Delta} \right) \left[-2\Delta \eta^{\mu\nu} + 2(2q^\nu q^\mu - \eta^{\mu\nu} q^2) x(x-1) \right] \end{aligned} \quad (3.45)$$

where $p = k - qx$ and $\Delta = m_t^2 + q^2 x(x-1)$. In the last step, we have neglected the finite terms. In the limit $m_t^2 \gg q^2 = m_Z^2$,

$$I_1 = \frac{i}{(4\pi)^2} \ln \left(\frac{\Lambda^2}{m_t^2} \right) \left[-2m_t^2 \eta^{\mu\nu} - \frac{2}{3} q^\mu q^\nu \right]. \quad (3.46)$$

The term proportional to q^ν vanishes for on-shell Z boson after summing over the polarizations. If the two projectors are different, the integral is

$$\begin{aligned}
I_2 &= \int \frac{d^4k}{(2\pi)^2} \frac{2m_t^2 \eta^{\mu\nu}}{(k^2 - m_t^2) \left((k - q)^2 - m_t^2 \right)} \\
&= \int_0^1 dx \int \frac{d^4p}{(2\pi)^2} \frac{2m_t^2 \eta^{\mu\nu}}{(p^2 - \Delta)^2} \\
&= \frac{i}{(4\pi)^2} \int_0^1 dx 2m_t^2 \eta^{\mu\nu} \ln \left(\frac{\Lambda^2}{\Delta} \right)
\end{aligned} \tag{3.47}$$

Neglecting again the Z mass, we obtain

$$I_2 = \frac{i}{(4\pi)^2} 2m_t^2 \eta^{\mu\nu} \ln \left(\frac{\Lambda_{cut}^2}{m_t^2} \right). \tag{3.48}$$

The $Z \rightarrow b\bar{b}$ is the most precisely measured branching ratio [9], *i.e.*

$$Br(Z \rightarrow b\bar{b}) = 15.12 \pm 0.05\%. \tag{3.49}$$

At the end, only the operators $\mathcal{O}_L^{(1)}$ and $\mathcal{O}_B^{(1)}$ correct the bottom quark left coupling through a top loop,

$$\delta_t g_L^b = 2(g_R - g_L) \left[2c_L^{(1)} - c_B^{(1)} \right] \frac{m_t^2}{\Lambda^2} \frac{1}{(4\pi)^2} \ln \frac{\Lambda_{cut}^2}{m_t^2}. \tag{3.50}$$

For $\Lambda = \Lambda_{cut} = 1 \text{ TeV}$,

$$Br(Z \rightarrow b\bar{b}) \approx Br(Z \rightarrow b\bar{b})_{SM} (1 + 0.003 [2c_L^{(1)} - c_B^{(1)}]). \tag{3.51}$$

Consequently, $c_L^{(1)}$ and $c_B^{(1)}$ should be at most of order one. The $Zb\bar{b}$ couplings do not receive contributions of the color octet operators due to a top loop. However, they also modify the $Zb\bar{b}$ coupling when a bottom quark is in the loop. In this case, the mass of the Z cannot be neglected anymore and will take more or less the place of the top mass. Taking into account the color factor and the integration over the Feynman parameter, we obtain

$$\delta_b g_L^b = \frac{8}{27} g_L c_L^{(8)} \frac{m_Z^2}{\Lambda^2} \frac{1}{(4\pi)^2} \ln \frac{\Lambda_{cut}^2}{m_Z^2} \tag{3.52}$$

or with the same numerical values as above

$$Br(Z \rightarrow b\bar{b}) \approx Br(Z \rightarrow b\bar{b})_{SM} (1 - 0.00012 c_L^{(8)}). \tag{3.53}$$

$c_L^{(8)}$ can thus be easily as big as 25. The last operator, $\mathcal{O}_B^{(8)}$ does not contribute because its color singlet part is as a product of two densities. The corresponding integral is then proportional to q^ν .

The operators in Eqs. (3.2) to (3.4) do not modify the couplings of the Z to the light quarks since they are color octets. However, both color octet and singlet can be present in the case of a t -channel exchange for example. Nevertheless, the constraints are weaker since the associated decay widths are less precisely measured [9] and the coefficients of those operators are of order one rather than order g_ρ^2 .

Chapter 4

Phenomenology of top pair productions



Based on

C. Degrande, J.-M. Gerard, C. Grojean, F. Maltoni, and G. Servant, "Non-resonant New Physics in Top Pair Production at Hadron Colliders", *JHEP*, vol. 03, p. 125, 2011, 1010.6304.

C. Degrande, J.-M. Gerard, C. Grojean, F. Maltoni, and G. Servant, "An effective approach to same sign top pair production at the LHC and the forward-backward asymmetry at the Tevatron", 2011, 1104.1798.

Tevatron has brought top physics from discovery [7, 8] to precision era. In fact, the D0 and CDF collaborations have already provided an impressive list of measurements

of the top properties (see for example Ref. [118] for a recent review). Tevatron data have been intensively used to put constraints on new physics like new resonances or direct production of new states decaying into top quarks. In this chapter, we complement those studies by constraining the new operators of the effective Lagrangians of Chap. 3. Only quark-antiquark annihilation can be probed at the Tevatron because this process is dominant in proton antiproton collisions. As a consequence, LHC opens the access to an almost unexplored territory, namely top pair productions by gluon fusion. Moreover, new processes like associated top pair productions might show up due to the higher energy of the collisions.

In this chapter, we compute several key observables for opposite sign top quark pair production. Those results together with both the Tevatron and the first LHC measurements are used to constrain the parameter space of our effective approach. The New Physics (NP) effects at the LHC are then analysed in the allowed region. Secondly, a similar analysis is done for the so far unobserved same sign top pair production. In particular, the production rate at the LHC, necessary to estimate the discovery potential, is given. Finally, the LHC signals for top pair production in association with two top or bottom quarks as well as with a Higgs are investigated.

4.1 Opposite sign top pair production

4.1.1 Partonic differential cross-sections

As already mentioned, top pair production is calculated at the same order in $1/\Lambda$ as the Lagrangian in Eq. (3.19)

$$|M|^2 = |M_{SM}|^2 + 2\Re(M_{SM}M_{NP}^*) + \mathcal{O}(\Lambda^{-4}), \quad (4.1)$$

where M_{NP} represents the matrix element of all the (new physics) dimension-six operators introduced in Section 3.1. The $\mathcal{O}(\Lambda^{-4})$ contributions can be divided into to part :

- The interference of the SM with either dimension-eight operators or with diagram with two effective vertices coming from dimension-six operators.
- The squared amplitude of all dimension-six operators, including non interfering ones like $\mathcal{O}_d^{(8)}$ or color singlets.

From the Lagrangian in Eq. (3.19), the two parton-level cross-sections for $t\bar{t}$ production at $\mathcal{O}(\Lambda^{-2})$ follow from the Feynman diagrams depicted in Fig. A.1 and A.2 of

App. A.2. Their expressions are :

$$\begin{aligned} \frac{d\sigma}{dt}(q\bar{q} \rightarrow t\bar{t}) &= \frac{d\sigma_{SM}}{dt} \left(1 + \frac{c_{Vv} \pm \frac{c'_{Vv}}{2}}{g_s^2} \frac{s}{\Lambda^2} \right) \\ &\quad + \frac{1}{\Lambda^2} \frac{\alpha_s}{9s^2} \left(\left(c_{Aa} \pm \frac{c'_{Aa}}{2} \right) s(\tau_2 - \tau_1) + 4g_s c_{hg} \sqrt{2} v m_t \right) \end{aligned} \quad (4.2)$$

$$\frac{d\sigma}{dt}(gg \rightarrow t\bar{t}) = \frac{d\sigma_{SM}}{dt} + \sqrt{2} \alpha_s g_s \frac{v m_t}{s^2} \frac{c_{hg}}{\Lambda^2} \left(\frac{1}{6\tau_1\tau_2} - \frac{3}{8} \right) \quad (4.3)$$

where the upper (lower) sign is for the up (down) quarks and

$$\frac{d\sigma_{SM}}{dt}(q\bar{q} \rightarrow t\bar{t}) = \frac{4\pi\alpha_s^2}{9s^2} \left(\tau_1^2 + \tau_2^2 + \frac{\rho}{2} \right) \quad (4.4)$$

$$\frac{d\sigma_{SM}}{dt}(gg \rightarrow t\bar{t}) = \frac{\pi\alpha_s^2}{s^2} \left(\frac{1}{6\tau_1\tau_2} - \frac{3}{8} \right) \left(\rho + \tau_1^2 + \tau_2^2 - \frac{\rho^2}{4\tau_1\tau_2} \right) \quad (4.5)$$

$$\text{with } \tau_1 = \frac{m_t^2 - t}{s}, \quad \tau_2 = \frac{m_t^2 - u}{s}, \quad \rho = \frac{4m_t^2}{s}. \quad (4.6)$$

The Mandelstam parameter t is related, in the $t\bar{t}$ center-of-mass frame, to the angle θ between the momenta of the incoming parton and the outgoing top quark by ($\beta = \sqrt{1 - \frac{4m_t^2}{s}}$)

$$m_t^2 - t = \frac{s}{2} (1 - \beta \cos \theta). \quad (4.7)$$

All the contributions to the $t\bar{t}$ differential cross-section but the one proportional to $c_{Aa} \pm \frac{c'_{Aa}}{2}$ are invariant under $\theta \rightarrow \pi - \theta$.

Similar results have already been derived in the literature. For instance, these cross-sections were recently fully computed in Ref. [93] and consistent with our expressions with the identifications given in Table 4.1. This non exhaustive table also gives the correspondences with respect to some other recent works [86–88, 119]. Note that the contribution of the chromomagnetic operator \mathcal{O}_{hg} was extensively discussed in the literature [81–84] and recently revisited for both processes in Ref. [88, 89].

As can be seen from Eqs. (4.5) and (4.3), the new physics and the SM contributions for gluon fusion have a common factor. In fact, this common factor is what is mainly responsible for the shape of the distributions of the SM. This is the reason why, as we will stress again in the following, the operator \mathcal{O}_{hg} can hardly be distinguished from the SM in gluon fusion.

	Ref. [93]	Ref. [86]	Ref. [119]	Ref. [87]	Ref. [88]
c_{hg}	$2C_{tG}$	$g_1 g_s$			$\frac{1}{2} C_{uG\phi}^{33}$
c_{Vv}	$\frac{1}{4} (C_u^1 + C_u^2 + C_d^1 + C_d^2)$	$-g_2 g_s^2 (*)$	$\frac{g_s^2}{4} (\kappa_R^u + \kappa_R^d + \kappa_L^u + \kappa_L^d) (*)$	$\frac{g_s^2}{2} (C_1 + C_2)$	
c_{Aa}	$\frac{1}{4} (C_u^1 - C_u^2 + C_d^1 - C_d^2)$		$\frac{g_s^2}{4} (\kappa_R^u + \kappa_R^d + \kappa_L^u + \kappa_L^d) (*)$	$\frac{g_s^2}{2} (C_1 - C_2)$	
c'_{Vv}	$\frac{1}{2} (C_u^1 + C_u^2 - C_d^1 - C_d^2)$		$\frac{g_s^2}{2} (\kappa_R^u - \kappa_R^d + \kappa_L^u - \kappa_L^d) (*)$		
c'_{Aa}	$\frac{1}{2} (C_u^1 - C_u^2 - C_d^1 + C_d^2)$		$\frac{g_s^2}{2} (\kappa_R^u - \kappa_R^d + \kappa_L^u - \kappa_L^d) (*)$		

Table 4.1: Dictionary between our parameters and those used in recent papers on the subject. They all agree up to a sign for those that are labeled by a (*). For Ref. [93], $C_{qq}^{(8,3)} = c_{Qq}^{(8,3)}$. Blank entries mean that the corresponding operators were not considered.

Equation (4.2) shows that only two kinds of four-fermion operators actually contribute to the differential cross-section after averaging over the final state spins:

- the first one is responsible for the even part in the scattering angle proportional to $c_{Vv} \pm \frac{c'_{Vv}}{2}$

$$\bar{t}\gamma^\mu T^A t \bar{q}\gamma^\mu T^A q \quad (4.8)$$

where here t and $q = u, d$ stand for the full 4-component Dirac spinor;

- the second one is responsible for the odd part in the scattering angle proportional to $c_{Aa} \pm \frac{c'_{Aa}}{2}$

$$\bar{t}\gamma^\mu \gamma_5 T^A t \bar{q}\gamma^\mu \gamma_5 T^A q. \quad (4.9)$$

4.1.2 Total cross-section

LHC–Tevatron complementarity

Since the dependence on c_{Aa} and c'_{Aa} vanishes after the integration over the kinematical variable t , the total cross-section only depends on the three parameters c_{hg} , c_{Vv} and c'_{Vv} . Moreover, the $t\bar{t}$ production by gluon fusion only depends on the coefficient of the operator \mathcal{O}_{hg} . Our results for $t\bar{t}$ production are obtained by the convolution of the analytic differential cross-section of Eqs. (4.2) and (4.3) with the pdf (taking CTEQ6L1 [120]). We have also implemented the new vertices in MadGraph [121] and used them to validate our results. At leading order, we have

— at the LHC ($\sqrt{s} = 14$ TeV):

$$\sigma(gg \rightarrow t\bar{t})/\text{pb} = 466_{-103}^{+146} + (127_{-23}^{+31}) c_{hg} \left(\frac{1 \text{ TeV}}{\Lambda}\right)^2, \quad (4.10)$$

$$\begin{aligned} \sigma(q\bar{q} \rightarrow t\bar{t})/\text{pb} &= 72_{-12}^{+16} + [(15_{-1}^{+2}) c_{Vv} + (17_{-2}^{+3}) c_{hg} \\ &\quad + (1.32_{-0.12}^{+0.12}) c'_{Vv}] \left(\frac{1 \text{ TeV}}{\Lambda}\right)^2, \end{aligned} \quad (4.11)$$

$$\begin{aligned} \sigma(pp \rightarrow t\bar{t})/\text{pb} &= 538_{-115}^{+162} + [(15_{-1}^{+2}) c_{Vv} + (144_{-25}^{+34}) c_{hg} \\ &\quad + (1.32_{-0.12}^{+0.12}) c'_{Vv}] \left(\frac{1 \text{ TeV}}{\Lambda}\right)^2. \end{aligned} \quad (4.12)$$

— at the LHC ($\sqrt{s} = 7$ TeV):

$$\begin{aligned} \sigma(pp \rightarrow t\bar{t})/\text{pb} &= 94_{-17}^{+22} + [(4.5_{-0.6}^{+0.7}) c_{Vv} + (25_{-5}^{+7}) c_{hg} \\ &\quad + (0.48_{-0.056}^{+0.068}) c'_{Vv}] \left(\frac{1 \text{ TeV}}{\Lambda}\right)^2. \end{aligned} \quad (4.13)$$

— at the Tevatron ($\sqrt{s} = 1.96$ TeV):

$$\sigma(gg \rightarrow t\bar{t})/\text{pb} = 0.35_{-0.12}^{+0.20} + (0.10_{-0.03}^{+0.05}) c_{hg} \left(\frac{1 \text{ TeV}}{\Lambda}\right)^2, \quad (4.14)$$

$$\begin{aligned} \sigma(q\bar{q} \rightarrow t\bar{t})/\text{pb} &= 5.80_{-1.49}^{+2.21} + [(0.87_{-0.16}^{+0.23}) c_{Vv} + (1.34_{-0.30}^{+0.42}) c_{hg} \\ &\quad + (0.31_{-0.06}^{+0.08}) c'_{Vv}] \left(\frac{1 \text{ TeV}}{\Lambda}\right)^2, \end{aligned} \quad (4.15)$$

$$\begin{aligned} \sigma(pp \rightarrow t\bar{t})/\text{pb} &= 6.15_{-1.61}^{+2.41} + [(0.87_{-0.16}^{+0.23}) c_{Vv} + (1.44_{-0.33}^{+0.47}) c_{hg} \\ &\quad + (0.31_{-0.06}^{+0.08}) c'_{Vv}] \left(\frac{1 \text{ TeV}}{\Lambda}\right)^2. \end{aligned} \quad (4.16)$$

Numerically, the contribution from the isospin-1 sector (c'_{Vv}) is suppressed compared to the contribution of the isospin-0 sector (c_{Vv}) and this suppression is more effective at the LHC than at the Tevatron. This is due to the fact that, at Tevatron, the top pair production by up-quark annihilation is between 5 and 6 times bigger than by down-quark annihilation. At the LHC, this ratio is reduced to 1.4 only. First, in a model independent analysis, we shall neglect the contribution from the isospin-1 sector since it is subdominant. They will be included in Sect. 4.1.6 for constraining the heavy particle exchange models.

The measurements of the total cross-section at the Tevatron and at the LHC are complementary as shown in Fig. 4.1. As expected, the LHC $pp \rightarrow t\bar{t}$ total cross-section strongly depends on c_{hg} . Consequently, it can be used to constrain directly the allowed range for c_{hg} . On the contrary, the corresponding Tevatron cross-section depends on both c_{hg} and c_{Vv} and constrains thus a combination of these parameters.

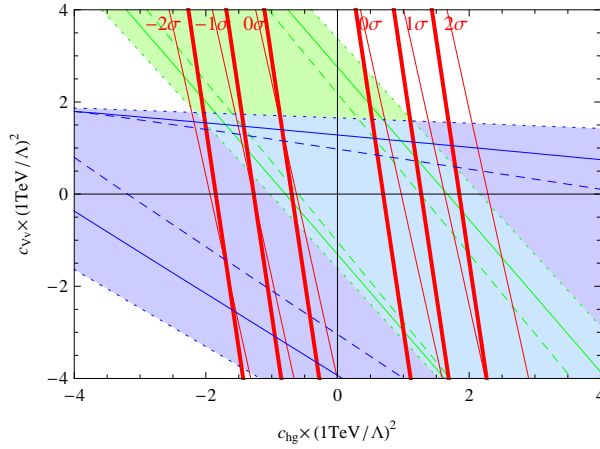


Figure 4.1: Region allowed by the Tevatron constraints (at 2σ) for $c'_{Vv} = 0$. The green region is allowed by the total cross-section measurement. The blue region is consistent with the $t\bar{t}$ invariant mass shape. The thin red lines show the limits set by the LHC at 7 TeV. The thick red lines show the limits that can be set by the LHC at 14 TeV (thick line) as soon as the precision on the top pair cross-section reaches 10%. The “ 0σ ” line delimits the region where the new physics contributions are smaller than the theoretical error on the SM cross-section. The dashed ($\mu_F = \mu_R = \frac{m_t}{2}$), dotted ($\mu_F = \mu_R = 2m_t$) and solid lines ($\mu_F = \mu_R = m_t = 174.3$ GeV) show the estimated theoretical uncertainties.

In Fig. 4.1, we use the NLO+NLL predictions for the SM cross-section of Eqs. (1.56) and (1.55) and combine the errors linearly. For the experimental values, we use the CDF and CMS combinations of all channels given in Eqs. (1.52) and (1.53) respectively and combine the errors quadratically. At 14 TeV, we assume that the observed value is the central value of the NLO+NLL prediction [28],

$$\sigma_{\text{th}}^{14 \text{ TeV}} = 832_{-78}^{+75}(\text{scale})_{-27}^{+28}(\text{pdf}) \text{ pb.} \quad (4.17)$$

with a experimental error of 10% since no measurement is available yet. Due to the rather large uncertainties on the theoretical normalization, the region allowed by the total cross-section measurement remains large. Even if the experimental precision

becomes very good, a rather large allowed region will remain due to the theoretical uncertainties. An improvement of the theoretical prediction for top pair production in SM is necessary to reduce the allowed region. The theoretical uncertainties for the new physics part are estimated by changing the factorisation scale μ_F and the renormalisation scale μ_R . The errors from the pdf are not computed. The errors on the exclusion regions at the LHC are not shown but are about 20% and are symmetric (10% on each side of the allowed region). A summary the exclusion regions is shown in Fig. 4.2.

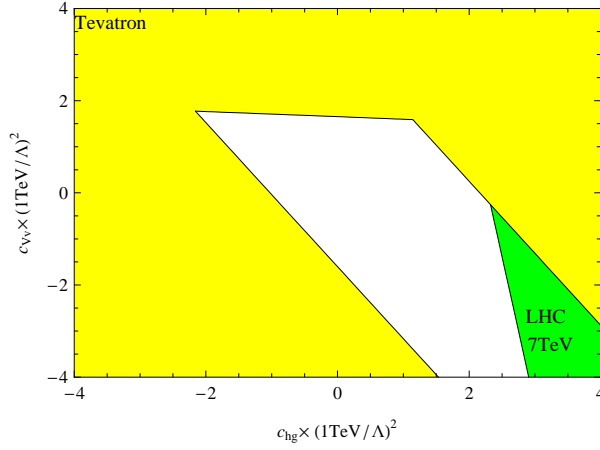


Figure 4.2: Summary plot (defining the exclusion region at 2σ). The yellow region is excluded by the Tevatron. The green region is excluded by LHC at 7 TeV.

The absence of a large deviation in the measurement of the cross-section at the Tevatron implies $c_{Vv} \approx -1.6 c_{hg}$ if the scale of new physics is rather low. From the discussion at the end of the classification of Section 3.2.1, it would mean that c_{hg} and c_{Vv} are both of the $\mathcal{O}(g_\rho^0)$, indicating that either both chiralities of the top or one chirality of the top and the Higgs boson are composite fields. Compared to the SM prediction, this would give a maximum deviation of the order of 25% for the $t\bar{t}$ production cross-section at the LHC when $c_{hg} \left(\frac{1\text{TeV}}{\Lambda}\right)^2 \sim 2$.

Domain of validity of the results

Our calculation is performed at order $\mathcal{O}(\Lambda^{-2})$ as we keep only the interference term between the dimension-six and the Standard Model and we neglect any contribution suppressed by higher power of Λ . The validity of our results is thus limited to values

of new coupling parameters and Λ satisfying

$$\sigma|_{\mathcal{O}(\Lambda^{-2})} \gtrsim \kappa \sigma|_{\mathcal{O}(\Lambda^{-n})} \quad (4.18)$$

where $n > 2$ and κ should be at least 2 in order to keep higher order the correction below 50%. We have estimated the size of the $\mathcal{O}(\Lambda^{-4})$ contributions by computing the squared amplitudes of each dimension-six operators with MadGraph and we find at the LHC for 14 TeV:

$$\sigma|_{\mathcal{O}(\Lambda^{-4})} \sim \sigma_{NP^2} = (22.5 c_{hg}^2 + 3.7 c_{Vv}^2) \times \left(\frac{1 \text{ TeV}}{\Lambda}\right)^4 \text{ pb} \quad (4.19)$$

and, at the Tevatron,

$$\sigma|_{\mathcal{O}(\Lambda^{-4})} \sim \sigma_{NP^2} = (0.103 c_{hg}^2 + 0.060 c_{Vv}^2) \times \left(\frac{1 \text{ TeV}}{\Lambda}\right)^4 \text{ pb} \quad (4.20)$$

Therefore, at the Tevatron, our results apply to a region of parameter space bounded by $|c_i| \left(\frac{1 \text{ TeV}}{\Lambda}\right)^2 \lesssim 14/\kappa$. At the LHC, since the center-of-mass energy is larger, the reliable region shrinks to $|c_{hg}| \left(\frac{1 \text{ TeV}}{\Lambda}\right)^2 \lesssim 6/\kappa$ and $|c_{Vv}| \left(\frac{1 \text{ TeV}}{\Lambda}\right)^2 \lesssim 4/\kappa$. Nevertheless, outside this region, the effects of the new physics should remain more or less of the same order excepted of course if there is some huge cancellation. Moreover, the cross-section is expected to be harder and harder as operators of higher dimensions are included in the effective Lagrangian. Ultimately some resonance threshold will be reached, leading to a radically different cross-section than the one predicted by the Standard Model.

It was found in Ref. [122] that for the four-fermion operators, there are $\mathcal{O}(\Lambda^{-4})$ corrections from non-interfering contributions that can be almost as large as the $\mathcal{O}(\Lambda^{-2})$ interfering contributions at the LHC if $\Lambda \sim 1 \text{ TeV}$. However, at the LHC, these four-fermion operators give small contributions compared to the chromomagnetic operator. So we can conclude that including non-interfering four-fermion operators will not change much our numerical analysis.

Finally, to have an idea on how heavy the particles associated with new physics should be to allow an effective field theory treatment at the LHC, we compare in Fig. 4.3 the correction to the SM cross-section at the LHC due to a W' (whose coupling to d and t quarks is 1) and the correction due to the corresponding effective operators ($C_{Vv} = -1/2$, $C'_{Vv} = -1$, $\Lambda = M_{W'}$). This plot shows that for $M_{W'} \gtrsim 1.5 \text{ TeV}$ the effective operators are a very good approximation (up to a few percents) at the LHC, although this depends on the coupling. We will show in Fig. 4.7 that a similar conclusion is reached at the Tevatron. Consequently, the resonance models cannot be constrained in our effective approach since the exclusion regions in Fig. 4.2 correspond, for example, to a relatively light resonance ($M \lesssim \text{TeV}$) with a coupling of order 1.

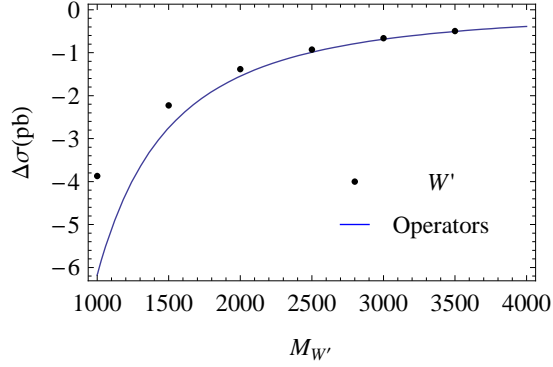


Figure 4.3: Correction to the SM cross-section at the LHC due to a W' and comparison with the effective field theory approach.

Comments on the non top-philic operators

The non top-philic operators only affect gluon fusion. Consequently, their effects at the Tevatron are very small,

$$\delta\sigma(pp \rightarrow t\bar{t})/\text{pb} = [0.019c_G - 0.0056c_{hG}] \left(\frac{1 \text{ TeV}}{\Lambda}\right)^2 \quad (4.21)$$

where the mass of the Higgs has been fixed at 180 GeV for the computation of the c_{hG} coefficient. However, even at the LHC (14 TeV), their contributions remain rather small,

$$\delta\sigma(pp \rightarrow t\bar{t})/\text{pb} = [38c_G - 8.8c_{hG}] \left(\frac{1 \text{ TeV}}{\Lambda}\right)^2. \quad (4.22)$$

On the one hand, it is known that it is very hard to see the interference of QCD amplitude with the Higgs boson at the LHC [78]. This contribution remains small even if we increase by about an order of magnitude the gluon-gluon-Higgs vertex. On the other hand, the interference between the \mathcal{O}_G operator and the SM is proportional $\beta^2 m_t^2$ because the color octet vector part of the SM amplitude is of the order β^2 [123]. Consequently, its contribution vanishes at threshold and is not enhanced at high energy. On the contrary, the amplitude squared of this operator is large because the β suppression disappears for \mathcal{O}_G and the cross-section grows like s . So quark pair production does not seem to be the best place to look for \mathcal{O}_G . Those results have been obtained with MadGraph 5 [124] for $\mu_R = \mu_F = m_t$ and using CTEQ6L1 pdf set [120]. The model has been automatically generated from a FeynRules [125] model using UFO [126] and ALOHA [127]. The FeynRules model has also been used to check the analytic results with Ref. [93] in FeynArts/FormCalc [70, 128].

To sum up, the contributions of the non top-philic operators are numerically small. Consequently, our analysis would not change drastically even if they would be included.

4.1.3 $t\bar{t}$ invariant-mass, p_T and η distributions

It was shown in Ref. [86] that the operators \mathcal{O}_{hg} and \mathcal{O}_{Rv} can modify the invariant mass distribution at the Tevatron without drastically affecting the total cross-section, although no constraint was derived explicitly. We use in this section the latest CDF data [30] to further constrain new physics. See also Ref. [119] for a similar study on the $\bar{L}L\bar{L}L$ and $\bar{R}R\bar{R}R$ operators with the first data [29]. Since we have already used the measured total cross-section to constrain the parameter space here we only employ the shape information.

For the sake of simplicity, in our analysis we assume that the measured values m_i are normally distributed around the corresponding theoretical predictions t_i with a standard deviation σ_i given by their errors. Errors coming from different sources have been combined quadratically. We multiply by a common free coefficient ζ the theoretical prediction to get rid of the normalization constraint. In practice, we use the best value for ζ . The quantity

$$\sum_{i=1}^n \frac{(m_i - \zeta t_i)^2}{\sigma_i^2} \quad (4.23)$$

is then distributed as a χ^2 with $n - 1$ degrees of freedom. The theoretical predictions are obtained by integrating Eqs. (4.2) and (4.3) over the scattering angle. The explicit formulas are given in App. A.3. The SM distribution is computed at the tree level and normalized to the NLO+NLL result. The errors on the contribution of the operators are estimated by changing the factorization and renormalization scales. We take into account the bins between 350 GeV and 600 GeV ($n = 13$). We cannot use the full distribution since our calculation only makes sense if $|g_{NP}| \frac{s}{\Lambda^2} \ll 1$. So $m_{t\bar{t}} \lesssim 1$ TeV if $\Lambda \sim 1$ TeV. The bound $m_{t\bar{t}} < 600$ GeV seems reasonable since, even in the region $|g_{NP}| (\frac{1\text{TeV}}{\Lambda})^2 \sim 4$, the estimation of the $1/\Lambda^4$ corrections from $|M_{NP}|^2$ are a bit less than 50% of the $1/\Lambda^2$ corrections. For the next bins, these next order corrections become too large.

In Fig. 4.1, we show the region consistent at 95% C.L. with the $t\bar{t}$ invariant mass constraints reported in Ref. [30]. As expected, the invariant mass shape is sensitive to a very different combination of the parameters than the total cross-section. The interferences with the operators \mathcal{O}_{Rv} and \mathcal{O}_{Lv} actually grow faster than the SM by a factor s , which is not the case for \mathcal{O}_{hg} . The shape depends thus strongly on c_{Vv} . The Tevatron measurement already excludes the region $c_{Vv} (\frac{1\text{TeV}}{\Lambda})^2 \gtrsim +2$.

The good constraints obtained with the invariant mass at the Tevatron suggest to look for similar effects at the LHC. However, at the LHC, the top pair is mainly produced by gluon fusion and the contributions of \mathcal{O}_{Rv} and \mathcal{O}_{Lv} are much smaller than the SM contribution. Moreover, the effect of these operators becomes important at high energy where our expansion breaks down. Only \mathcal{O}_{hg} has an important contribution. However, this contribution has a similar shape as that of the SM for reasons already mentioned in Section 4.1.1 and confirmed by Fig. 4.4. The effects of the new operators will be much harder to be seen in the $m_{t\bar{t}}$ distribution but also in the p_T and η at the LHC, as shown in Fig. 4.4.

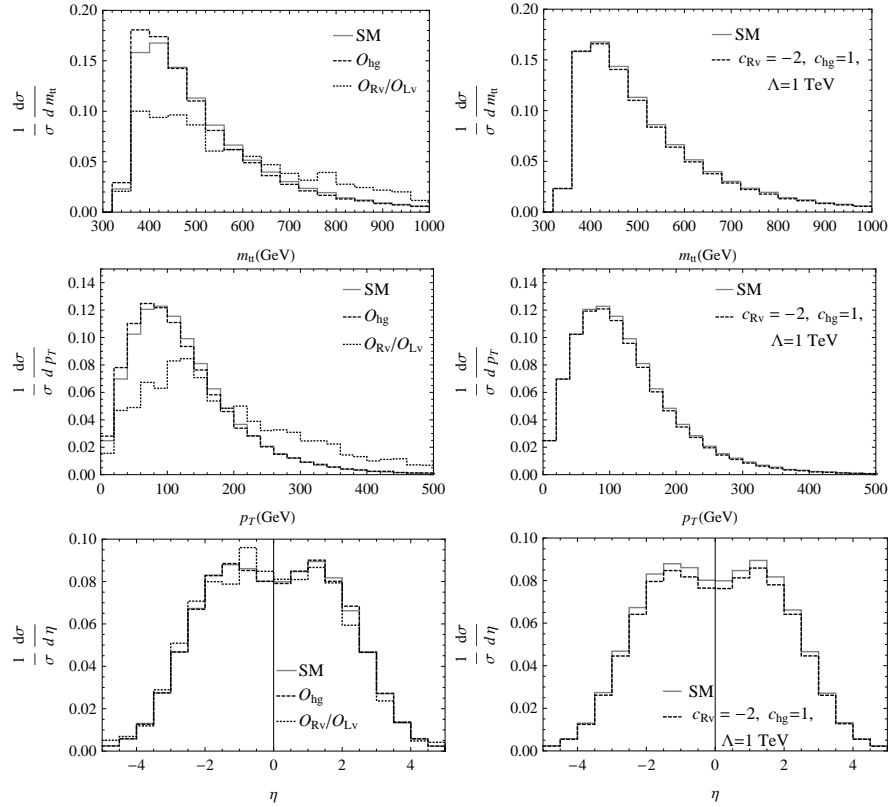


Figure 4.4: On the left: normalized differential cross-sections of the SM, $\frac{1}{\sigma_{SM}} \frac{d\sigma_{SM}}{dX}$, and of the interferences of the SM with \mathcal{O}_{hg} and with \mathcal{O}_{Rv} and \mathcal{O}_{Lv} , $\frac{1}{\sigma_{NP}} \frac{d\sigma_{NP}}{dX}$, as a function of $m_{t\bar{t}}$, p_T and η for the LHC at 14TeV. On the right: normalized cross-section of the SM, $\frac{1}{\sigma_{SM}} \frac{d\sigma_{SM}}{dX}$, and of the SM and the interference with the new physics, $\frac{1}{\sigma_{SM} + \sigma_{NP}} \frac{d\sigma_{SM} + \sigma_{NP}}{dX}$ (for $c_{hg} = 1$, $c_{Vv} = -2$ and $\Lambda = 1$ TeV).

4.1.4 Forward-backward asymmetry

As we saw in Sect. 1.3, the forward-backward asymmetry measured at the Tevatron is well above its predicted value in the Standard Model. While a thorough investigation within the SM and in particular of the impact of the unknown higher order QCD corrections would be certainly welcome, it is tempting to explain this discrepancy as the effect of new physics in various models [87, 108–110, 119, 129–136]. An attractive, simple and model-independent alternative is to consider the low energy effective field theory of Sect. 3.1. A first obvious observation is that no asymmetry can arise in gluon fusion in which the initial state is symmetric. From Eq. (4.2), we see that the asymmetry can only depend on c_{Aa} and c'_{Aa} . Since their contribution is a purely odd function of the scattering angle θ defined in Eq. (4.7), these coefficients are only constrained by the asymmetry and not by the total cross-section nor the invariant mass distribution. After integration with the pdf, we find in the lab frame

$$\begin{aligned} \sigma(\cos\theta_t > 0) - \sigma(\cos\theta_t < 0) &= (0.235^{+0.067}_{-0.042} c_{Aa} \\ &\quad + 0.088^{+0.024}_{-0.016} c'_{Aa}) \times \left(\frac{1 \text{ TeV}}{\Lambda}\right)^2 \text{ pb} \end{aligned} \quad (4.24)$$

where again the errors are estimated by varying the factorization and renormalization scales. Assuming that the total cross-section is given by Eq. (1.55), the corrections to the SM asymmetry can be expressed as

$$\delta A_{FB}^{\text{lab}} = (0.0342^{+0.016}_{-0.009} c_{Aa} + 0.0128^{+0.0064}_{-0.0036} c'_{Aa}) \times \left(\frac{1 \text{ TeV}}{\Lambda}\right)^2 \quad (\text{Tevatron}). \quad (4.25)$$

We see once again that the leading contribution comes from the isospin-0 operators. The region of parameter space in the (c_{Aa}, Λ) plane that can explain the A_{FB} for $c'_{Aa} = 0$ is shown in Fig. 4.5.

Since all the observables asymmetric in the scattering angle only depend on those two parameters, a more precise determination of the parameters (shown on Fig. 4.5) can be made from the measured asymmetry in the high invariant mass region (1.60). From the effective Lagrangian (3.19), we obtain

$$\delta A_{FB}^{t\bar{t}}(M_{t\bar{t}} \geq 450 \text{ GeV}) = (0.087^{+10}_{-9} c_{Aa} + 0.032^{+4}_{-3} c'_{Aa}) \left(\frac{1 \text{ TeV}}{\Lambda}\right)^2 \quad (4.26)$$

$$\delta A_{FB}^{t\bar{t}}(M_{t\bar{t}} < 450 \text{ GeV}) = (0.023^{+3}_{-1} c_{Aa} + 0.0081^{+6}_{-4} c'_{Aa}) \left(\frac{1 \text{ TeV}}{\Lambda}\right)^2. \quad (4.27)$$

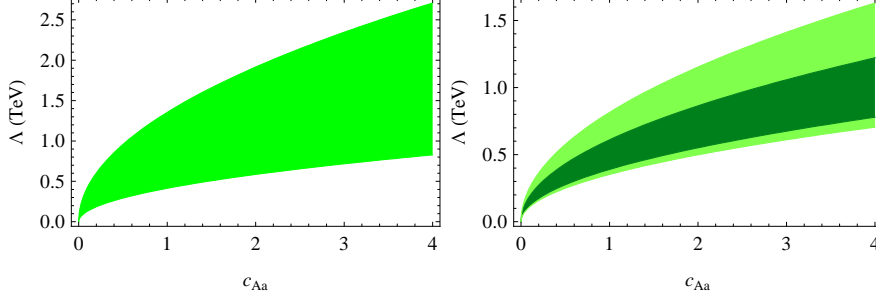


Figure 4.5: On the left, the region of parameter space that can explain the A_{FB} measurement at the Tevatron at one σ for $c'_{Aa} = 0$. On the right, the region of parameter space that can explain the $A_{FB}(m_{t\bar{t}} \geq 450 \text{ GeV})$ measurement at the Tevatron at one (dark green) and two (light green) σ for $c'_{Aa} = 0$.

In our approach, the asymmetry increases with the $t\bar{t}$ center of mass energy consistently with the CDF observations. Those corrections to the asymmetries have been obtained using only the SM for the symmetric total cross-section above or below 450 GeV. The invariant mass distribution measurement, consistent with the SM prediction, tells us that it is at least a reliable approximation. However, the other four-fermion operators might slightly change this rise by modifying the invariant mass distribution.

As an illustration of the simplicity of such an approach, we consider the forward-backward asymmetry at LHC. In this case the symmetry of the pp collision and the dominance of the gg channel for $t\bar{t}$ make it particularly challenging. A possibility is to build the so-called central rapidity asymmetry

$$A_C(y_C) \equiv \frac{\sigma_t(|y| < y_C) - \sigma_{\bar{t}}(|y| < y_C)}{\sigma_t(|y| < y_C) + \sigma_{\bar{t}}(|y| < y_C)} \quad (\text{lab frame}), \quad (4.28)$$

where y_C is the rapidity cut defining the ‘‘centrality’’ of an event. The value $y_C = 1$ has been shown to be close to optimal in Ref. [33]. A straightforward calculation using $c_{Aa} \left(\frac{1 \text{ TeV}}{\Lambda}\right)^2 = 2$ as an extraction from the Tevatron data gives rise to very small asymmetries, $A_C \lesssim 1\%$, at the LHC both at 14 TeV and 7 TeV. However, a better option is to use the charge asymmetry as defined by CMS,

$$\delta A_C = (0.0073^{+0.0030}_{-0.0022} c_{Aa} + 0.0017^{+0.0007}_{-0.0004} c'_{Aa}) \left(\frac{1 \text{ TeV}}{\Lambda}\right)^2. \quad (4.29)$$

The region allowed by CMS measurement (1.66) (Fig. 4.6) is still compatible with the region allowed by the Tevatron. Nevertheless, CMS might exclude in the near future a deviation of the forward-backward asymmetry from the SM as large as the

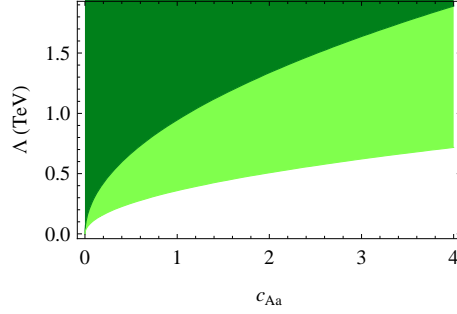


Figure 4.6: The region allowed by the CMS measurement [41] of the charge asymmetry at one (dark green) and two (light green) σ for $c'_{Aa} = 0$.

one required by CDF data at 95% C.L. for $c'_{Aa} = 0$. c'_{Aa} is much harder to constrain at the LHC due to the small contribution from the isospin-1 operators.

It is instructive to link the simple analysis given above with models featuring an axigluon A , *i.e.*, a massive color octet gauge boson coupled to chiral fermionic currents. These models do generate a forward-backward asymmetry due to the interference between the SM amplitude and that of $q\bar{q} \rightarrow A \rightarrow t\bar{t}$. If the scattering energies are smaller than the mass of the axigluon, the interference terms exactly match the term in Eq. (4.2) proportional to c_{Aa} . If the axigluon has a flavor-universal coupling to fermions with a strength proportional to the QCD couplings, g_s , as in Ref. [33], then the relation $c_{Aa}/\Lambda^2 = -2g_s^2/m_A^2$ (where m_A is the axigluon mass) obviously leads to a negative asymmetry. To generate a positive asymmetry that could explain the Tevatron result, a flavor non-universal axigluon is needed. More precisely, the coupling of the axigluon to the third generation and to the light quarks should be of opposite sign [132, 135, 137]: $c_{Aa}/\Lambda^2 = -2g_A^q g_A^t/m_A^2$ is then positive and can potentially explain the Tevatron data for a mass of the axigluon around 1.5 TeV provided that its couplings are of the same order as the QCD coupling.¹

In Fig. 4.7, we plot the prediction for A_{FB} from an axigluon with coupling g_s to all fermions and the prediction obtained with the corresponding effective operator ($c_{Aa} = -2g_s^2$, $c'_{Aa} = 0$, $\Lambda = M_A$). This shows that our effective field theory approach is a good approximation at the Tevatron for masses $M_A \gtrsim 1.5$ TeV, comparably to the LHC (see Fig. 4.3).

¹It was noted [135] recently that concrete realizations of this axigluon idea [132] are endangered by data on neutral B_d -meson mixing.

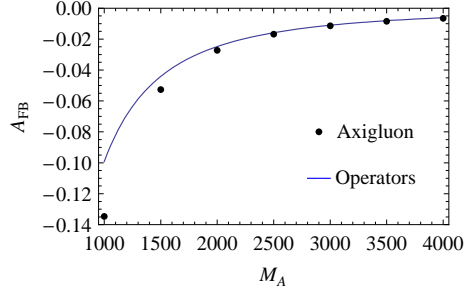


Figure 4.7: A_{FB} prediction at the Tevatron due to an axigluon and comparison with the effective field theory approach.

4.1.5 Spin correlations

We are here focusing on spin correlations which can provide further information on the coupling structure of the production mechanism (for alternative approaches see Ref. [138]). Spin correlations are good observables to disentangle the contributions from the two operators \mathcal{O}_{Rv} and \mathcal{O}_{Lv} since at high energy $\mathcal{O}_{R/Lv}$ should produce mainly right/left-handed top quarks and left/right-handed antitop quarks.

We assume that there is no modification of the top decay. In fact, there is only one dimension-six operator affecting the W-top-bottom vertex, $(H\bar{Q})\sigma^{\mu\nu}\sigma^I tW_{\mu\nu}^I$, which however does not modify the maximal spin-correlation in the leptonic decays of the top quark [93, 139, 140]. For this study, we chose the helicity basis². There is a one-to-one relation between the parameters C and b_{\pm} and the helicity cross-sections,

$$C = \frac{1}{\sigma} (\sigma_{+-} + \sigma_{-+} - \sigma_{++} - \sigma_{--}), \quad (4.30)$$

$$b_+ = \frac{1}{\sigma} (\sigma_{+-} - \sigma_{-+} + \sigma_{++} - \sigma_{--}), \quad (4.31)$$

$$b_- = \frac{1}{\sigma} (\sigma_{+-} - \sigma_{-+} - \sigma_{++} + \sigma_{--}). \quad (4.32)$$

The explicit formulas for the helicity cross-sections are given in App. A.3 and lead to (neglecting the contributions from the isospin-1 sector):

²It was shown [42] that spin correlation effects in the SM are more important at the Tevatron in the beam basis. However, it appears that the deviations from the SM values due to the operators \mathcal{O}_{hg} , \mathcal{O}_{Rv} and \mathcal{O}_{Lv} are on the contrary smaller in the beam basis.

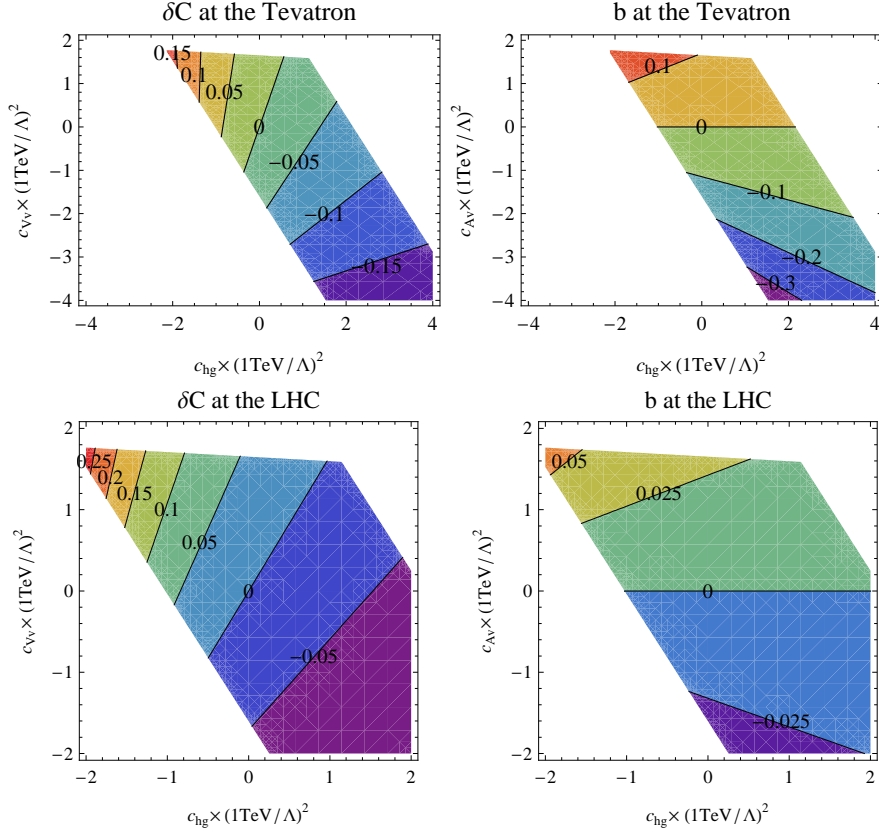


Figure 4.8: *Top panel:* Deviations from the SM prediction at the Tevatron ($C = 0.47$, $b = 0$) [45] for the parameters C (on the left) and $b = b_+ = b_-$ for $c_{Av} = c_{Vv}$ (on the right) in the region allowed by the Tevatron. *Bottom panel:* Deviations at the LHC from the SM prediction ($C = -0.31$, $b = 0$) [45].

$$C \times \sigma/\text{pb} = 2.82^{+1.06}_{-0.72} + [(0.37^{+0.10}_{-0.08}) c_{hg} + (0.50^{+0.13}_{-0.10}) c_{Vv}] \times \left(\frac{1\text{ TeV}}{\Lambda}\right)^2, \quad (4.33)$$

$$b \times \sigma/\text{pb} = (0.45^{+0.12}_{-0.09}) c_{Av} \times \left(\frac{1\text{ TeV}}{\Lambda}\right)^2, \quad (4.34)$$

at the Tevatron, and

$$C \times \sigma/\text{pb} = -166_{-37}^{+52} + [(-69_{-13}^{+17}) c_{hg} + (11_{-1}^{+1}) c_{Vv}] \times \left(\frac{1 \text{ TeV}}{\Lambda}\right)^2, \quad (4.35)$$

$$b \times \sigma/\text{pb} = (10_{-1}^{+1}) c_{Av} \times \left(\frac{1 \text{ TeV}}{\Lambda}\right)^2, \quad (4.36)$$

at the LHC. The parameters b_{\pm} are exactly proportional to the difference $c_{Rv} - c_{Lv}$ and thus allow us to distinguish between right or left handed top quarks. Additionally, the parameter C quite strongly depends on c_{hg} and c_{Vv} and can be used to detect the presence of new physics as shown in Fig. 4.8 for the Tevatron and the LHC respectively. The errors on the contour lines are only of a few percents.

As expected, the parameters $b = b_+ = b_-$ only differ slightly from zero at the LHC where the contributions of \mathcal{O}_{Rv} and \mathcal{O}_{Lv} are small. A possible modification of the spin distribution both at the Tevatron and the LHC is shown in Figs. 4.9. The non vanishing b parameter is at the origin of the asymmetry of the distribution clearly visible for the Tevatron. However, it will be quite difficult to measure spin correlation with sufficient precision at the Tevatron where only a few hundreds of events are expected and observed (Ref. [141] and Ref. [7] therein), while at the LHC we expect about a few millions of events after 100 fb^{-1} [142, 143]. In fact, the error on the C parameter are about 0.3 for 5.4 fb^{-1} at the Tevatron [144]³ and are mainly statistical (see Sect. 1.3.3).

4.1.6 Bosons exchanges

As we saw in Sect. 3.2.2, the chromomagnetic operator cannot be generated at the tree-level by the exchange of a new boson. In this section, we assume that $c_{hg} \approx 0$. Consequently, the cross-section and the invariant mass distribution as well as the forward-backward asymmetry depend each on two parameters only even without neglecting the isospin-1 operators. The allowed region are shown on Fig. 4.10 for both pairs of parameters. The total cross-section and the invariant mass constraints have been derived as in Sects. 4.1.2 and 4.1.3. The combination is done by assuming that the total cross-section measurement also follows a gaussian distribution and is not correlated with the invariant mass shape data. For the asymmetry above and below 450 GeV, we use the predictions for the SM of Eqs. (1.62) and (1.63) and for the new physics of Eqs. (4.26) and (4.27) respectively. We make again the hypothesis of uncorrelated measurements with gaussian distributions.

³This measurement is done in the beam basis.

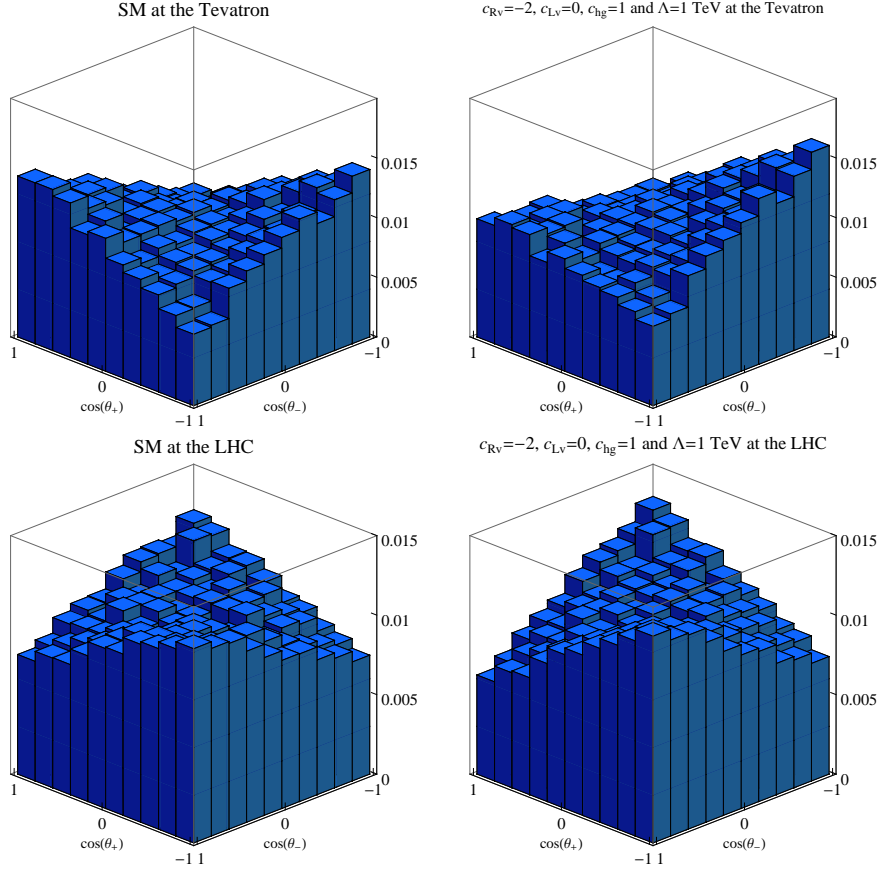


Figure 4.9: Distribution of events at the Tevatron/LHC (top panel/bottom panel) for the SM (on the left) and for $c_{Rv} = -2$, $c_{Lv} = 0$, $c_{hg} = 1$ and $\Lambda = 1$ TeV (on the right) with $\mu_F = \mu_R = mt$.

It can be seen from Tab. 3.2 that the t -channel models are already disfavored by the Tevatron data due to the relation between the vector and axial coefficients ($|c_{Vv}| = |c_{Aa}|$ and $|c'_{Vv}| = |c'_{Aa}|$). On the one hand, the agreement of the measured total cross-section and the $m_{t\bar{t}}$ distribution with the SM predictions requires $c_{Vv}^{(j)}$ to be small as shown on Fig. 4.10. On the other hand, the observed deviation for A_{FB} [38] implies that $c_{Aa}^{(j)}$ should be large. In fact, the color singlet vector [130] and the color octet scalar are immediately ruled out since they give the wrong sign for A_{FB} (see Eq. (4.26)).

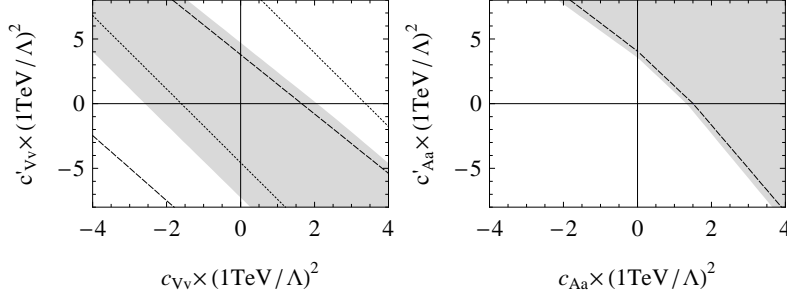


Figure 4.10: On the left, in gray, the region for c_{Vv} and c'_{Vv} allowed at 95% by the cross-section (delimited by dotted line) and the shape of the invariant mass distribution (delimited by dashed line). On the right, in gray, the region for c_{Aa} and c'_{Aa} allowed at 95% by A_{FB} for $m_{t\bar{t}} < 450$ GeV (the full region plotted is allowed) and for $m_{t\bar{t}} \geq 450$ GeV (above the dashed line) [38].

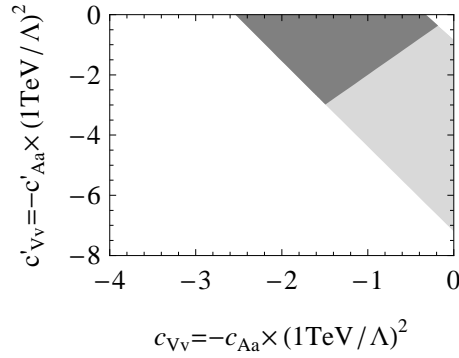


Figure 4.11: The allowed region by all these observables for $c_{Vv} = -c_{Aa}$ and $c'_{Vv} = -c'_{Aa}$ which corresponds to the still allowed spin 0 case (see Table 3.2). Only the dark gray region can be obtained for a t -channel scalar.

After combining all the constraints, we conclude that a color octet vector is also excluded while a small region, depicted in Fig. 4.10, remains for the case of a color singlet scalar. This region disappears if we change the C.L. to 85%. This last case is also constrained for low masses by the Tevatron search for $t\bar{t}$ production [47].

We note that when the interference between the new physics and the SM is negative, the new physics squared (NP²) can cancel the effect of the interference on the total cross-section for large values of the coupling or for small masses. It was shown [112, 113, 130] that the asymmetry can be explained with a rather light color singlet vector only coupled to the right-handed u and t quarks. Of course, this region

of the parameter space cannot be probed in our effective approach. However, the invariant mass distribution shape for a light state in the t -channel is also only marginally consistent with the data (Ref. [145] suggests, though, that this problem could be alleviated thanks to a reduced acceptance rate of the top quarks in the forward region). As a matter of fact, there is a large overlap between the allowed regions by the cross-section⁴ and the forward-backward asymmetry above 450 GeV but not with the region allowed by the shape of the invariant mass distribution as shown on Fig. 4.12. The distortion of the invariant mass shape due to a flavor violating vector explaining A_{FB} is also illustrated on Fig. 4.12.

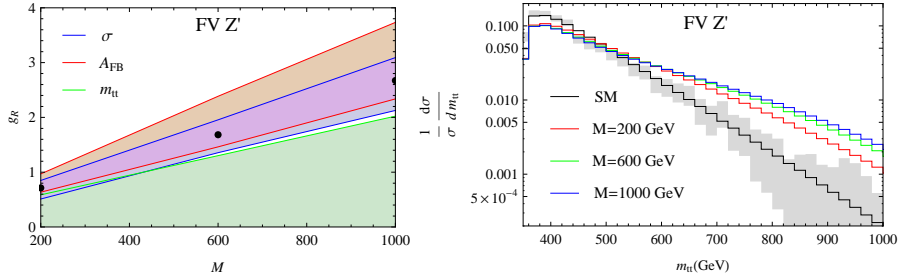


Figure 4.12: On the left, the allowed regions for a Flavor Violating (FV) Z' coupled to the right-handed top and up quarks by the total cross-section σ , the forward-backward asymmetry above 450 GeV and the invariant mass for $\mu_R = \mu_F = m_t$. On the right, the normalized invariant mass distribution for different masses of the new vector at the Tevatron. The 1σ region of the CDF measurement is shown in gray [30]. The cases displayed on the right graph are represented by dots on the left graph.

For a color singlet scalar, the NP² contribution to the asymmetry is negative and implies that $\delta A(m_{t\bar{t}} \geq 450 \text{ GeV}) < 0.2$. Moreover, the maximum for the forward-backward asymmetry does not correspond to the region where the new physics contributions to the total cross-section barely cancel each other as illustrated on Fig. 4.13. So, unfortunately, the only class of models linking same and opposite sign top pair productions, *i.e.* a t -channel exchange, seems disfavored by the Tevatron data.

⁴The allowed region for small values of g_R is not displayed since the resulting asymmetry is either too small or negative.

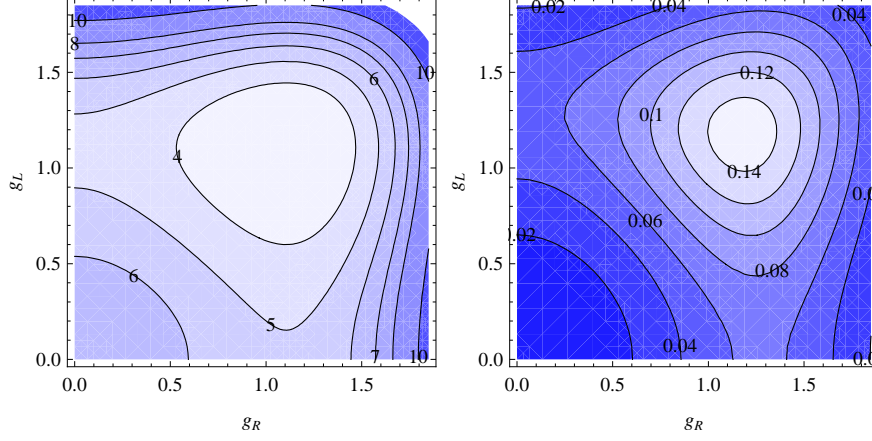


Figure 4.13: For a color singlet scalar with a mass of 200 GeV, the cross-section (on the left) and the forward-backward asymmetry above 450 GeV (on the right) at the Tevatron for $\mu_R = \mu_F = m_t = 174.3$ GeV.

4.2 Same Sign top pair production

At the partonic level, the leading order cross-section for same sign top pair production is given by

$$\begin{aligned}
 \frac{d\sigma}{dt} = & \frac{1}{\Lambda^4} \left[\left(|c_{RR}|^2 + |c_{LL}|^2 \right) \frac{(s - 2m_t^2)}{3\pi s} \right. \\
 & + \left(|c_{LR}^{(1)}|^2 + \frac{2}{9} |c_{LR}^{(8)}|^2 \right) \frac{(m_t^2 - t)^2 + (m_t^2 - u)^2}{16\pi s^2} \\
 & \left. - \left(|c_{LR}^{(1)}|^2 + \frac{8}{3} \Re(c_{LR}^{(1)} c_{LR}^{(8)*}) - \frac{2}{9} |c_{LR}^{(8)}|^2 \right) \frac{m_t^2}{24\pi s} \right]. \quad (4.37)
 \end{aligned}$$

The dominant contribution to this cross-section is due to the new physics amplitudes squared because the one-loop SM process depicted in Fig. 4.14 is strongly suppressed by the squares of the V_{ub} CKM matrix element and of the bottom quark mass. Lowest order contributions are thus $\mathcal{O}(\Lambda^{-4})$ contrary to opposite sign top pair production for which the largest corrections arise from the $\mathcal{O}(\Lambda^{-2})$ interference. After integration over t , the cross-section grows like s as expected from dimensional analysis. In fact, only the interference between the LR operators is proportional to m_t^2 , see Eq. (4.37), and does not have this behavior. As a consequence, a large part of the total cross-section at the LHC comes from the region where $m_{tt} \sim 1$ TeV as shown on Fig. 4.15. In this region, however, the $1/\Lambda$ expansion cannot be trusted for values of Λ around

1 TeV we consider in our study. Figure 4.16 displays the cross-section with an upper cut on m_{tt} at $\Lambda/3$ as a function of Λ for $c_i = 1$, where c_i is a generic label for the coefficients in Eq. (3.23). This choice ensures that the m_{tt} distribution is at most about 20% below (above) its true value for an s - (t -) channel exchange. The general case can easily be inferred since the coefficient dependences factorise in Eq. (4.37). At 14 TeV, the cross-section increases by a factor 2 for $\Lambda \sim 2$ TeV up to a factor 4 for $\Lambda \sim 14$ TeV.

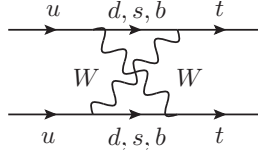


Figure 4.14: SM contribution to $uu \rightarrow tt$

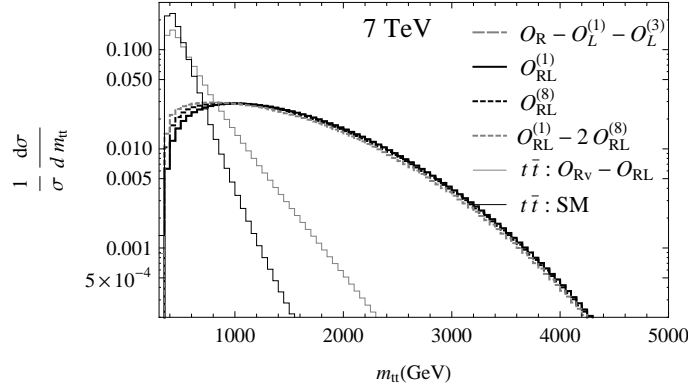


Figure 4.15: Normalized invariant mass distribution for same sign top pair production at the LHC. The distribution can be trusted for $m_{tt} \ll \Lambda$ only. The interference between the SM and the four-fermion operators as well as the SM for $t\bar{t}$ production are also displayed for comparison.

At the Tevatron, the same sign top pair production is small due to the PDF. Moreover, their damping is such that the m_{tt} distribution is peaked instead below 500 GeV. The

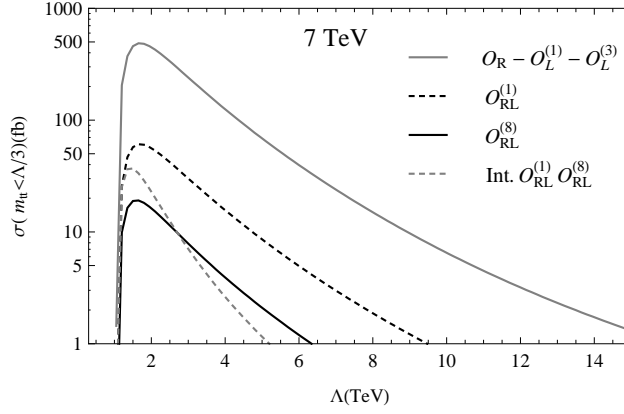


Figure 4.16: Cross-section of $pp \rightarrow tt$ at the LHC with an upper cut on the invariant mass at $\frac{\Lambda}{3}$ for $c_i = 1$. Parameters: $m_t = 174.3$ GeV, CTEQ6L1 pdf set [120], $\mu_F = \mu_R = m_t$.

total cross-section is given by

$$\begin{aligned} \sigma^{\text{TeV}}(p\bar{p} \rightarrow tt + \bar{t}\bar{t})/\text{fb} &= 2 \left[62 \left(|c_{RR}|^2 + |c_{LL}|^2 \right) + 7.7 |c_{LR}^{(1)}|^2 + 2.3 |c_{LR}^{(8)}|^2 \right. \\ &\quad \left. - 3.6 \Re \left(c_{LR}^{(1)} c_{LR}^{(8)*} \right) \right] \left(\frac{1 \text{ TeV}}{\Lambda} \right)^4. \end{aligned} \quad (4.38)$$

Assuming the same acceptance (0.5%) as in [47], we find that $c_i \sim 1$ are still allowed. A very recent analysis based on operators in Eq. (3.22) gives similar constraints [146].

Figure 4.15 shows that the m_{tt} shapes given by the different operators appear to be quite similar. The maximal effect of the interference term corresponds approximately to the linear combination $\mathcal{O}_{LR}^{(1)} - 2\mathcal{O}_{LR}^{(8)}$. As foreseen, the interference can only give a sizeable effect for low m_{tt} since it does not grow with s . Again, there are no significant changes at 14 TeV. The distribution is only stretched to the higher invariant mass region.

In contrast with the m_{tt} distribution, the spin correlations provide in principle a very efficient observable to discriminate among the contributions from the various operators in Eq. (3.22). The main reason is that the latter have a well defined chirality structure and no interference with the Standard Model is possible. Let us define the normalized differential tt cross-section

$$\frac{1}{\sigma} \frac{d\sigma}{d \cos \theta_1 d \cos \theta_2} = \frac{1}{4} [1 + C \cos \theta_1 \cos \theta_2 + b (\cos \theta_1 + \cos \theta_2)], \quad (4.39)$$

where θ_1 (θ_2) is the angle between the momentum in the top rest frame of the charged lepton resulting from the first (second) top decay and the top momentum in the tt rest frame. Then, the C and b parameters can directly be computed from the helicity cross-sections, namely

$$\begin{aligned} C &= \frac{1}{\sigma} (\sigma_{++} + \sigma_{--} - \sigma_{+-} - \sigma_{-+}) \\ b &= \frac{1}{\sigma} (\sigma_{++} - \sigma_{--}), \end{aligned} \quad (4.40)$$

where the first (second) index refers to the helicity of the first (second) top quark. For \mathcal{O}_{RR} , $C = 1$ and $b = 0.997$. For $\mathcal{O}_{LL}^{(1)}$ and $\mathcal{O}_{LL}^{(3)}$, only the sign of b changes. The two remaining operators in Eq. (3.22) are characterized by $C \approx 1$ and $b \approx 0$. C and b are here calculated on the full cross-section, *i.e.*, without any cut on m_{tt} . However, $C = 1$ for \mathcal{O}_{RR} , $\mathcal{O}_{LL}^{(1)}$ and $\mathcal{O}_{LL}^{(3)}$ is independent of such a cut. As a result, such strong spin correlations could be used to enhance the sensitivity to the signal and to identify the possible contributing operators.

4.3 Associated top pair productions

4.3.1 $t\bar{t}b\bar{b}$ and $t\bar{t}t\bar{t}$ productions at the LHC

While $t\bar{t}$ production appears as the leading process to probe any new physics in the top sector, there are physical situations where the operators of $\mathcal{L}_{t\bar{t}}$ are parametrically suppressed. As shown in Section 3.2.1, this is the case if the top quark is not an elementary particle but rather a composite bound state: the dominant operators are the ones involving composite states only. The $t\bar{t}$ process is still probing the dominant operators but at the loop level only. In these situations, a much better probe of the dominant dynamics (Eqs.(3.26) to (3.28)) is the direct production of four top quarks or the production of two top and two bottom quarks [98].

The SM cross-section for 4-top production is rather small (of the order of 5 fb at the LHC) and the operators of Eqs. (3.26)–(3.28) can easily give larger contributions. Contrary to pair production, the smallness of the SM cross-section urges us to keep the squared amplitude from new physics instead of the interference with the SM as shown in Table 4.2. The two contributions are equal for $0.2 \lesssim c_i \left(\frac{1 \text{ TeV}}{\Lambda}\right)^2 \lesssim 1$ where c_i generically denotes the coefficient of the operator \mathcal{O}_i . The range of this critical value is due to the different operators. Thus, we are effectively computing the cross-sections at the order $\mathcal{O}(\Lambda^{-4})$ and we also neglect the interference between the SM and any dimension-eight operators. This approximation is valid if the coefficients are

large and cannot be used for the operator $\mathcal{O}_L^{(1)}$ and $\mathcal{O}_B^{(1)}$ since their coefficients have to be at most of order one (see Sect. 3.4). The associated cross-sections for both the interferences and the squared amplitudes of the new operators are of the order of the fb like the SM and would likely be too small to be observed.

	σ_{4t}	$\sigma_{4t}^{\Lambda^{-2}}$	$\sigma_{4t}^{\Lambda^{-4}}$	$\sigma_{t\bar{t}b\bar{b}}$	$\sigma_{t\bar{t}b\bar{b}}^{\Lambda^{-2}}$	$\sigma_{t\bar{t}b\bar{b}}^{\Lambda^{-4}}$	$\sigma_{t\bar{t}b\bar{b}}^{\text{cut}}$	$\sigma_{t\bar{t}b\bar{b}}^{\text{cut}}/\sigma_{4t}$
	(fb)	(fb)	(fb)	(pb)	(pb)	(pb)	(pb)	
SM	5.26	-	-	7.7	-	-	0.306	58.2
$\mathcal{O}_R^{(1)}$	-	-20.8	574	-	-	-	-	-
$\mathcal{O}_B^{(1)}$	-	-11	193	-	0.2	3.89	2.38	12
$\mathcal{O}_B^{(8)}$	-	-4	47	-	0.9	0.9	0.52	11
$\mathcal{O}_L^{(1)}$	-	-37.2	569	-	<0.03	15.49	9.35	16
$\mathcal{O}_L^{(8)}$	-	-0.9	63	-	0.49	3.5	2.09	33

Table 4.2: The $t\bar{t}t\bar{t}$ ($\mu_F = \mu_R = 4m_t$) and $t\bar{t}b\bar{b}$ ($\mu_F = \mu_R = 2m_t$) cross-sections for $\Lambda = 1$ TeV and $c_i = 4\pi$. The interferences between the SM and the new physics, given in the third and sixth columns, can be neglected. The squared amplitudes from new physics are in the fourth, seventh and eighth columns. The new physics contributions for a different scale Λ and different couplings c_i are simply obtained by multiplying those last numbers by a factor $(c_i/(4\pi))^2 \times (1 \text{ TeV}/\Lambda)^4$.

The SM $t\bar{t}b\bar{b}$ production is not as suppressed as the 4-top production, so the same approximation would be a priori valid for smaller values of the scale of new physics only (or for larger couplings). However, we can use the particular kinematics associated to the new physics operators to improve our approximation. In fact, the new physics squared amplitudes grow with the energy as shown in Fig. 4.17. Therefore the $b\bar{b}$ pair will be produced with a higher invariant mass in presence of new physics, and a cut on the $b\bar{b}$ invariant mass will suppress the $\mathcal{O}(\Lambda^{-2})$ terms compared to the $\mathcal{O}(\Lambda^{-4})$ ones. Moreover, such a cut will also improve the ratio of the signal over the SM background as shown on Fig. 4.18. Again the two operators $\mathcal{O}_L^{(1)}$ and $\mathcal{O}_B^{(1)}$, can only give small (10-30%) corrections to the SM process. Those corrections are relatively as large as the corrections from the operators in Eq.(3.19) to $t\bar{t}$ production but will be harder to see since the cross-section is a few orders of magnitude smaller. The interference and the amplitude squared for $\mathcal{O}_B^{(8)}$ are more or less the same for $\frac{c_B^{(8)}}{\Lambda^2} = 4\pi \text{ TeV}^{-2}$. How-

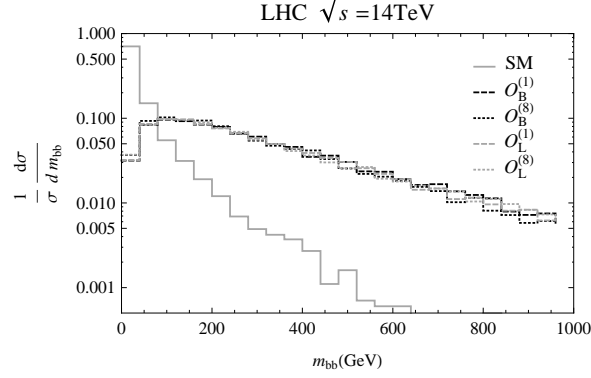


Figure 4.17: Normalized cross-sections at the LHC for the $t\bar{t}b\bar{b}$ production as a function of the $b\bar{b}$ invariant-mass. Since we neglected the interference terms between the SM and the new physics contribution, the distributions are independent of the new physics scale and of the actual couplings in front of the dimension-6 operators.

ever, there are no constraint at all from the Z decay widths. Consequently, only larger values of its coefficient for which our approximations are valid can be tested.

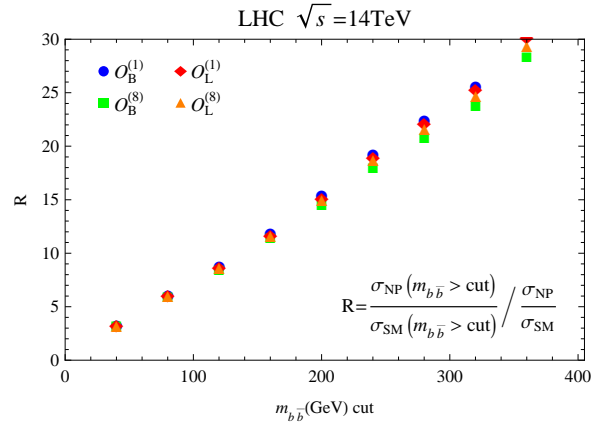


Figure 4.18: Effect of the $b\bar{b}$ invariant-mass cut on the signal over background ratio. $R = \frac{\sigma_{NP}(m_{b\bar{b}} > \text{cut})}{\sigma_{SM}(m_{b\bar{b}} > \text{cut})} / \frac{\sigma_{NP}}{\sigma_{SM}}$ is the double ratio of the signal (contribution from new operators) over the background (contribution of the SM) with and without the cut on the $b\bar{b}$ invariant mass. In our approximations, R is independent of the new physics scale and of the actual couplings in front of the dimension-6 operators.

For both $t\bar{t}\bar{t}$ and $t\bar{t}b\bar{b}$ productions, the operators defined in Eqs. (3.26)–(3.28) give cross-sections of the same order of magnitude (see Table 4.2) and it is not possible to distinguish them just by a measurement of one of the two total cross-sections. Furthermore, as Fig. 4.17 suggests, they also generate similar distributions for all the spin-independent variables. However, the ratio of the two cross-sections appears to be very different for the three still allowed operators and is also independent of the new physics scale and of the actual couplings in front of the dimension-six operators provided that the interferences with the SM can be safely neglected. A detailed study of four-top production at the LHC will be presented in Ref. [147] (see Ref. [148] for a preview).

4.3.2 $t\bar{t}$ production in association with a Higgs

As we have already mentioned, the chromomagnetic operator also modifies the Higgs boson interactions with the top and the gluons. Top pair production in association with a Higgs might thus provide further constraints on its coefficient. The diagrams can be easily obtained from those of Fig. A.1 by adding a Higgs leg attached to the top line or to the effective vertex as illustrated on Fig. 4.19. In this last case, the diagrams contain only one chirality flip such that no other chirality flip is needed to interfere with the SM amplitude. On the contrary, there are two chirality flips by diagram in the former case. So, one mass insertion is required to interfere with the SM amplitude in this case. Contrary to opposite sign top pair production, the interference might thus have a different behavior than the SM at high energy since proportionality to the top mass and to the Higgs vev can be avoided for some of the diagrams.

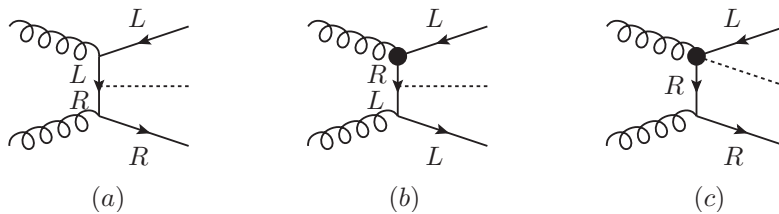


Figure 4.19: Examples of diagrams for $t\bar{t}h$ production from the SM (a) and from the chromomagnetic operator (b) and (c).

The total cross-section at the LHC (14 TeV) is given by

$$\sigma(pp \rightarrow t\bar{t}h)/\text{fb} = 604_{-152}^{+192} + 482_{-115}^{+124}c_{hg} \left(\frac{1 \text{ TeV}}{\Lambda}\right)^2 + 520_{-101}^{+140}c_{hg}^2 \left(\frac{1 \text{ TeV}}{\Lambda}\right)^4 \quad (4.41)$$

for $m_h = 120$ GeV. The cross-section for different values of Higgs mass is displayed on Fig. 4.20. The other operators have not been included since they cannot modify the main process, *i.e.* gluon fusion. Since this process requires more energy, both the interference and the NP² terms are of the same magnitude for $\frac{c_{hg}}{\Lambda^2} \gtrsim 1 \text{ TeV}^{-2}$. For consistency, $\frac{c_{hg}}{\Lambda^2} < \frac{1}{2} \text{ TeV}^{-2}$ at least. The same factorization and renormalization scales as for opposite sign top pair production have been used since we have only considered a light Higgs boson. The cross-section would decrease if higher values taking into account the Higgs mass are chosen.

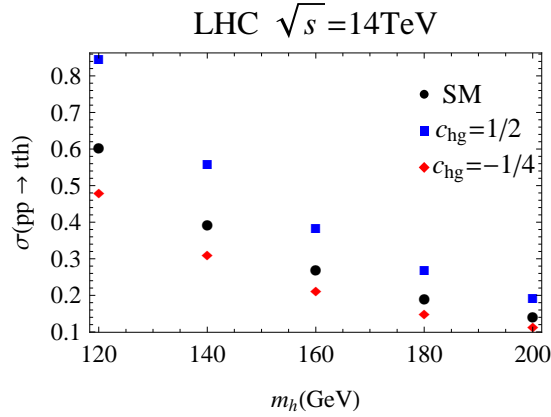


Figure 4.20: Cross-sections for $pp \rightarrow t\bar{t}h$ as a function of the Higgs mass using CTEQ611 pdf set and $\mu_R = \mu_F = m_t = 174.3$ GeV for the SM and for the SM and the interference with the chromomagnetic operator.

The total transverse energy as well as the invariant mass distribution of the Higgs and the top are displayed on Fig. 4.21. The shape of the NP² is also shown for comparison. The NP² part is clearly stretched to high energy while the interference and the SM have a very similar behavior. Consequently, the interference with the diagrams in which the Higgs is connected at the effective vertex are suppressed. These results have been obtained with MadGraph 5 [124] similarly as for the non top-philic operators.

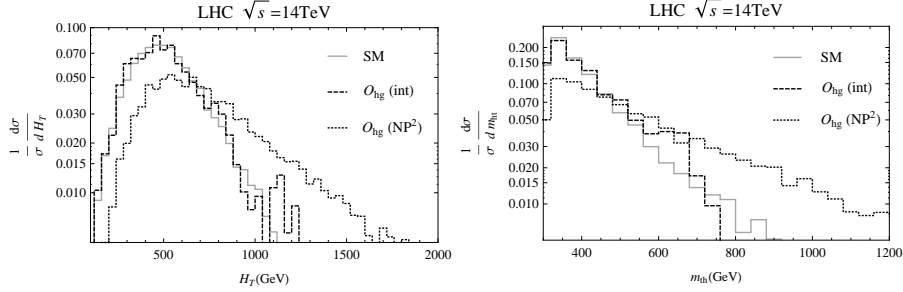


Figure 4.21: Normalized distributions of the total transverse energy H_T and the top-Higgs invariant mass m_{th} using CTEQ611 pdf set and $\mu_R = \mu_F = m_t = 174.3$ GeV for the SM, its interference with the chromomagnetic operator and the squared of the amplitudes with one effective vertex.

4.4 Summary

In theories that provide a mechanism for mass generation, new physics must have a large coupling to the top quark. It is, therefore, natural to use top quark observables to test the mechanism responsible for electroweak symmetry breaking. We have shown how non-resonant top-philic new physics can be probed using measurements in top quark pair productions at hadron colliders.

Some of our results have already appeared in the literature, although only subsets of dimension-six operators were considered. For instance, there is an extensive literature [81–84, 88, 89] on the operator \mathcal{O}_{hg} , the chromomagnetic dipole moment of the top quark, while other works focused on the effect of additional four-fermion operators on top pair production at the Tevatron [85–87, 119]. Recently, all relevant operators were properly accounted for in Ref. [93] which, however, did not cover the corresponding phenomenological analysis. In our work, the aim is to provide a complete and self-consistent treatment in a model-independent approach and, especially, to extract the physics by combining information from the Tevatron and the LHC.

The analysis of opposite sign top pair production can be performed in terms of eight operators, suppressed by the square of the new physics energy scale Λ . Observables depend on different combinations of only four main parameters

$\sigma(gg \rightarrow t\bar{t}), d\sigma(gg \rightarrow t\bar{t})/dt$	\leftrightarrow	c_{hg}
$\sigma(q\bar{q} \rightarrow t\bar{t})$	\leftrightarrow	c_{hg}, c_{Vv}
$d\sigma(q\bar{q} \rightarrow t\bar{t})/dm_{t\bar{t}}$	\leftrightarrow	c_{hg}, c_{Vv}
A_{FB}	\leftrightarrow	c_{Aa}
spin correlations	\leftrightarrow	c_{hg}, c_{Vv}, c_{Av}

where c_{hg} is the parameter associated with the chromomagnetic dipole moment operator and c_{Vv} , c_{Aa} and c_{Av} correspond to particular combinations of four-fermion operators defined in Section 3.1.1. Let us summarize our main results on these observables.

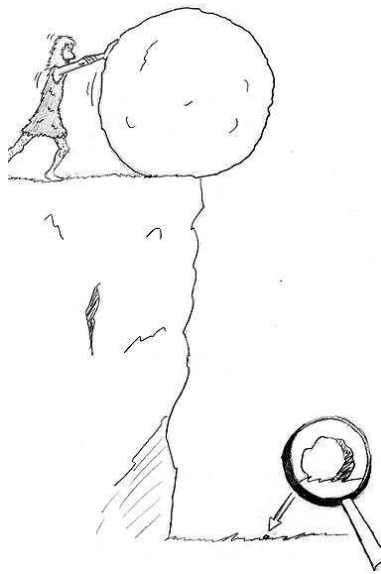
1. Since top pairs are mainly produced by gluon fusion at the LHC, the measurement of the $t\bar{t}$ cross-section at the LHC determines the allowed range for c_{hg} . In contrast, the Tevatron cross-section is also sensitive to the four-fermion operators and constrains a combination of c_{hg} and c_{Vv} . Consequently, the measurements of the total cross-sections at the Tevatron and at the LHC are complementary and combining the two pins down the allowed region in the (c_{hg}, c_{Vv}) plane.
2. The shape of the invariant mass distribution at the Tevatron is sensitive to a combination of the parameters c_{Vv} and c_{hg} which is different from the combination controlling the total cross-section. It quite strongly depends on the presence of four-fermion operators and was used to further reduce the parameter space mainly along the c_{Vv} direction.
3. The forward-backward asymmetry that probes different operators than those affecting the cross-section or the invariant mass distribution could be the first sign of new physics at the Tevatron. The scale of the new interaction(s) can then be estimated from the value predicted by our effective Lagrangian approach if a deviation from the SM is confirmed.
4. The three observables σ , $d\sigma/dm_{t\bar{t}}$ and A_{FB} are unable to disentangle between theories coupled mainly to right- or left-handed top quark. However, spin correlations allow us to determine which chiralities of the top quark couple to new physics, and in the case of composite models, whether one or two chiralities of the top quark are composite.

For heavy particle exchange models, the \mathcal{O}_{hg} operator can only be generated at the loop-level and c_{hg} is then expected to be small. Assuming $c_{hg} = 0$, the allowed regions for the four-fermion operators show that the t -channel scenarios are disfavored by the Tevatron data. The relation between opposite and same sign top pair productions can then not directly be used to fix the production rate of the latter at the LHC. However, other production mechanisms can lead to tt production. Only five independent effective operators of dimension-six contribute to this process. Among them two operators are already severely constrained by flavor data and cannot play any role in processes at the TeV scales. The cross-sections can be of the order of a pb both at 7 TeV and at 14 TeV if the scale of the new physics is about 2 TeV. LHC searches in the same-sign dilepton channel will be probing these cross-sections this year. It makes this channel particularly competitive to search for new physics in the top sector (see also [149] for probing like-sign top production using single lepton events). The strong spin correlations can, in principle, be used to distinguish the different operators. Contrary to flavor experiment, the LHC has definitely the potential to directly constrain those $\Delta F = 2$ operators.

In composite models, the ratio of c_{Vv} and c_{hg} is very important since it reflects the number of composite fields in the SM. However, the peculiar hierarchy between dominant and subdominant operators cannot be tested in $t\bar{t}$ or tt productions that depend on one class of operators only. Fortunately, composite models can be further tested through the golden four-top channel and $t\bar{t}b\bar{b}$ production at the LHC. Both processes are necessary to identify the dominant operators and thus to extract their coefficients. The hierarchy between the operators can be tested and used to estimate the strength of the new strong interaction, g_ρ . We stress that the results for top pair productions are generic while those for $t\bar{t}t\bar{t}$ and $t\bar{t}b\bar{b}$ productions require the enhancement due to a new strong interaction. These two processes would disappear in the SM background if they are not enhanced by a factor g_ρ^2 . Such an enhancement is already forbidden by the Z decay constraints for two of the five dominant operators.

Finally, the chromomagnetic operator can induce significant deviation for Higgs and $t\bar{t}h$ productions by gluon fusion. Those processes are sensitive to a higher energy domain and can thus put stronger constraints on c_{hg} . However, they will again be mainly limited by the errors on the overall normalisation of the processes since no significant shape distortions are expected.

Conclusion



The largest part of this thesis (Chaps. 3 and 4) was devoted to the study of beyond the Standard Model top physics with the help of effective field theories. The SM Lagrangian is then the lowest order term of the expansion in the momenta of the process over the mass of the heavy new states $\frac{p^2}{\Lambda^2}$. The scale Λ should not be too large to observe the deviations from the SM. Namely, the new physics contributions should be bigger than the expected experimental and theoretical errors, *i.e.* about 10-15% for $t\bar{t}$ production at hadron colliders. As a consequence, the errors due to the truncation of the effective Lagrangian at the $\mathcal{O}(\Lambda^{-2})$ are not very small. The reliability of our predictions was checked by a partial evaluation of the $\mathcal{O}(\Lambda^{-4})$ corrections. Numerically, they are estimated to be smaller than 25% of the new physics contributions for $\Lambda = 1$ TeV (and $c_i = 1$). The comparison between the exact computation based on the exchanges of heavy particles and the result from the corresponding effective theory shows that the corrections might slightly be underestimated. A complete computation of the $\mathcal{O}(\Lambda^{-4})$ corrections is quite complicated, but the effective theory for the light

pseudoscalar mesons of Chap. 2 tells us that effective theories are still meaningful even if the expansion parameter is rather large. In fact, the corrections to this effective theory from the next order in p^2 are expected to be of about 20% $\sim \frac{p^2}{1 \text{ GeV}^2}$. Taking this into account, the predictions from the effective Lagrangian at leading order in p^2 and in $1/N_c$ agree with the experimental data. In particular, the tree-level $\eta - \eta'$ mixing angle $\theta \cong -27^\circ$, stable against quadratic quantum corrections, is about 20% below the value $\theta = -22^\circ$ extracted from the radiative J/ψ decay.

The effective theory for opposite sign top pair production put forward many differences between the two dominant mechanisms. First, seven four-fermion and one two-fermion operators affect quark annihilation while only one top-philic operator, the chromomagnetic operator, contributes to gluon fusion at $\mathcal{O}(\Lambda^{-2})$. Secondly, the interference between the dimension-six operators and the SM is expected to grow faster with the energy than the pure SM contribution since $\frac{p^2}{\Lambda^2} \sim \frac{s}{\Lambda^2}$. As a matter of fact, the contributions to the cross-section from the four-fermion operators have an extra factor s compared to the SM. Since the center of mass energy is, in average, larger at the LHC than at the Tevatron, the ratio of the four-fermion operators and the SM contributions to $q\bar{q} \rightarrow t\bar{t}$ is bigger at the LHC. On the contrary, the contribution of the chromomagnetic operator is helicity suppressed and has no extra s factor. As a consequence, the ratio of its contribution and the SM one to $gg \rightarrow t\bar{t}$ is roughly the same at both colliders despite that the difference of the averaged center of mass energy for a two gluons initial state is larger than for quark antiquark. Consequently, the sensitivity to the chromomagnetic operator is quite low at the LHC. Even if we relax our assumption of top-philic new physics, the conclusion for gluon fusion remains the same at this order in Λ . Finally, the shape distortions, important to distinguish the new physics and the SM, are mainly caused by the four-fermion operators. The invariant mass distribution, the angular distribution and, in particular, the forward-backward asymmetry and the spin correlations are all affected by those operators. On the contrary again, the chromomagnetic operator significantly modifies the spin correlations only in addition to the cross-section.

The search for new physics with effective field theories were also extended beyond $t\bar{t}$ production. For example, we attempted to overcome the suppression of the chromomagnetic operator by looking rather at the top pair production in association with a Higgs boson. Unfortunately, there are also no sizeable enhancement of the cross-section with the energy for this process at $\mathcal{O}(\Lambda^{-2})$. Nevertheless, the larger energy required by this final state still allows us to probe higher values of Λ . Furthermore, the effects of the chromomagnetic operator on Higgs production by gluon fusion was shown to be quite large compared with the SM. Four top quarks production was also studied in this thesis. If the new physics is strongly interacting like in composite

models, this process has been shown, by copying the rules derived from the effective theory for the light mesons, to be the golden channel. Similarly, top pair production in association with two bottom quarks can strongly be enhanced if the left-handed doublet of the heaviest quarks interacts with the new strong sector. Despite being already constrained by the Z decay width, the remaining operators with four heavy quarks can be identified by the ratio of the cross-sections of those two processes. Last but not least, the effective Lagrangian for same sign top pair production was built. Being initiated by two quarks, this process overcomes the difficulty to find an antiquark in a proton at the LHC. Same sign top pair production offers the possibility to constrain a new set of flavor violating four-fermion operators. Moreover, this process, strongly suppressed in the SM, allows us to probe large value for the energy scale of the new physics Λ by getting rid of the SM theoretical errors. Moreover, same sign top pair production can easily be distinguished from any SM background because its invariant mass distribution is far from being peaked at threshold.

We have shown that effective field theories are useful for colliders phenomenology. In particular, they have been shown to be suitable to quantify the (allowed) size of the new physics in a model independent way when no resonances are found like at the Tevatron. Despite that the LHC is now surpassing the Tevatron, all the contributions of our effective Lagrangian to its dominant process for the top pair production, *i.e.* gluon fusion, are suppressed. The last hope at this order in Λ are the CP violating operators. However, they deserve a careful analysis since they can generate CP violation for the strong interaction at one-loop. Otherwise, shape distortion at the LHC would require to go to the $\mathcal{O}(\Lambda^{-4})$ for gluon fusion. Those contributions might still be observable. For example, the unsuppressed squared amplitude of the \mathcal{O}_G operator gives a contribution as large as 15% for $\Lambda = 1$ TeV and $c_G = 1$. Contrary to quark annihilation, the parameter space at this order is not expected to become very large since no new dimension-six operators should be added. Finally, effective theories could be used for other processes. For example, we have also mentioned the multijet events to look for dimension-six operators and, in particular, for the \mathcal{O}_G operator. Dijets have already been used to constrain the four-fermion operators at the LHC [49]. However, we can expect that much stronger constraints could be set on the operators involving gluons.

Appendix **A**

Appendix for top pair productions

A.1 Fierz transformations

We are collecting here some Fierz transformations that are needed to reduce the basis of independent dimension-six operators. The same transformations are also useful to compute the effective Lagrangian obtained after integrating out some heavy resonances.

$$\delta_{ij}\delta_{kl} = \frac{1}{2}\sigma_{il}^I\sigma_{kj}^I + \frac{1}{2}\delta_{il}\delta_{kj}, \quad (\text{A.1})$$

$$\delta_{ab}\delta_{cd} = 2T_{ad}^A T_{cb}^A + \frac{1}{3}\delta_{ad}\delta_{cb}, \quad (\text{A.2})$$

$$(\gamma_\mu P_{L/R})_\alpha^\beta (\gamma^\mu P_{L/R})_\gamma^\delta = -(\gamma_\mu P_{L/R})_\alpha^\delta (\gamma^\mu P_{L/R})_\gamma^\beta \quad (\text{A.3})$$

$$(\gamma_\mu P_R)_\alpha^\beta (\gamma^\mu P_L)_\gamma^\delta = 2(P_L)_\alpha^\delta (P_R)_\gamma^\beta, \quad (\text{A.4})$$

$$(P_{L/R})_\alpha^\beta (P_{L/R})_\gamma^\delta = -\frac{1}{2}(P_{L/R})_\alpha^\delta (P_{L/R})_\gamma^\beta + \frac{1}{8}(\gamma^{\mu\nu} P_{L/R})_\alpha^\delta (\gamma_{\mu\nu} P_{L/R})_\gamma^\beta, \quad (\text{A.5})$$

where $P_{L/R} = (1 \mp \gamma^5)/2$ are the usual chirality projectors and $\gamma^{\mu\nu} = \frac{1}{2}[\gamma^\mu, \gamma^\nu]$.

A.2 Feynman diagrams for $t\bar{t}$ production at order $\mathcal{O}(\Lambda^{-2})$

At the $\mathcal{O}(\Lambda^{-2})$ order, the two parton-level cross sections for $t\bar{t}$ production follow from the Feynman diagrams depicted in Fig. A.1 and A.2.

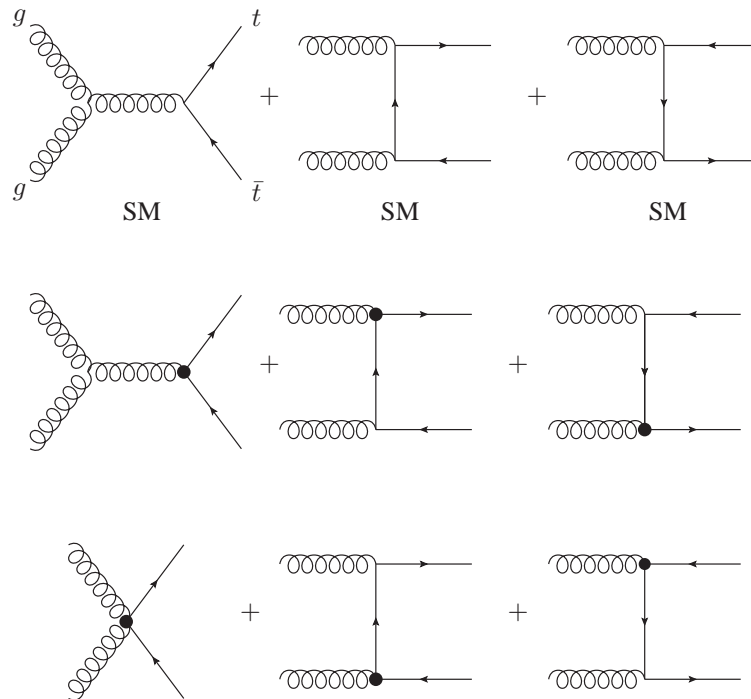


Figure A.1: Feynman diagrams for $gg \rightarrow t\bar{t}$ up to $\mathcal{O}(\Lambda^{-2})$. The dark blobs denote interactions generated by the operator \mathcal{O}_{hg} .

A.3 Helicity amplitude for $t\bar{t}$

As explained in Section 3.1.1, when summed over the helicities of the final top, the cross section for the $t\bar{t}$ production depends only on the sum $c_{Vv} = c_{Rv} + c_{Lv}$ (we neglect the contribution for the isospin-1 sector). However the individual helicity

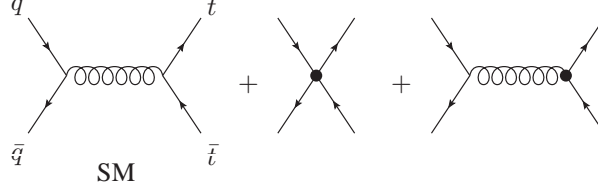


Figure A.2: Feynman diagrams for $q\bar{q} \rightarrow t\bar{t}$ up to $\mathcal{O}(\Lambda^{-2})$. The diagram in the middle originates from the four-fermion interactions induced by the operators $\mathcal{O}_{L/Rv}$, $\mathcal{O}_{L/Ra}$ and $\mathcal{O}_{Qq}^{(8,3)}$. The diagram on the right is the contribution from the operator \mathcal{O}_{hg} .

cross sections are sensitive to c_{Rv} and c_{Lv} individually since at high energy \mathcal{O}_{Rv} (\mathcal{O}_{Lv}) should produce mainly right (left) handed top and left (right) handed antitop. Explicitly, the helicity cross sections are given by (we recall that $c_{Av} = c_{Rv} - c_{Lv}$)

$$\begin{aligned}
\sigma_{++}(gg \rightarrow t\bar{t}) &= \frac{\pi\alpha_s^2}{24(4m_t^2 - s)s^3} \left\{ -2\sqrt{s(s-4m_t^2)}(62m_t^4 - 7sm_t^2 + 2s^2) \right. \\
&\quad + (16m_t^4 + 58sm_t^2 + s^2)m_t^2 \log\left(\frac{s + \sqrt{s(s-4m_t^2)}}{s - \sqrt{s(s-4m_t^2)}}\right) \\
&\quad - \frac{c_{hg}}{g_s\Lambda^2} 2\sqrt{2}svm_t \left[\sqrt{s(s-4m_t^2)}(14m_t^2 + 13s) \right. \\
&\quad \left. \left. + (4m_t^4 - 34m_t^2s) \log\left(\frac{s + \sqrt{s(s-4m_t^2)}}{s - \sqrt{s(s-4m_t^2)}}\right) \right] \right\}, \\
\sigma_{--}(gg \rightarrow t\bar{t}) &= \sigma_{++}(gg \rightarrow t\bar{t}), \\
\sigma_{+-}(gg \rightarrow t\bar{t}) &= \left(1 + \frac{c_{hg}}{g_s\Lambda^2} 4\sqrt{2}m_tv\right) \frac{\pi\alpha_s^2}{24(s-4m_t^2)s^2} \times \\
&\quad \left[11\sqrt{s(s-4m_t^2)}(m_t^2 - s) \right. \\
&\quad \left. + (2m_t^4 - sm_t^2 - 4s^2) \log\left(\frac{s - \sqrt{s(s-4m_t^2)}}{s + \sqrt{s(s-4m_t^2)}}\right) \right], \\
\sigma_{-+}(gg \rightarrow t\bar{t}) &= \sigma_{+-}(gg \rightarrow t\bar{t}). \tag{A.6}
\end{aligned}$$

and for the quark annihilation, by

$$\begin{aligned}
\sigma_{++}(q\bar{q} \rightarrow t\bar{t}) &= \frac{8m_t^2\pi\alpha_s^2}{27s^{5/2}}\sqrt{s-4m_t^2}\left(1 + \frac{c_{hg}}{g_s\Lambda^2}\sqrt{2}\frac{vs}{m_t} + \frac{c_{Vv}}{g_s^2\Lambda^2}s\right), \\
\sigma_{--}(q\bar{q} \rightarrow t\bar{t}) &= \sigma_{++}(q\bar{q} \rightarrow t\bar{t}), \\
\sigma_{+-/-+}(q\bar{q} \rightarrow t\bar{t}) &= \frac{4\pi\alpha_s^2}{27s^{3/2}}\sqrt{s-4m_t^2}\left(1 + \frac{c_{hg}}{g_s^2\Lambda^2}4\sqrt{2}vm_t\right. \\
&\quad \left. + \frac{\sqrt{s}}{g_s^2\Lambda^2}(c_{Vv}\sqrt{s} \pm c_{Av}\sqrt{s-4m_t^2})\right) \quad (\text{A.7})
\end{aligned}$$

The first/second index indicates the helicity of the top/antitop. There are no effects of the operators \mathcal{O}_{Ra} and \mathcal{O}_{La} on the spin correlation because after integration over the variable t , their helicity cross sections vanish.

When summing over the final helicities, we arrive at

$$\sigma(q\bar{q} \rightarrow t\bar{t}) = \sigma_{SM}^{q\bar{q}}\left(1 + \frac{c_{Vv}}{g_s^2}\frac{s}{\Lambda^2}\right) + \frac{1}{\Lambda^2}\frac{\alpha_s}{9s^{3/2}}4g_sc_{hg}\sqrt{2}vm_t\sqrt{s-4m_t^2}, \quad (\text{A.8})$$

$$\begin{aligned}
\sigma(gg \rightarrow t\bar{t}) &= \sigma_{SM}^{gg} - \frac{vm_t\alpha_s g_s}{12\sqrt{2}\Lambda^2 s^2}c_{hg} \times \\
&\quad \left(8s \log\left(\frac{s - \sqrt{s(s-4m_t^2)}}{s + \sqrt{s(s-4m_t^2)}}\right) + 9\sqrt{s(s-4m_t^2)}\right), \quad (\text{A.9})
\end{aligned}$$

where

$$\sigma_{SM}^{q\bar{q}} = \frac{8\pi\alpha_s^2\sqrt{s-4m_t^2}(2m_t^2 + s)}{27s^{5/2}}, \quad (\text{A.10})$$

$$\begin{aligned}
\sigma_{SM}^{gg} &= \frac{\pi\alpha_s^2}{12s^3}\left[4(m^4 + 4sm^2 + s^2)\log\left(\frac{s + \sqrt{s(s-4m_t^2)}}{s - \sqrt{s(s-4m_t^2)}}\right)\right. \\
&\quad \left.- \sqrt{s(s-4m_t^2)}(31m^2 + 7s)\right]. \quad (\text{A.11})
\end{aligned}$$

These expressions correspond to the differential cross sections (4.2) and (4.3) integrated over the scattering angle.

Bibliography

- [1] C. Degrande and J. M. Gerard, “A theoretical determination of the eta-eta’ mixing”, *JHEP*, vol. 05, p. 043, 2009, 0901.2860.
- [2] C. Degrande, J.-M. Gerard, C. Grojean, F. Maltoni, and G. Servant, “Non-resonant New Physics in Top Pair Production at Hadron Colliders”, *JHEP*, vol. 03, p. 125, 2011, 1010.6304.
- [3] C. Degrande, J.-M. Gerard, C. Grojean, F. Maltoni, and G. Servant, “An effective approach to same sign top pair production at the LHC and the forward-backward asymmetry at the Tevatron”, 2011, 1104.1798.
- [4] A. Strumia and F. Vissani, “Neutrino masses and mixings and..”, 2006, hep-ph/0606054.
- [5] G. Rolandi, “Compilation of results on electroweak parameters from SLC and LEP”, Presented at 25th Rencontre de Moriond: Electroweak Interactions and Unified Theories, Les Arcs, France, Mar 4- 11, 1990.
- [6] P. Langacker and M.-x. Luo, “Implications of precision electroweak experiments for $M(t)$, $\rho(0)$, $\sin^2\theta(W)$ and grand unification”, *Phys. Rev.*, vol. D44, pp. 817–822, 1991.
- [7] F. Abe *et al.*, “Observation of top quark production in anti-p p collisions”, *Phys. Rev. Lett.*, vol. 74, pp. 2626–2631, 1995, hep-ex/9503002.
- [8] S. Abachi *et al.*, “Observation of the top quark”, *Phys. Rev. Lett.*, vol. 74, pp. 2632–2637, 1995, hep-ex/9503003.
- [9] K. Nakamura *et al.*, “Review of particle physics”, *J. Phys.*, vol. G37, p. 075021, 2010.
- [10] D. B. Kaplan, “Five lectures on effective field theory”, 2005, nucl-th/0510023.

-
- [11] A. V. Manohar, “Effective field theories”, 1996, hep-ph/9606222.
- [12] A. Pich, “Effective field theory”, 1998, hep-ph/9806303.
- [13] M. E. Peskin and D. V. Schroeder, “An Introduction to quantum field theory”, Reading, USA: Addison-Wesley (1995) 842 p.
- [14] E. Fermi, “An attempt of a theory of beta radiation. 1”, *Z. Phys.*, vol. 88, pp. 161–177, 1934.
- [15] T. Appelquist and J. Carazzone, “Infrared Singularities and Massive Fields”, *Phys. Rev.*, vol. D11, p. 2856, 1975.
- [16] F. Sannino and K. Tuominen, “Orientifold theory dynamics and symmetry breaking”, *Phys. Rev.*, vol. D71, p. 051901, 2005, hep-ph/0405209.
- [17] M. Beneke *et al.*, “Top quark physics”, 2000, hep-ph/0003033.
- [18] W. Bernreuther, “Top quark physics at the LHC”, *J. Phys.*, vol. G35, p. 083001, 2008, 0805.1333.
- [19] T. Han, “The ‘Top Priority’ at the LHC”, *Int. J. Mod. Phys.*, vol. A23, pp. 4107–4124, 2008, 0804.3178.
- [20] R. Frederix, “Top quark phenomenology”, 2010, 1009.6199.
- [21] T. Christiansen, “Top quark study at cms.” Talk presented at ICHEP2010.
- [22] A. Lucotte, “Top quark studies with atlas.” Talk presented at ICHEP2010.
- [23] F.-P. Schilling, “First top results (cms).” Talk presented at HCP2010.
- [24] G. Cortiana, “First top results (atlas).” Talk presented at HCP2010.
- [25] “Combination of top pair production cross sections in pp collision at $\sqrt{s} = 7$ TeV and comparisons with theory”, *CMS note*, vol. PAS TOP-11-001, 2011.
- [26] L. Cerrito, “Top quark and Electroweak measurements at the Tevatron”, *J. Phys. Conf. Ser.*, vol. 259, p. 012019, 2010, 1010.1735.
- [27] “A combined measurement of the top quark pair production cross-section using dilepton and single-lepton final states”, *Atlas note*, vol. 040, 2011.
- [28] M. Cacciari, S. Frixione, M. L. Mangano, P. Nason, and G. Ridolfi, “Updated predictions for the total production cross sections of top and of heavier quark pairs at the Tevatron and at the LHC”, *JHEP*, vol. 09, p. 127, 2008, 0804.2800.

- [29] T. Aaltonen *et al.*, “First Measurement of the $t\bar{t}$ Differential Cross Section $d\sigma/dM_{t\bar{t}}$ in $p\bar{p}$ Collisions at $\sqrt{s} = 1.96$ TeV”, *Phys. Rev. Lett.*, vol. 102, p. 222003, 2009, 0903.2850.
- [30] N. Goldschmidt, “Search for T-Tbar Resonances at the Tevatron”, *Proceedings of Science*, 2010. Talk at the 35th International Conference of High Energy Physics, to be published.
- [31] “Search for $t\bar{t}$ Resonances in the Lepton+Jets Final Stat in $p\bar{p}$ Collisions at $\sqrt{s} = 1.96$ TeV”, *D0 note*, vol. 5882-CONF, 2011.
- [32] “Search for Resonances in Semi-leptonic Top-pair Decays Close to production Threshold”, *CMS note*, vol. PAS TOP-10-007, 2011.
- [33] O. Antunano, J. H. Kuhn, and G. Rodrigo, “Top quarks, axiguons and charge asymmetries at hadron colliders”, *Phys. Rev.*, vol. D77, p. 014003, 2008, 0709.1652.
- [34] T. A. Schwarz, “Measurement of the front back asymmetry in top-antitop quark pairs produced in proton-antiproton collisions at center of mass energy = 1.96 TeV”, FERMILAB-THESIS-2006-51.
- [35] V. M. Abazov *et al.*, “First measurement of the forward-backward charge asymmetry in top quark pair production”, *Phys. Rev. Lett.*, vol. 100, p. 142002, 2008, 0712.0851.
- [36] T. Aaltonen *et al.*, “Forward-Backward Asymmetry in Top Quark Production in $p\bar{p}$ Collisions at $\sqrt{s} = 1.96$ TeV”, *Phys. Rev. Lett.*, vol. 101, p. 202001, 2008, 0806.2472.
- [37] “Measurement of the Inclusive Forward-Backward Asymmetry and its Rapidity Dependence $A_{fb}(\Delta y)$ in $t\bar{t}$ Production in 5.3 fb^{-1} of Tevatron Data”, *CDF note*, vol. 10224, 2010.
- [38] T. Aaltonen *et al.*, “Evidence for a Mass Dependent Forward-Backward Asymmetry in Top Quark Pair Production”, 2011, 1101.0034.
- [39] V. M. Abazov *et al.*, “Forward-backward asymmetry in top quark-antiquark production”, 2011, 1107.4995.
- [40] “Measurement of the Forward Backward Asymmetry in Top Pair Production in the Dilepton Decay Channel using 5.1 fb^{-1} ”, *CDF note*, vol. 10436, 2011.
- [41] “Measurement of the charge asymmetry in top pair production”, *CMS note*, vol. PAS TOP-11-014, 2011.

- [42] G. Mahlon and S. J. Parke, “Angular correlations in top quark pair production and decay at hadron colliders”, *Phys. Rev.*, vol. D53, pp. 4886–4896, 1996, hep-ph/9512264.
- [43] G. Mahlon and S. J. Parke, “Maximizing spin correlations in top quark pair production at the Tevatron”, *Phys. Lett.*, vol. B411, pp. 173–179, 1997, hep-ph/9706304.
- [44] V. M. Abazov *et al.*, “Measurement of spin correlation in $t\bar{t}$ production using dilepton final states”, 2011, 1103.1871.
- [45] W. Bernreuther, A. Brandenburg, Z. G. Si, and P. Uwer, “Top quark pair production and decay at hadron colliders”, *Nucl. Phys.*, vol. B690, pp. 81–137, 2004, hep-ph/0403035.
- [46] T. Aaltonen *et al.*, “Measurement of $t\bar{t}$ Spin Correlation in $p\bar{p}$ Collisions Using the CDF II Detector at the Tevatron”, *Phys. Rev.*, vol. D83, p. 031104, 2011, 1012.3093.
- [47] T. Aaltonen *et al.*, “Search for Maximal Flavor Violating Scalars in Same-Charge Lepton Pairs in p anti- p Collisions at $\sqrt{s} = 1.96$ TeV”, *Phys. Rev. Lett.*, vol. 102, p. 041801, 2009, 0809.4903.
- [48] T. Aaltonen *et al.*, “Search for new particles decaying into dijets in proton-antiproton collisions at $\sqrt{s} = 1.96$ TeV”, *Phys. Rev.*, vol. D79, p. 112002, 2009, 0812.4036.
- [49] V. Khachatryan *et al.*, “Measurement of Dijet Angular Distributions and Search for Quark Compositeness in pp Collisions at 7 TeV”, *Phys. Rev. Lett.*, vol. 106, p. 201804, 2011, 1102.2020.
- [50] T. Feldmann, “Quark structure of pseudoscalar mesons”, *Int. J. Mod. Phys.*, vol. A15, pp. 159–207, 2000, hep-ph/9907491.
- [51] R. Escribano and J.-M. Frere, “Study of the η η' system in the two mixing angle scheme”, *JHEP*, vol. 06, p. 029, 2005, hep-ph/0501072.
- [52] J.-M. Gerard, “Mass Issues in Fundamental Interactions”, 2008, 0811.0540.
- [53] E. Witten, “Large N Chiral Dynamics”, *Ann. Phys.*, vol. 128, p. 363, 1980.
- [54] S. R. Coleman and E. Witten, “Chiral Symmetry Breakdown in Large N Chromodynamics”, *Phys. Rev. Lett.*, vol. 45, p. 100, 1980.
- [55] G. 't Hooft, “Symmetry breaking through Bell-Jackiw anomalies”, *Phys. Rev. Lett.*, vol. 37, pp. 8–11, 1976.

- [56] H. Georgi, “A bound on $m(\eta) / m(\eta\text{-prime})$ for large $n(c)$ ”, *Phys. Rev.*, vol. D49, pp. 1666–1667, 1994, hep-ph/9310337.
- [57] S. Weinberg, “Mixing angle in renormalizable theories of weak and electromagnetic interactions”, *Phys. Rev.*, vol. D5, pp. 1962–1967, 1972.
- [58] S. Weinberg, “The U(1) Problem”, *Phys. Rev.*, vol. D11, pp. 3583–3593, 1975.
- [59] H. J. Lipkin, “FSI rescattering in B^{\pm} decays via states with η , η' , ω and Φ ”, *Phys. Lett.*, vol. B433, pp. 117–124, 1998.
- [60] J. M. Gerard and E. Kou, “Anomalous enhancement of a penguin hadronic matrix element in $B \rightarrow K \eta$ ”, *Phys. Rev. Lett.*, vol. 97, p. 261804, 2006, hep-ph/0609300.
- [61] R. Slansky, “Group Theory for Unified Model Building”, *Phys. Rept.*, vol. 79, pp. 1–128, 1981.
- [62] G. C. Branco and J. M. Gerard, “On the calculability of $W^+(L) - W^+(R)$ gauge mixing”, *Phys. Lett.*, vol. B124, p. 415, 1983.
- [63] J. A. Cronin, “Phenomenological model of strong and weak interactions in chiral $U(3) \times U(3)$ ”, *Phys. Rev.*, vol. 161, pp. 1483–1494, 1967.
- [64] R. Kaiser and H. Leutwyler, “Large $N(c)$ in chiral perturbation theory”, *Eur. Phys. J.*, vol. C17, pp. 623–649, 2000, hep-ph/0007101.
- [65] C. G. Callan, Jr., S. R. Coleman, J. Wess, and B. Zumino, “Structure of phenomenological Lagrangians. 2”, *Phys. Rev.*, vol. 177, pp. 2247–2250, 1969.
- [66] S. R. Coleman, J. Wess, and B. Zumino, “Structure of phenomenological Lagrangians. 1”, *Phys. Rev.*, vol. 177, pp. 2239–2247, 1969.
- [67] M. Capdequi-Peyranere, F. M. Renard, and M. Talon, “Leptonic and hadronic corrections to mass and propagator of w and z bosons”, *Z. Phys.*, vol. C5, p. 337, 1980.
- [68] M. A. Diaz, “Diagonalization of coupled scalars and its application to the supersymmetric neutral Higgs sector”, 1997, hep-ph/9705471.
- [69] N. D. Christensen and C. Duhr, “FeynRules - Feynman rules made easy”, *Comput. Phys. Commun.*, vol. 180, pp. 1614–1641, 2009, 0806.4194.
- [70] T. Hahn, “Generating Feynman diagrams and amplitudes with FeynArts 3”, *Comput. Phys. Commun.*, vol. 140, pp. 418–431, 2001, hep-ph/0012260.

- [71] H. Leutwyler, “Bounds on the light quark masses”, *Phys. Lett.*, vol. B374, pp. 163–168, 1996, hep-ph/9601234.
- [72] P. Herrera-Siklody, J. I. Latorre, P. Pascual, and J. Taron, “eta eta’ mixing from $U(3)_L \times U(3)_R$ chiral perturbation theory”, *Phys. Lett.*, vol. B419, pp. 326–332, 1998, hep-ph/9710268.
- [73] J. M. Gerard and E. Kou, “eta - eta’ masses and mixing: A large $N(c)$ reappraisal”, *Phys. Lett.*, vol. B616, pp. 85–92, 2005, hep-ph/0411292.
- [74] P. Di Vecchia, F. Nicodemi, R. Pettorino, and G. Veneziano, “Large n , Chiral Approach to Pseudoscalar Masses, Mixings and Decays”, *Nucl. Phys.*, vol. B181, p. 318, 1981.
- [75] S. Fajfer and J. M. Gerard, “Hadronic decays of eta and eta-prime in the large n limit”, *Z. Phys.*, vol. C42, p. 431, 1989.
- [76] V. Barger, T. Han, and D. G. E. Walker, “Top Quark Pairs at High Invariant Mass: A Model- Independent Discriminator of New Physics at the LHC”, *Phys. Rev. Lett.*, vol. 100, p. 031801, 2008, hep-ph/0612016.
- [77] D. Choudhury, R. M. Godbole, R. K. Singh, and K. Wagh, “Top production at the Tevatron/LHC and nonstandard, strongly interacting spin one particles”, *Phys. Lett.*, vol. B657, pp. 69–76, 2007, 0705.1499.
- [78] R. Frederix and F. Maltoni, “Top pair invariant mass distribution: a window on new physics”, *JHEP*, vol. 01, p. 047, 2009, 0712.2355.
- [79] “Precision electroweak measurements on the Z resonance”, *Phys. Rept.*, vol. 427, p. 257, 2006, hep-ex/0509008.
- [80] C. T. Hill and S. J. Parke, “Top production: Sensitivity to new physics”, *Phys. Rev.*, vol. D49, pp. 4454–4462, 1994, hep-ph/9312324.
- [81] D. Atwood, A. Kagan, and T. G. Rizzo, “Constraining anomalous top quark couplings at the Tevatron”, *Phys. Rev.*, vol. D52, pp. 6264–6270, 1995, hep-ph/9407408.
- [82] K.-m. Cheung, “Probing the chromoelectric and chromomagnetic dipole moments of the top quark at hadronic colliders”, *Phys. Rev.*, vol. D53, pp. 3604–3615, 1996, hep-ph/9511260.
- [83] K. Whisnant, J.-M. Yang, B.-L. Young, and X. Zhang, “Dimension-six CP conserving operators of the third family quarks and their effects on collider observables”, *Phys. Rev.*, vol. D56, pp. 467–478, 1997, hep-ph/9702305.

- [84] K.-i. Hikasa, K. Whisnant, J. M. Yang, and B.-L. Young, “Probing anomalous top quark interactions at the Fermilab Tevatron collider”, *Phys. Rev.*, vol. D58, p. 114003, 1998, hep-ph/9806401.
- [85] B. Lillie, J. Shu, and T. M. P. Tait, “Top Compositeness at the Tevatron and LHC”, *JHEP*, vol. 04, p. 087, 2008, 0712.3057.
- [86] K. Kumar, T. M. P. Tait, and R. Vega-Morales, “Manifestations of Top Compositeness at Colliders”, *JHEP*, vol. 05, p. 022, 2009, 0901.3808.
- [87] D.-W. Jung, P. Ko, J. S. Lee, and S.-h. Nam, “Model independent analysis of the forward-backward asymmetry of top quark production at the Tevatron”, *Phys. Lett.*, vol. B691, pp. 238–242, 2010, 0912.1105.
- [88] Z. Hioki and K. Ohkuma, “Search for anomalous top-gluon couplings at LHC revisited”, *Eur. Phys. J.*, vol. C65, pp. 127–135, 2010, 0910.3049.
- [89] D. Choudhury and P. Saha, “Probing Top Anomalous Couplings at the Tevatron and the Large Hadron Collider”, 2009, 0911.5016.
- [90] J. A. Aguilar-Saavedra, “A minimal set of top anomalous couplings”, *Nucl. Phys.*, vol. B812, pp. 181–204, 2009, 0811.3842.
- [91] J. A. Aguilar-Saavedra, “A minimal set of top-Higgs anomalous couplings”, *Nucl. Phys.*, vol. B821, pp. 215–227, 2009, 0904.2387.
- [92] J. A. Aguilar-Saavedra and J. Bernabeu, “W polarisation beyond helicity fractions in top quark decays”, *Nucl. Phys.*, vol. B840, pp. 349–378, 2010, 1005.5382.
- [93] C. Zhang and S. Willenbrock, “Effective-Field-Theory Approach to Top-Quark Production and Decay”, *Phys. Rev.*, vol. D83, p. 034006, 2011, 1008.3869.
- [94] J. Drobnak, S. Fajfer, and J. F. Kamenik, “New physics in $t \rightarrow b W$ decay at next-to-leading order in QCD”, *Phys. Rev.*, vol. D82, p. 114008, 2010, 1010.2402.
- [95] W. Buchmuller and D. Wyler, “Effective Lagrangian Analysis of New Interactions and Flavor Conservation”, *Nucl. Phys.*, vol. B268, p. 621, 1986.
- [96] B. Grzadkowski, M. Iskrzynski, M. Misiak, and J. Rosiek, “Dimension-Six Terms in the Standard Model Lagrangian”, *JHEP*, vol. 10, p. 085, 2010, 1008.4884.
- [97] K. Agashe, R. Contino, L. Da Rold, and A. Pomarol, “A custodial symmetry for $Z b \text{ anti-}b$ ”, *Phys. Lett.*, vol. B641, pp. 62–66, 2006, hep-ph/0605341.

- [98] A. Pomarol and J. Serra, “Top Quark Compositeness: Feasibility and Implications”, *Phys. Rev.*, vol. D78, p. 074026, 2008, 0806.3247.
- [99] P. L. Cho and E. H. Simmons, “Looking for gluon substructure at the tevatron”, *Phys. Lett.*, vol. B323, pp. 401–407, 1994, hep-ph/9307345.
- [100] P. L. Cho and E. H. Simmons, “Searching for G3 in t anti-t production”, *Phys. Rev.*, vol. D51, pp. 2360–2370, 1995, hep-ph/9408206.
- [101] E. H. Simmons and P. L. Cho, “Anomalous gluon selfinteractions and t anti-t production”, 1995, hep-ph/9504401.
- [102] M. Bona *et al.*, “Model-independent constraints on $\Delta F=2$ operators and the scale of new physics”, *JHEP*, vol. 03, p. 049, 2008, 0707.0636.
- [103] H. Georgi, L. Kaplan, D. Morin, and A. Schenk, “Effects of top compositeness”, *Phys. Rev.*, vol. D51, pp. 3888–3894, 1995, hep-ph/9410307.
- [104] G. F. Giudice, C. Grojean, A. Pomarol, and R. Rattazzi, “The Strongly-Interacting Light Higgs”, *JHEP*, vol. 06, p. 045, 2007, hep-ph/0703164.
- [105] H. Georgi, “Generalized dimensional analysis”, *Phys. Lett.*, vol. B298, pp. 187–189, 1993, hep-ph/9207278.
- [106] A. Manohar and H. Georgi, “Chiral Quarks and the Nonrelativistic Quark Model”, *Nucl. Phys.*, vol. B234, p. 189, 1984.
- [107] J. M. Gerard and S. Trine, “QCD anomalies in hadronic weak decays”, *Phys. Rev.*, vol. D69, p. 113005, 2004, hep-ph/0402158.
- [108] J. Shu, T. M. P. Tait, and K. Wang, “Explorations of the Top Quark Forward-Backward Asymmetry at the Tevatron”, *Phys. Rev.*, vol. D81, p. 034012, 2010, 0911.3237.
- [109] A. Arhrib, R. Benbrik, and C.-H. Chen, “Forward-backward asymmetry of top quark in diquark models”, *Phys. Rev.*, vol. D82, p. 034034, 2010, 0911.4875.
- [110] I. Dorsner, S. Fajfer, J. F. Kamenik, and N. Kosnik, “Light colored scalars from grand unification and the forward-backward asymmetry in top quark pair production”, *Phys. Rev.*, vol. D81, p. 055009, 2010, 0912.0972.
- [111] Z. Ligeti, M. Schmaltz, and G. M. Tavares, “Explaining the t tbar forward-backward asymmetry without dijet or flavor anomalies”, 2011, 1103.2757.
- [112] E. L. Berger, Q.-H. Cao, C.-R. Chen, C. S. Li, and H. Zhang, “Top Quark Forward-Backward Asymmetry and Same-Sign Top Quark Pairs”, *Phys. Rev. Lett.*, vol. 106, p. 201801, 2011, 1101.5625.

- [113] J. Cao, L. Wang, L. Wu, and J. M. Yang, “Top quark forward-backward asymmetry, FCNC decays and like-sign pair production as a joint probe of new physics”, 2011, 1101.4456.
- [114] T. Han, I. Lewis, and Z. Liu, “Colored Resonant Signals at the LHC: Largest Rate and Simplest Topology”, *JHEP*, vol. 12, p. 085, 2010, 1010.4309.
- [115] E. L. Berger, Q.-H. Cao, C.-R. Chen, G. Shaughnessy, and H. Zhang, “Color Sextet Scalars in Early LHC Experiments”, *Phys. Rev. Lett.*, vol. 105, p. 181802, 2010, 1005.2622.
- [116] H. Zhang, E. L. Berger, Q.-H. Cao, C.-R. Chen, and G. Shaughnessy, “Color Sextet Vector Bosons and Same-Sign Top Quark Pairs at the LHC”, *Phys. Lett.*, vol. B696, pp. 68–73, 2011, 1009.5379.
- [117] K. Agashe, R. Contino, and R. Sundrum, “Top compositeness and precision unification”, *Phys. Rev. Lett.*, vol. 95, p. 171804, 2005, hep-ph/0502222.
- [118] B. Stelzer, “Review of Top Quark Measurements”, 2010, 1004.5368.
- [119] Q.-H. Cao, D. McKeen, J. L. Rosner, G. Shaughnessy, and C. E. M. Wagner, “Forward-Backward Asymmetry of Top Quark Pair Production”, *Phys. Rev.*, vol. D81, p. 114004, 2010, 1003.3461.
- [120] P. M. Nadolsky *et al.*, “Implications of CTEQ global analysis for collider observables”, *Phys. Rev.*, vol. D78, p. 013004, 2008, 0802.0007.
- [121] J. Alwall *et al.*, “MadGraph/MadEvent v4: The New Web Generation”, *JHEP*, vol. 09, p. 028, 2007, 0706.2334.
- [122] J. A. Aguilar-Saavedra, “Effective four-fermion operators in top physics: a roadmap”, *Nucl. Phys.*, vol. B843, pp. 638–672, 2011, 1008.3562.
- [123] F. Maltoni, *Quarkonium phenomenology*. Ph.D. Thesis, 1998.
- [124] J. Alwall, M. Herquet, F. Maltoni, O. Mattelaer, and T. Stelzer, “MadGraph 5 : Going Beyond”, 2011, 1106.0522.
- [125] N. D. Christensen *et al.*, “A comprehensive approach to new physics simulations”, *Eur. Phys. J.*, vol. C71, p. 1541, 2011, 0906.2474.
- [126] C. Degrande, C. Duhr, B. Fuks, D. Grellscheid, O. Mattelaer, and T. Reiter, “Ufo - the universal feynrules output”, 2011. (in preparation).
- [127] P. de Aquino, W. Link, F. Maltoni, O. Mattelaer, and T. Stelzer, “Aloha: Automatic libraries of helicity amplitudes for feynman diagram computations”, 2011. (in preparation).

- [128] T. Hahn, “FormCalc 6”, *PoS*, vol. ACAT08, p. 121, 2008, 0901.1528.
- [129] A. Djouadi, G. Moreau, F. Richard, and R. K. Singh, “The forward-backward asymmetry of top quark production at the Tevatron in warped extra dimensional models”, *Phys. Rev.*, vol. D82, p. 071702, 2010, 0906.0604.
- [130] S. Jung, H. Murayama, A. Pierce, and J. D. Wells, “Top quark forward-backward asymmetry from new t-channel physics”, *Phys. Rev.*, vol. D81, p. 015004, 2010, 0907.4112.
- [131] K. Cheung, W.-Y. Keung, and T.-C. Yuan, “Top Quark Forward-Backward Asymmetry”, *Phys. Lett.*, vol. B682, pp. 287–290, 2009, 0908.2589.
- [132] P. H. Frampton, J. Shu, and K. Wang, “Axigluon as Possible Explanation for $p\bar{p} \rightarrow t\bar{t}$ Forward-Backward Asymmetry”, *Phys. Lett.*, vol. B683, pp. 294–297, 2010, 0911.2955.
- [133] J. Cao, Z. Heng, L. Wu, and J. M. Yang, “Top quark forward-backward asymmetry at the Tevatron: a comparative study in different new physics models”, *Phys. Rev.*, vol. D81, p. 014016, 2010, 0912.1447.
- [134] V. Barger, W.-Y. Keung, and C.-T. Yu, “Asymmetric Left-Right Model and the Top Pair Forward- Backward Asymmetry”, *Phys. Rev.*, vol. D81, p. 113009, 2010, 1002.1048.
- [135] R. S. Chivukula, E. H. Simmons, and C. P. Yuan, “Axigluons cannot explain the observed top quark forward- backward asymmetry”, *Phys. Rev.*, vol. D82, p. 094009, 2010, 1007.0260.
- [136] M. Bauer, F. Goertz, U. Haisch, T. Pfoh, and S. Westhoff, “Top-Quark Forward-Backward Asymmetry in Randall-Sundrum Models Beyond the Leading Order”, *JHEP*, vol. 11, p. 039, 2010, 1008.0742.
- [137] P. Ferrario and G. Rodrigo, “Constraining heavy colored resonances from top-antitop quark events”, *Phys. Rev.*, vol. D80, p. 051701, 2009, 0906.5541.
- [138] R. M. Godbole, K. Rao, S. D. Rindani, and R. K. Singh, “On measurement of top polarization as a probe of $t\bar{t}$ production mechanisms at the LHC”, *JHEP*, vol. 11, p. 144, 2010, 1010.1458.
- [139] B. Grzadkowski and Z. Hioki, “New hints for testing anomalous top quark interactions at future linear colliders”, *Phys. Lett.*, vol. B476, pp. 87–94, 2000, hep-ph/9911505.
- [140] B. Grzadkowski and Z. Hioki, “Decoupling of anomalous top-decay vertices in angular distribution of secondary particles”, *Phys. Lett.*, vol. B557, pp. 55–59, 2003, hep-ph/0208079.

-
- [141] S. Jabeen, “Top quark properties measurement with the $D0$ detector”, 2009, 0910.4220.
- [142] G. L. Bayatian *et al.*, “CMS physics: Technical design report”, CERN-LHCC-2006-001.
- [143] “ATLAS detector and physics performance. Technical design report. Vol. 2”, CERN-LHCC-99-15.
- [144] V. M. Abazov *et al.*, “Measurement of spin correlation in $t\bar{t}$ production using a matrix element approach”, 2011, 1104.5194.
- [145] S. Jung, A. Pierce, and J. D. Wells, “Top quark asymmetry from a non-Abelian horizontal symmetry”, 2011, 1103.4835.
- [146] “Search for like-sign top quark pair production at cdf with 6.1 fb^{-1} ”, *CDF public note 10466*, 2011.
- [147] L. Gauthier and G. Servant In Preparation.
- [148] G. Brooijmans, C. Grojean, G. Kribs, C. Shepherd-Themistocleous, K. Agashe, *et al.*, “New Physics at the LHC. A Les Houches Report: Physics at TeV Colliders 2009 - New Physics Working Group”, 2010, arXiv:1005.1229.
- [149] A. Rajaraman, Z. Surujon, and T. M. P. Tait, “Asymmetric Leptons for Asymmetric Tops”, 2011, 1104.0947.